Bendix
Aerospace Systems Division

APOLLO 12 PSE THERMAL ANOMALY FINAL REPORT

NO.	REV. NO.
ATM 887	

DATE 5 June 1970

This ATM summarizes the results of the BxA study conducted to investigate the ALSEP Flight 1 PSE Thermal Anomaly. The purpose of the study was to (1) correlate the Flight 1 PSE sensor lunar performance results, (2) determine the most probable cause of the temperature related anomalies, (3) recommend possible thermal modifications to the Flight 4 PSE (Apollo 14) and subsequent units, (4) resolve thermal problems encountered in the implementation of the modifications, (5) provide thermal performance predictions for Apollo 14 and (6) supply recommendations for future efforts to improve the experiment's performance and capability as a scientific research instrument. This report has been generated in response to MSC directive BG 931/L115-70/T94, "Analysis of Apollo 12 PSE Data Anomalies", dated 13 February 1970.

Prepared by J. C. Griffin, Jr.
J. Griffin

Prepared by G. Psaros
G. Psaros

Approved by J. McNaughton
J. McNaughton

CONTENTS

ILLUSTRATIONS

ILLUSTRATIONS (CONT.)

TABLES

1.0 INTRODUCTION

Thermal performance of the PSE during the first seven lunar days of operation is shown in Figure 1-1. The temperature of the PSE sensor increased from the first lunation maximum of 134°F at a sun angle of approximately 126 degrees to a temperature of 145°F during the third day. Since the third day of operation, maximum temperatures have remained essentially constant with only slight increases due to material properties degradation. The specified upper operating temperature limit of the PSE is 143°F which is also the upper limit of the telemetry range.

During the first two lunar nights, the sensor temperature had gone below the lower limit of the PSE telemetry range of 107°F. An estimation of the sensor's lowest lunar night temperature had been obtained through curve fitting of the experiment's temperature profile during transition from lunar evening to night. It was estimated that the sensor reached a low temperature of 75°F. This temperature is below the specified lower operation temperature of 107°F. The design goal for the PSE was 126.0 ± 0.4°F. It was immediately evident that modifications of the thermal control system were required. The nominal power dissipated by SN05 electronics and heaters is 3.10 watts. By actively commanding on the PSE sensor Z axis leveling motor and dissipating an additional 3.05 watts inside the experiment, the seismometer temperature has stablilized at 125.9°F for all lunar night operations from the third to the present.

The out-of-tolerance temperature variation of the seismometer reduces the possibility of obtaining full tidal data of the lunar surface. In addition to the loss of tidal data, a considerable amount of signal noise was recorded during terminator crossing at lunar sunrise and sunset which may possibly be attributed to tugging on the seismometer base due to thermal expansion and contraction of the insulation layers of the thermal skirt or the cable leading to the central station.

To improve upon the present thermal design, a thermal model of the lunar subsurface and PSE was developed to evaluate possible modifications. A detailed discussion of the thermal model is included in the present document. The thermal model was used to direct and influence design changes resulting in a more acceptable operation of the experiment. Included in

BENDIX AEROSPACE SYSTEMS DIVISION - THERMOPHYSICS GROUP

FIGURE I-1

APOLLO LUNAR SURFACE EXPERIMENTS PACKAGE (FLIGHT 1 - APOLLO 12) - 7 TH ALSEP LUNATION

SUNRISE DAY 135 (MAY 15, 1970) AT 0700 GMT

SUNRISE DAY 164 (JUNE 13, 1970) AT 1800 GMT

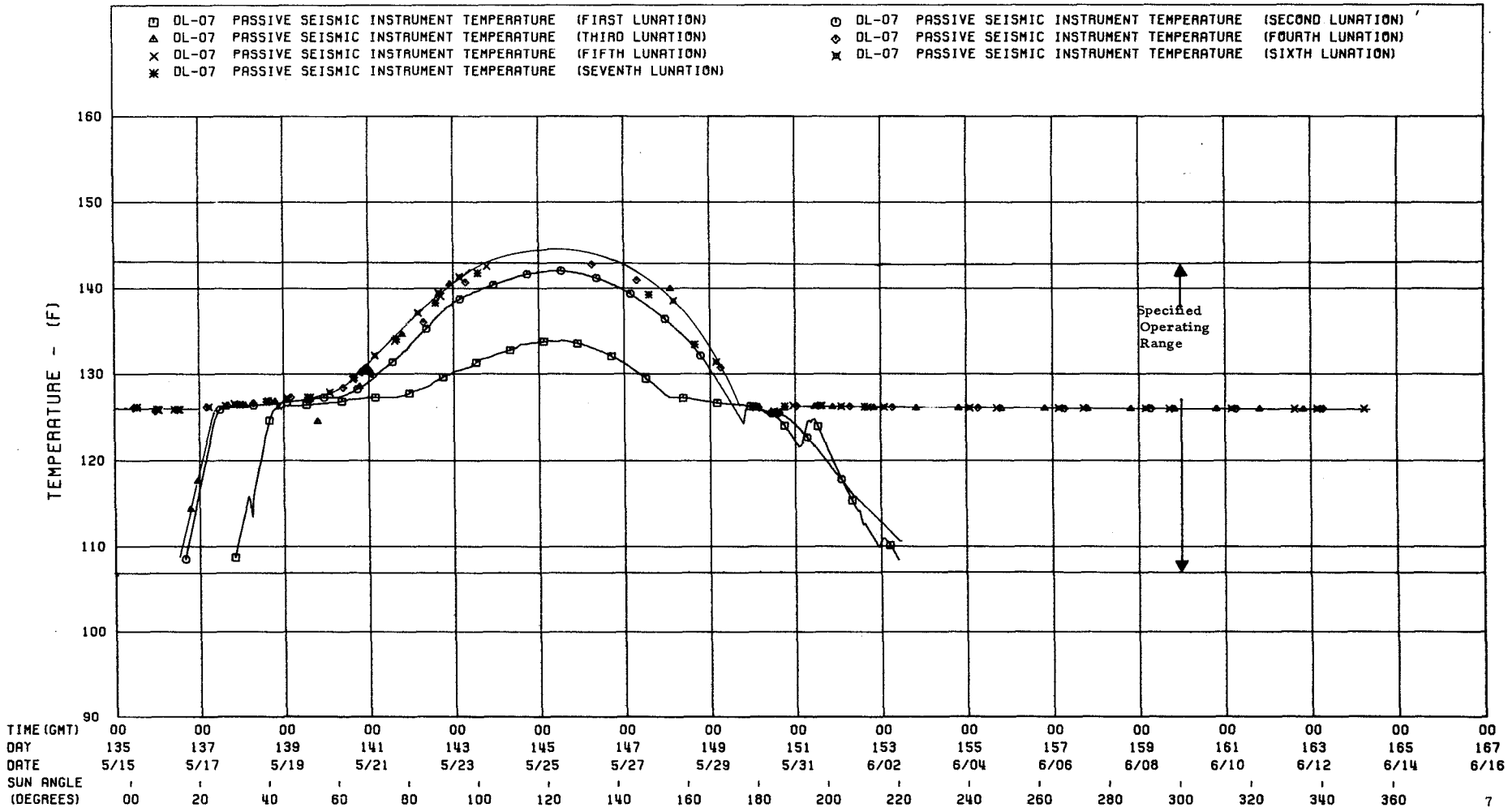

the present report are discussions of the thermal subsurface and experiment models, investigation of thin film material properties and the proposed modifications of the Apollo 14 PSE thermal control system. Potential long term modifications and design concepts to eliminate terminator noise problems are presented.

In addition, a study of the experiment solar illumination at lunar sunrise which may be the cause of the terminator noise problems is presented. A proposed modification to reduce skirt tugging is also discussed.

Other work which has been completed since the interim thermal anomaly report, reference 1, is off equatorial deployment studies of the PSE for latitudes up to 60 degrees. Thermal control performance and lunar surface temperatures beneath the skirt are given for these off-equator deployment sites.

In the redesign of the heater control system, electrical and reliability problems arose due to high thermal dissipations in transistors which required thermal analyses, modification and thermal-vacuum testing of the components. These results are also included in the report.

Finally, thermal performance predictions for the PSE deployment at the possible Apollo 14 landing site of Frau Mauro as well as Littrow Rille are presented. These predictions include the modifications to the thermal control subsystem and off equatorial deployment of the sensor.

2.0 STATEMENT OF WORK

The following statement of work is taken from MSC directive BG 931/L115-70/T94 Analysis of Apollo 12 PSE Data Anomalies.

2.1 Temperature anomaly.

2.1.1 From photos ascertain extent of dust coverage and estimate thermal degradation of shroud therefrom. (See figure 2-1)

2.1.2 Revise thermal shroud from evidence obtained from 2.1.1.

2.1.3 Conduct parametric thermal studies to evaluate effect of PSE skirt lifting, dust coverage, internal sensor power dissipation, predicted lunar surface temperature range, sensor emittance (clean and dusty) etc., on PSE transient performance.

2.1.4 Establish possible quick fix thermal modifications to PSE based on results of 2.1.3.

2.1.5 Identify additional long-term design modifications to improve PSE skirt deployment and sensor day to night temperature range.

2.1.6 Summarize overall thermal study in BxA ATM.

2.2 Noise at terminator crossing anomaly.

2.2.1 Analyze shroud design to devise a method of shroud modification to eliminate possible shroud problem due to strain accumulation and releases.

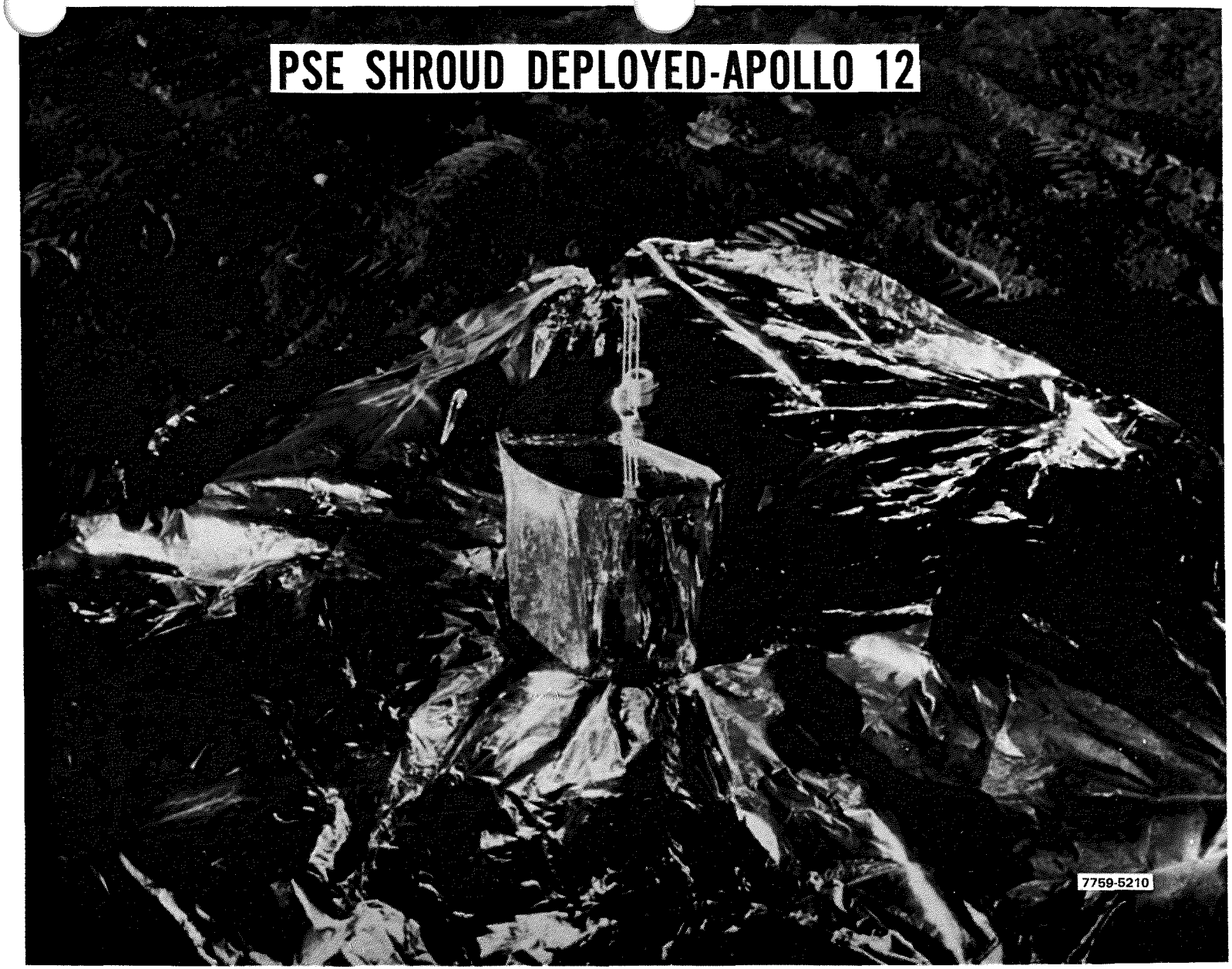

Figure 2-1

3.0 SUMMARY

This BxA study was conducted to resolve the Apollo 12 PSE sensor lunar performance and to investigate the thermal noise generated during terminator crossing per statement of work in Section 2.0. An analytical model of the PSE and local lunar surface and subsurface has been generated for correlation of the Apollo 12 PSE lunar performance and to determine the most probable cause of the out-of-tolerance temperature anomaly.

A detailed discussion of the analytical thermal model including shroud insulation, the lunar surface properties, and the effect of latitude on the lunar surface temperature and in-depth temperature profiles is presented. Temperature profiles of the Apollo 11 soil thermal properties as obtained from references 14 and 15, and the dust design thermal-physical properties as specified in reference 13 have been completed. Profiles are shown for the equator and at latitudes up to 60°. Adiabatic depths have been shown to remain the same with latitude; however, adiabatic temperatures are shown to decrease with latitude.

Transient thermal responses on the external surfaces of the thermal shroud due to solar illumination during terminator crossing at sunrise and sunset have been considered to determine the possibility of erroneous signals to the sensor. This effort has been preliminary and should be further refined.

Thermal modifications to the Apollo 14 PSE thermal control system required to maintain the sensor at its specified temperature set point of 126°F presented in Table 3-1 are discussed in detail including the necessity for each modification. These discussions are reinforced with analytical results where necessary.

In the process of arriving at the required heater modification, it was determined that the transistors in the circuit were unreliable due to over heating. This prompted an analytical study to determine the required thermal modification to assure junction temperatures below 100°C. The modification was then tested and verified. Before the thermal investigation, regulator transistor junction and case temperatures reached 183 and 168.5°C, respectively, while dissipating a nominal power of 800 milliwatts. After thermal modifications were implemented, junction and case temperatures under similar operating conditions were reduced to 87 and 62°C.

TABLE 3-1

PROPOSED MODIFICATIONS TO APOLLO 14 PSE THERMAL CONTROL SUBSYSTEM

	Modification	Description	Required Materials	On Apollo 13 Kit?	Reasons for Implementation	Requalification Required	Engineering Retest Required
1.	Perforate Mylar Insulation Layers in Skirt (Include 1/2 Mil Bare Mylar)	1. Punch Vent Holes 1/8 inch dia. 2. Adjacent Sheets Must have Alternate Patterns	None	Yes	Assures Positive Venting of Entrapped Air to: 1. Improve stowage and deployment 2. Eliminate possible rupture of shroud during launch phase	No	No
2.	Add one sheet of Silverized or Aluminized Teflon over outer surface of shroud	1. Teflon film outward 2. Stitch to outer surface of skirt 1/2 inches from cyld. cannister 3. Cylindrical section sown and slid over cannister	1. 2 Mil FEP Type-A Teflon Silverized or Aluminized one side ($\alpha/\epsilon \leq 0.11$) - Manu. - Schjeldahl 2. Tufbraid 50 Dor 16	Yes	Decreases Solar Absorptance to Infrared Emittance Ratio to: 1. Reduce temperature excursion of lunar surface beneath sensor and results in lower sensor lunar day temperature 2. Reduce heat loads to sensor through cannister	No	No
3.	Incorporate weights to each deployment Tab	Sew weights firmly to tabs	1. Mallory 1000 2. Tufbraid 50 Dor 16	Yes	1. Improves skirt deployment 2. Eliminates adverse thermal effects of tunneling 3. Improves skirt thermal isolation	No	No
4.	(A) Button skirt in three concentric circles of 8, 16 and 28 inch radii (B) Stitch periphery of skirt 1/2 inch from edge	A. Loosely button 8, 16 and 32 buttons on each circle respectively B. 1/2 inch loose stitching C. Leave spaces on edge to insure proper outgassing	1. 5 Mil Kapton buttons 3/8 inch dia 2. Dacron Thread V69	Yes	Eliminates individual layers from repelling and pealing back due to: 1. Electrostatic charges 2. Impingement of LM ascent engine exhaust and debris	No	No
5.	Add 10 sheets of Mylar insulation in skirt	1. Insert between every other sheet 2. Mylar side up	1. 1/4 Mil Mylar Type-S Aluminized one side ($\alpha/\epsilon < 0.5$)	No	Decreases effective conductivity of skirt to: 1. Reduce temperature excursion of lunar surface beneath skirt 2. Reduce effect of degradation of external skirt surface properties	No	Yes
6.	(A) Increase heater power from 2.5W to 5.5W in auto mode (B) Manual mode power increased from 2.9 to 5.57 watts	Replace present resistance heaters	Minco resistance heaters	No	1. To maintain temperature set point during lunar night phase	No	Yes
7.	Bond Teflon Compass Rose over present Compass Rose	Bond per M.P. #66	1. 2 Mil Fep Type-A Teflon Silverized one side ($\alpha/\epsilon \leq 0.11$) - Manu. - Schjeldal 2. Narmco 7343/7139	No	Decreases solar absorptance to infrared emittance to: Reduce heat loads to sensor through cannister	No	No
8.	Interim Decoupled shroud from Sensor	1. Skirt construction identical to present skirt with MODs 1, 2, 4 and 5 2. Suspend primary skirt by flexible mount	1. 30 layers of 1/4 Mil Mylar Aluminized one side 2. Dacron thread V-69 3. Nylon support ring	No	1. Decouple mechanically the skirt from sensor	No	Yes
9.	Add temperature sensor to underside of skirt or to cable	Bond temperature sensor 1' from PSE	Mylar Tape	No	Measures temperature external to sensor to: more effectively determine thermal sink temperature of soil beneath sensor.	No	Yes

Predictions for the Apollo 14 PSE sensor at possible deployment sites such as Frau Mauro and Littrow Rille at latitudes of 4° south and 22° north respectively have been made. In addition predictions for deployment sites up to 45° latitude have been made. All predictions show that the PSE sensor will remain at its temperature set point of 126°F providing the required modifications presented in Section 5.3 are implemented.

A material evaluation has been made to establish the surface properties of both aluminized and silverized 2 mil teflon films for use on the external surface of the thermal shroud. The surface properties of silverized teflon film were found to be a 63% improvement over aluminized teflon film. This corresponds to a decrease in peak temperature on the external surface of the shroud of approximately 100°F.

The long term degradation of teflon films with respect to ultraviolet radiation and to charged particles has been briefly investigated. It is generally accepted that teflon film is inert to ultraviolet radiation. However, considerable degradation occurs with 40 KEV proton bombardment at fluence levels beyond 2×10^{14} particles/cm^2. At fluence levels of the order of 1×10^{12} particles/cm^2 teflon films degrade approximately 50% from their original values corresponding to an increase in external shroud temperatures of approximately 50°F.

Subsequent efforts required have been defined which include (1) a thermal analysis to evaluate the PSE thermal control system at deployment sites of high soil thermal conductances and densities such as the rock design properties of reference 13. Latitudes up to 60 degrees will be considered (2) a parametric study of totally decoupled shroud concepts to eliminate thermal noise at terminator crossing, (3) evaluation of the proposed stool design, (4) correlation of the Apollo 14 PSE flight data incorporating the lunar soil sample thermal-physical data of Apollo 12 and 14, (5) further evaluation of silverized teflon films for long-term stability in charged particle environments.

4.1 Thermal Properties of Lunar Soil

The thermal simulation of the PSE on the lunar surface is dependent upon closely simulating the experiment and the lunar soil beneath it. A brief discussion of the assumptions and numerical values of thermal parameters used to obtain the near correlation of reference 1 is presented in this section.

Until the results of the investigation of Apollo 11 lunar sample thermal properties were presented, reference (13) was used as the source of thermal-physical lunar data. The numerical values of lunar soil conductivity, density and specific heat are important parameters in the determination of the adiabatic temperature and depth.

A comprehensive study of the thermal-physical data of the lunar samples obtained from the Apollo 11 mission has been made. The results have been evaluated and nominal lunar thermal properties selected for use in the lunar subsurface model.

4.1.1 Thermal Conductivity of Lunar Soil, K_{Soil}

The thermal conductivity of lunar surface and subsurface material has been determined previously using analytical models and infrared measurement techniques. The primary source of thermal conductivities has been reference 13. With the return of lunar samples from Apollo 11 it has been possible to obtain laboratory measurements of thermal conductivity and determine numerical values with precision. However, the values may not be truly representative of the entire lunar composition. This is evidenced by the wide variation of thermal conductivities reported in reference 14. Substantial variations in thermal conductivity resulted due to the sample type. In general, igneous rock was reported to possess a thermal conductivity on the order of 1 Btu/hr/ft°F. Breccia types were on the order of 1×10^{-1} Btu/hr/ft°F. Finally, the lunar fines possessed thermal conductivities on the order of 1×10^{-3} Btu/hr/ft°F.

The selection of a lunar model for Apollo 12 correlation purposes was based on the fact that core tube samples in the immediate area of the PSE indicated a loose soil type of lunar material. Core tubes encountered

only moderate resistance indicating the absence of massive concentrations of igneous or breccia rock in the landing site area. Photographs of the local lunar terrain gave an indication that the surface was of a sandy and loose nature. Therefore, the thermal conductivity of lunar fines was selected based on these facts and observations.

The thermal conductivity of lunar fines was investigated in reference 15 as a function of temperature. Although the investigators indicated some uncertainty in the temperature effects, they were used in the analyses since no other information is available to date.

The thermal conductivity was determined using the line heat source technique. Values at three soil temperatures were reported. The three values are plotted in figure 4-1. The three points indicate a linear variation of thermal conductivity with temperature. A linear extrapolation of the data below -100°F is shown. Thermal conductivities range from 0.71×10^{-3} Btu/hr/ft°F at lunar night to a value of 1.4×10^{-3} Btu/hr/ft°F at lunar noon. Furthermore, it was indicated by these and other investigators that the thermal conductivity is a function of the packing of the lunar fines. Values indicating this effect were not reported.

As a result of the uncertainty expressed by the investigators (reference 15) of soil thermal conductivity temperature dependence, packing factor influences and soil variations due to locale, a constant value was assumed at a mean temperature of 0°F. The value used in the model is $k_{soil} = 1.1 \times 10^{-3}$ Btu/hr/ft°F. The value of thermal conductivity used previously was 2.41×10^{-3} Btu/hr/ft°F (reference 13). The sample measured values differs from the LED-520 design value for lunar soil by a factor of two. The lower conductivity value indicates a better insulating of the soil beneath the skirt from external temperatrue fluctuations than previously expected. Furthermore, the adiabatic depth is decreased and sensitivity of the sensor to external temperature variations is reduced. The soil possesses insulating qualities approaching those of multilayer insulation.

As a result of the relatively low thermal conductivity, surface radial temperature variations are very small. The primary temperature drop occurred at the outer edge of the skirt in the analytical model. The

Figure 4-1
THERMAL CONDUCTIVITY OF LUNAR
SOIL(POWDER) - APOLLO 11*

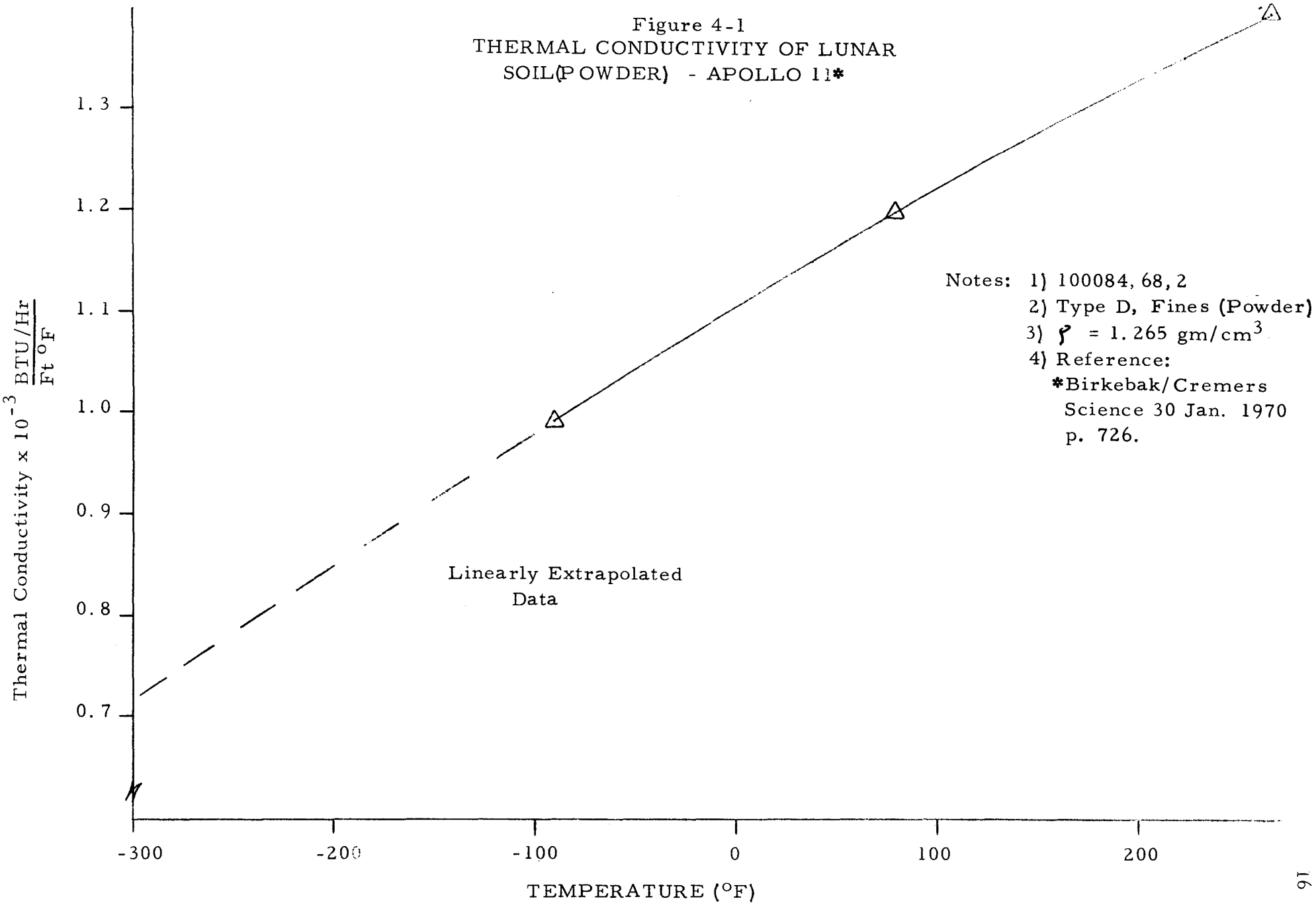

effect is desirable in attenuating external fluctuations, however, the potential usefulness as a lunar heat sink is not fully realized due to the restricted heat path resulting from the decreased thermal conductivity. This may be a cause of rising daytime temperatures since the rejection of internally dissipated power to the lunar heat sink is essential.

It was assumed that soil thermal conductivity was independent of latitude in all studies. There is no reason to assume any dependence other than that due to temperature effects as discussed above.

4.1.2 Lunar Soil Density, ρ_{soil}

It was assumed that the contents of the core tube samples better represented the "average" lunar material than any of the particular breccia or igneous rock samples. The core samples of 10 and 13.5 cm in length indicated the existence of a thick soil stratum rather than solid rock at that location.

The density of the core tube samples was assumed and used in the analyses. A numerical value of $\rho = 6.14 \times 10^{-2}$ lb/in^3 (1.70 gm/cm^3) was measured. LED-S20-IF had specified 3.24×10^{-2} lb/in^3 (0.9 gm/cm^3).

4.1.3 Lunar Soil Specific Heat, C_p

Measured specific heats of the lunar materials varied the least of any of the thermal properties. A nominal value of C_p = 0.2 Btu/lb°F (0.2 cal/gm°c) was used in the thermal analyses.

4.1.4 Thermal Inertial Parameter, γ^{-1}

The resulting numerical value of γ using

$k = 1.1 \times 10^{-3}$ Btu/hr/ft°F (4.55×10^{-6} cal/sec cm°C)

$\rho = 6.14 \times 10^{-2}$ lb/in^3 (1.70 gm/cm^3)

C_p = 0.2 Btu/lb°F (0.2 cal/gm°C)

is

$\gamma = 6.54$ ft^2°F hr$^{1/2}$/Btu (800 cm^2°C sec$^{1/2}$/cal)

4.2 Lunar Subsurface Models

4.2.1 One Dimensional Lunar Subsurface Model

The 12 node, one dimensional lunar subsurface model shown in figure 4-2 was used to determine subsurface temperature profiles. The lunar surface temperature was impressed on node 13. All other nodes were allowed to float. The convergence to desired temperature time histories for a given depth was attained after 10 lunations. It was then possible to determine the adiabatic depths and corresponding temperatures for various types of lunar material. Using the numerical values of the thermal properties of section 4.1 and the equatorial lunar surface temperatures for the dust model of reference 13, an adiabatic temperature of -60°F occuring at a depth of 8 inches was obtained. Presented in figure 4-3 are the temperatures vs. soil depths for a few selected times. The temperature profiles for the lunar dust model of LED-520-IF is also shown in figure 4-4. An adiabatic temperature of -46°F occurring at a depth of 13 inches was obtained.

4.2.2 Lunar Surface and Subsurface Temp Variation with Latitude

Lunar surface temperatures vary with latitude. Presented in figure 4-5 is the surface temperature as a function of latitude assuming the relation:

$$T(R^\circ) = T_e(R^\circ) \cos^{1/4} \theta$$

where T_e is the lunar surface temperature at the equator at a given time. A one dimensional thermal model of the lunar surface was constructed to determine the influence of latitude on adiabatic temperature and depths. A study was made (reference 6) to determine lunar soil responses for three types of lunar materials. The dust and rock design thermal properties of LED-520-IF were used as well as thermal data resulting from analysis of core tube samples of Apollo 11 (reference 15). The one dimensional analyses were performed for latitudes of 0°, 22°, 45° and 60°. The lunar surface temparature time histories were impressed on the node representing the lunar surface. As many as 10 successive lunations were run until a convergence to desired subsurface responses were attained.

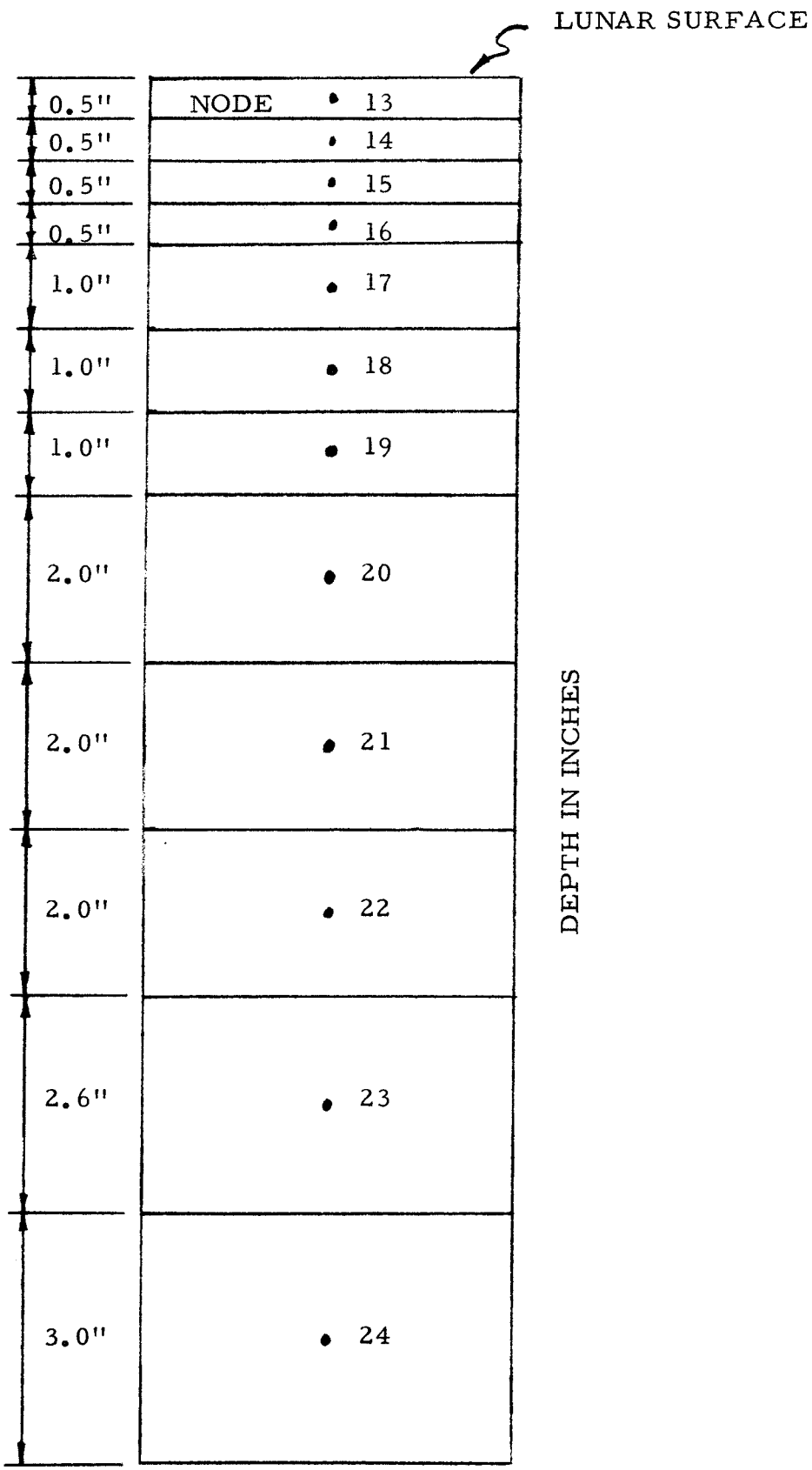

Figure 4-2 1 Dimensional Soil Model

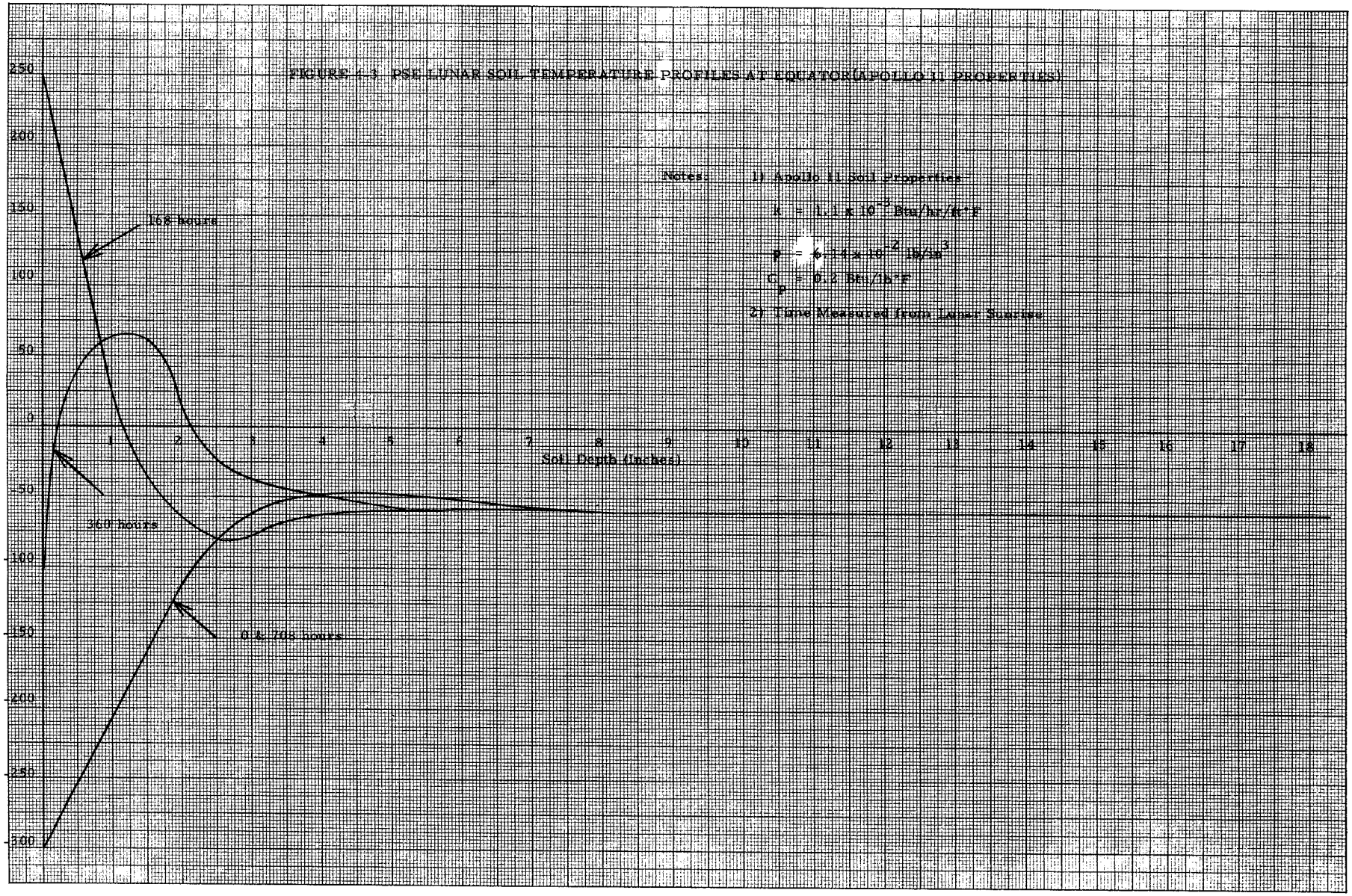
FIGURE 4-3 PSE LUNAR SOIL TEMPERATURE PROFILES AT EQUATOR(APOLLO 11 PROPERTIES)
Notes: 1) Apollo 11 Soil Properties
k = 1.1 x 10⁻³ Btu/hr/ft°F
ρ = 6.14 x 10⁻² lb/in³
Cp = 0.2 Btu/lb°F
2) Time Measured from Lunar Sunrise
Soil Temperature (°F)
Soil Depth (inches)
168 hours
360 hours
0 & 708 hours

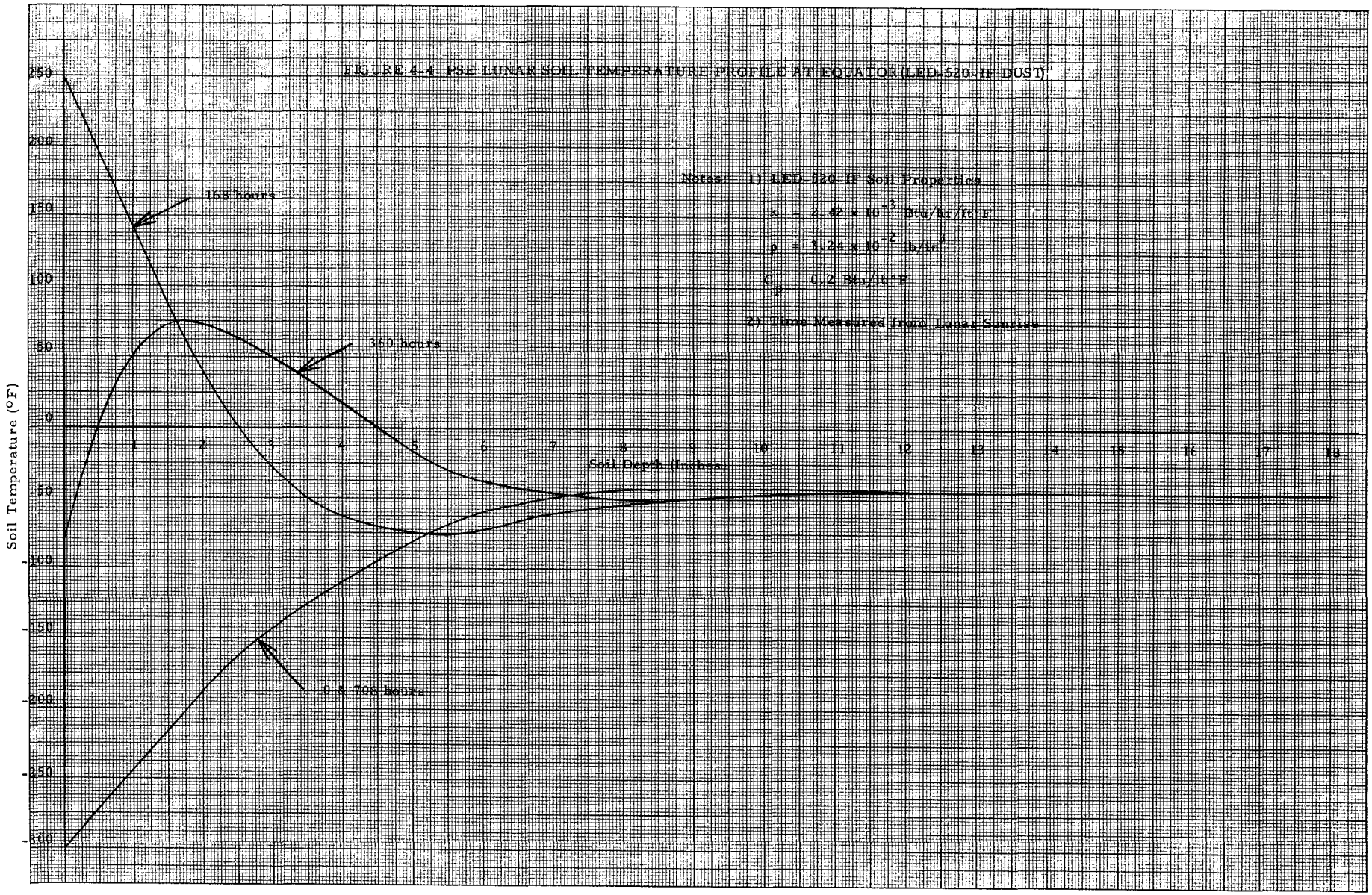

FIGURE 4-4 PSE LUNAR SOIL TEMPERATURE PROFILE AT EQUATOR (LED-520-IF DUST)

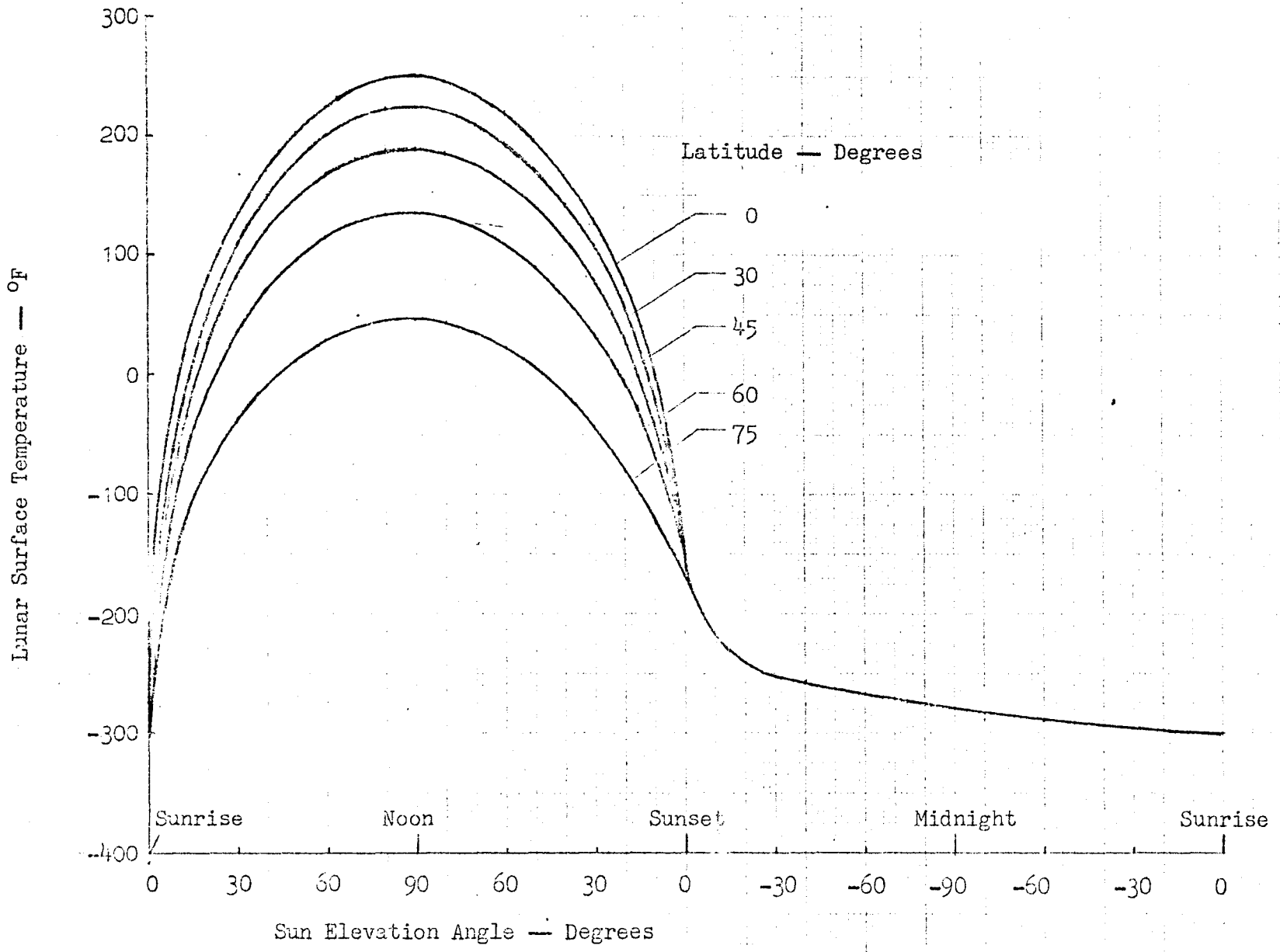

Figure 4-5. Lunar Surface Temperature vs Sun Angle and Latitude

The results of reference 21 were verified in the number of lunations required for transients to die out and the thermal subsurface response to attain steady state conditions.

The results of the study reveal that latitude influence on adiabatic depth is minimal for any particular soil. However, as shown in figures 4-6 and 4-7 the adiabatic depth is different for each of the lunar materials investigated. Adiabatic depths for Apollo 11 soil, and LED-520 dust are 8 and 13 inches respectively at the equator.

The adiabatic soil temperatures which exist at these depths are presented in figure 4-8 for these lunar materials at various latitudes. The relatively close comparison between Apollo 11 soil and LED-520 dust adiabatic temperatures reflect the similarity of thermal properties. In particular, the thermal conductivities are so low that they result in nearly the same adiabatic temperatures and depths.

In addition to obtaining the adiabatic depth and temperature, the one dimensional model was useful in determining the time varying temperatures imposed as boundary conditions on the subsurface model shown in figure 4-9.

4.2.3 Three dimensional Lunar Subsurface Model

The lunar subsurface model consists of 12 cylindrical nodes beneath the PSE base, 72 annular nodes beneath the skirt and 12 exterior nodes used to impose the time varying boundary conditions. A diagram showing the location of the nodes in shown in figure 4-9.

4.3 Passive Seismic Thermal Model

Thermal simulation of the PSE assumed the 14 node model as shown in figure 4-9. A listing of the nodal breakdown and numbering scheme is as follows:

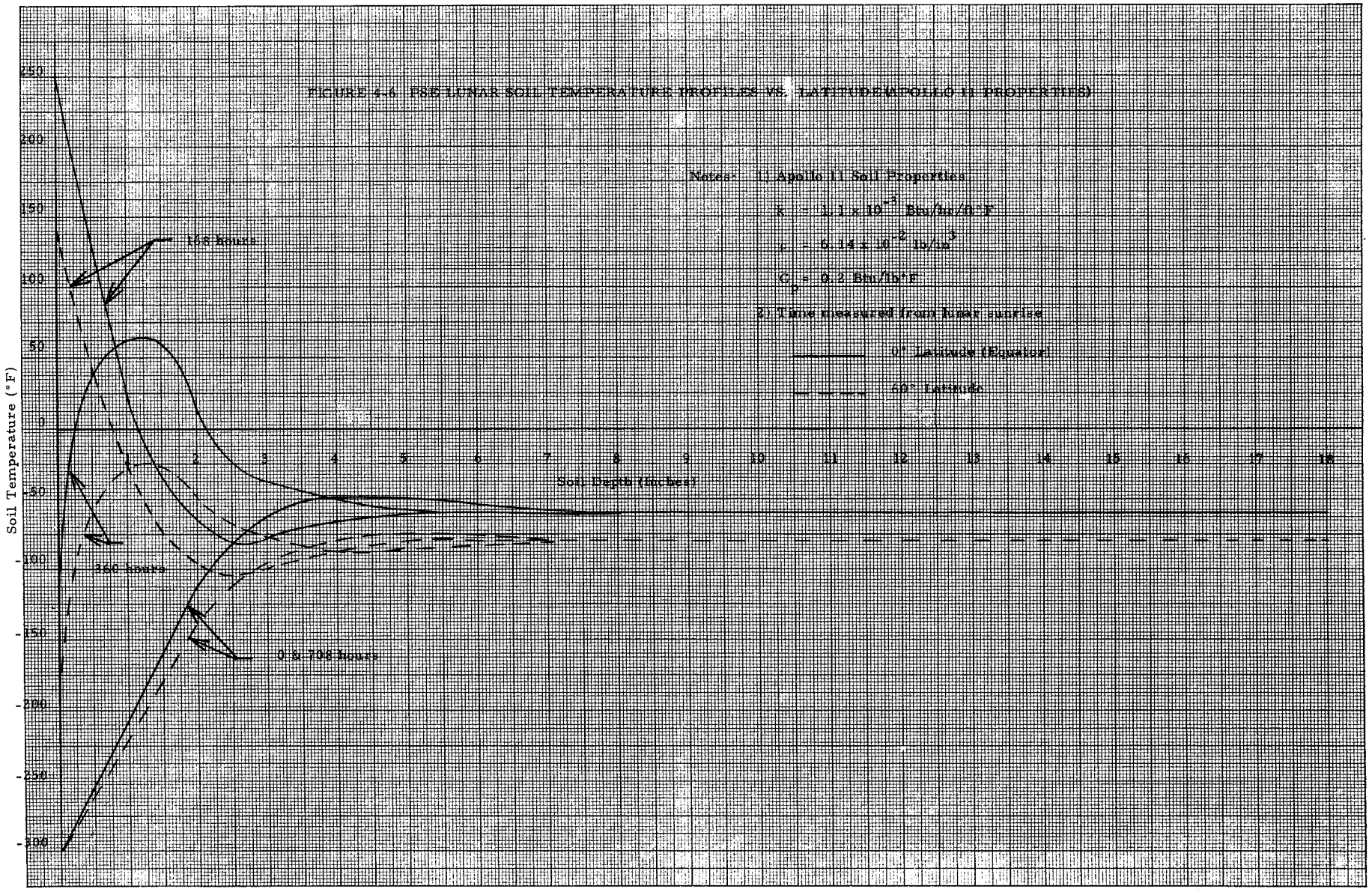

FIGURE 4-6 FSE LUNAR SOIL TEMPERATURE PROFILES VS. LATITUDE (APOLLO 11 PROPERTIES)

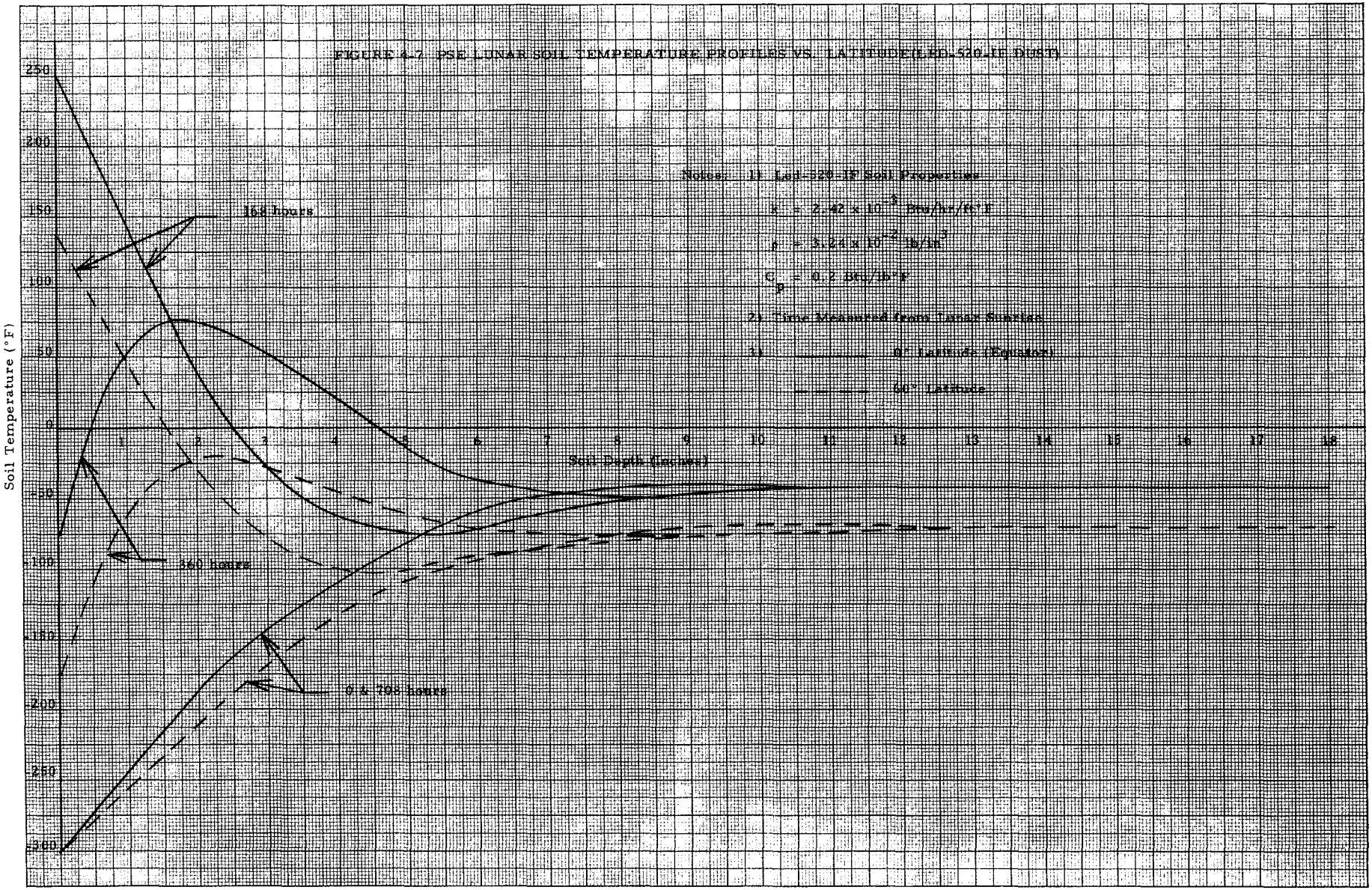
FIGURE 4-7 PSE LUNAR SOIL TEMPERATURE PROFILES VS. LATITUDE(LED-520-IF DUST)
Notes: 1) Led-520-IF Soil Properties
k = 2.42 x 10^-3 Btu/hr/ft°F
ρ = 3.24 x 10^-2 lb/in^3
Cp = 0.2 Btu/lb°F
2) Time Measured from Lunar Sunrise
1) 0° Latitude (Equator)
60° Latitude
164 hours
360 hours
0 & 708 hours
Soil Temperature (°F)
Soil Depth (Inches)
250
200
150
100
50
0
-50
-100
-150
-200
-250
-300
1
2
3
4
5
6
7
8
9
10
11
12
13
14
15
16
17
18

FIGURE 4-8 ADIABATIC SOIL TEMPERATURE VS. LATITUDE

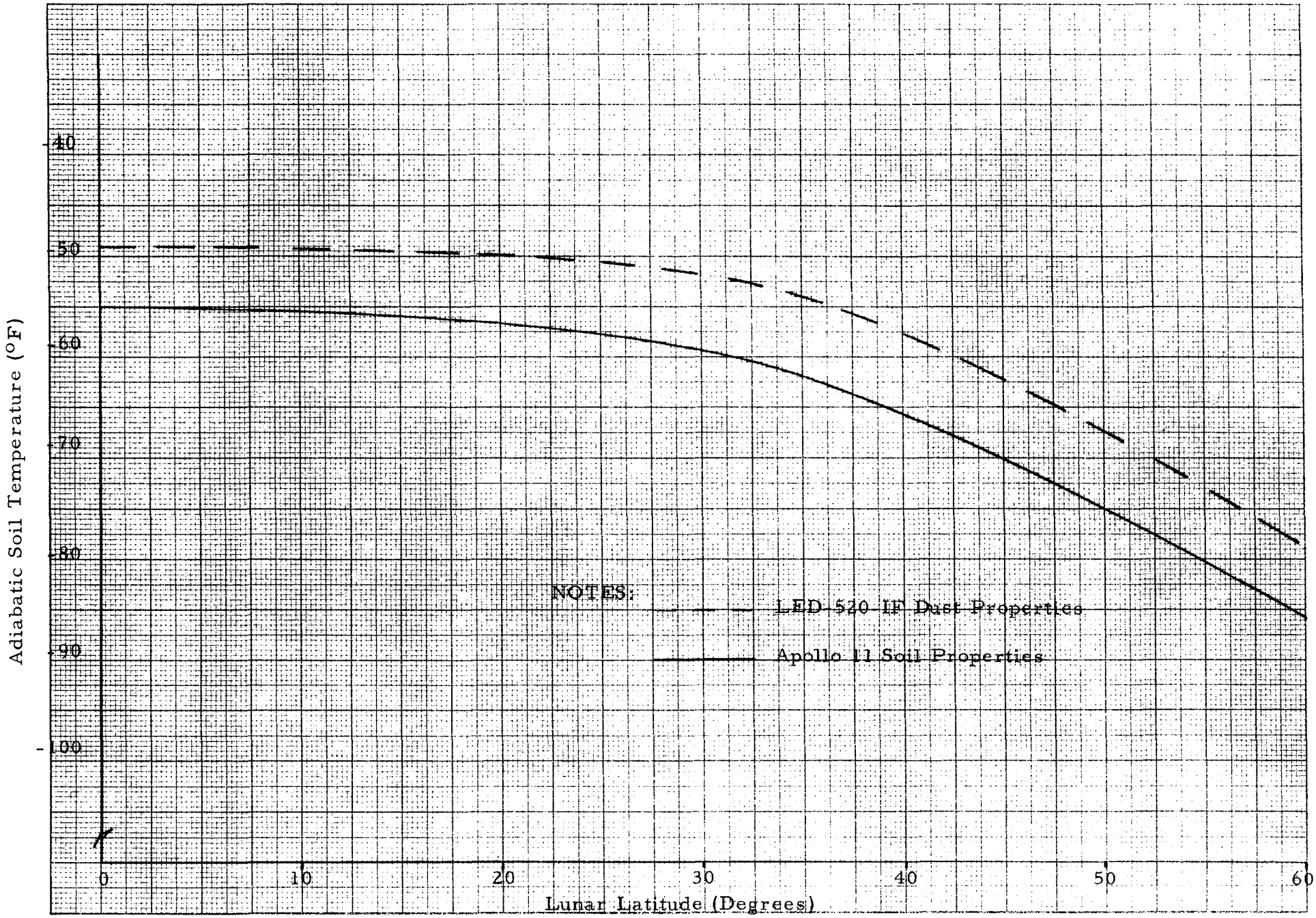

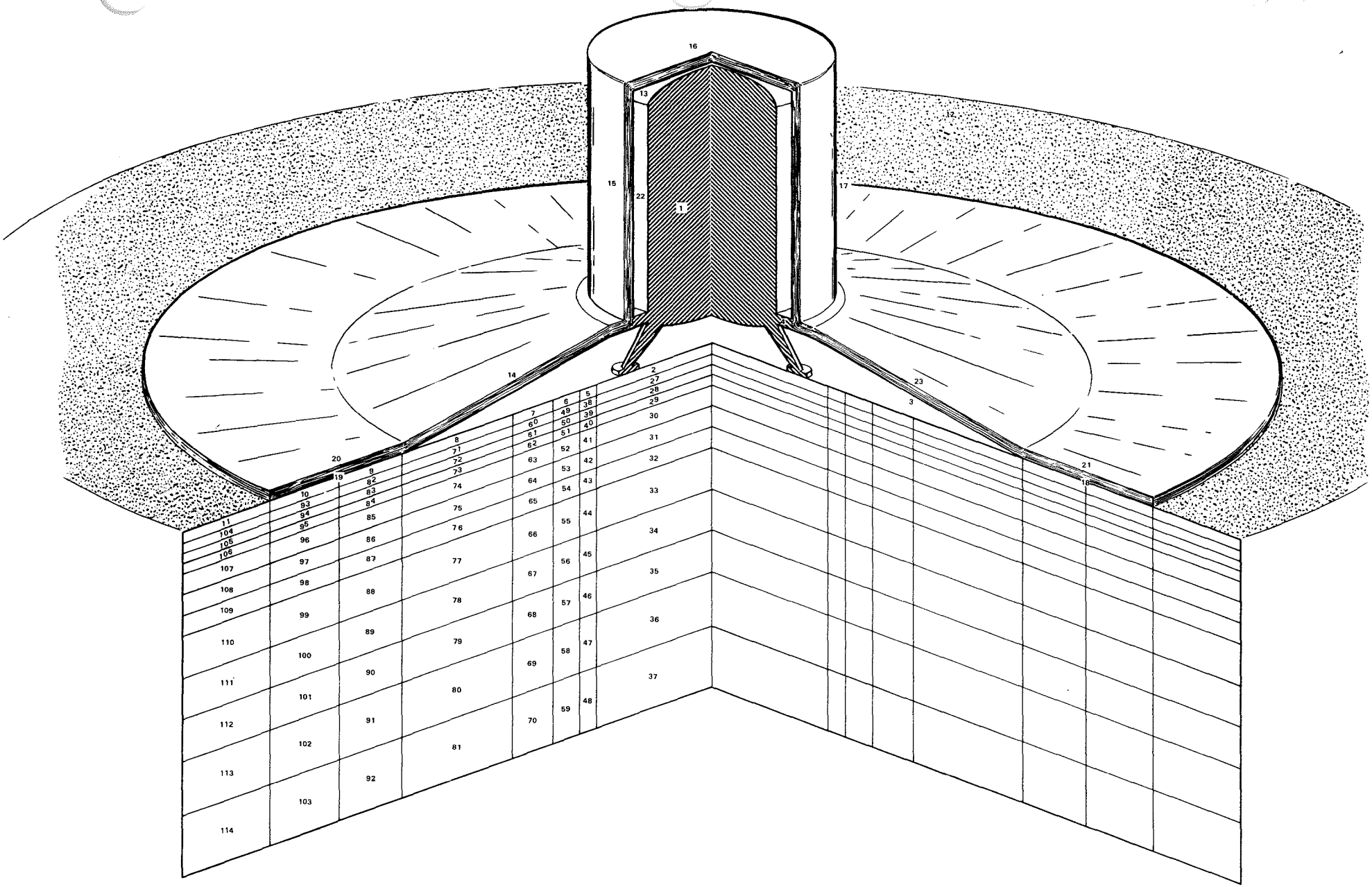

FIGURE 4-9 PSE SENSOR AND LUNAR SUBSURFACE THERMAL MODEL

Node No.	Description
(1)	PSE sensor
(3)	inside of conical skirt
(4)	radiation barrier
(13)	inside of multilayer insulation disc
(14)	east half of sloped skirt
(15)	east half of cylindrical shroud
(16)	outside of multilayer insulation disc
(17)	west half of cylindrical shroud
(18)	west half of horizontal underside of skirt
(19)	east half of horizontal underside of skirt
(20)	east half of horizontal topside of skirt
(21)	west half of horizontal topside of skirt
(22)	inside of cylindrical shroud
(23)	west half of sloped skirt.

4.3.1 Multilayer Insulation Conductivity

An important parameter of the PSE thermal control system is the effective thermal conductivity of the multilayer insulation shroud and skirt.

Heat transfer through multilayer insulation takes place by radiation and conduction. The thermal characteristics of the material are usually described by an "effective" thermal conductivity. The radiative heat transfer component between layers is usually accounted for by specifying the "effective" thermal conductivity at a specified temperature or in a temperature range. Emissivity, geometric effects between layers, perforations due to sewing, etc., are accounted for in the determination of "effective" conductivity by laboratory tests. Particular applications of the material requires a testing of the material under service conditions. Ideal laboratory conditions are rarely realized in application of the material and in general laboratory values can be used only to determine orders of magnitude.

The values of the shroud and skirt conductivity used in reference 1 were determined in the correlation of the Apollo 12 PSE sensor temperatures. The sensor temperature is primarily influenced by the lunar soil

temperature beneath the skirt. Shown in figure 4-10 are the temperatures of the lunar soil under the skirt as a function of skirt conductivity. A study of the curves reveal that there is only a small difference in soil temperatures for $k = 5.3 \times 10^{-4}$ and $k = 7.5 \times 10^{-4}$ Btu/hr/ft°F.

Early correlation attempts were made assuming different thermal conductivities for lunar day and night. Conductivity was essentially made as a function of temperature in that a lower value was used from lunar sunset to lunar sunrise than was used during lunar day. However, by assuming a particular value and identical changes in values for both shroud and skirt portions it was not possible to obtain the correlation presented in reference 1. The best correlation occured when the skirt and shroud conductivities were constant for both lunar day and night. The numerical values indicated the skirt to have a lower conductivity than the shroud. A constant value of $k = 7.5 \times 10^{-4}$ Btu/hr/ft°F was used for the shroud and $k = 5.3 \times 10^{-4}$ Btu/hr/ft°F was used for the skirt portion. The thermal model does allow for the thermal conductivity to vary continuously with temperature if the relationship is known. The complexity and computer time increases with this modification but an attempt will be made and the results reported at a later date.

4.4 Parametric Transient Thermal Analyses and Results

A parametric thermal study was performed in reference 1 to correlate ALSEP-1 PSE temperature data.

The parameters varied in the study were the following:

(1) solar absorptance of shroud and skirt (external surfaces)
(2) infrared emittance of shroud and skirt (external surfaces)
(3) aluminized mylar vs. aluminized teflon
(4) skirt conductivity (day and night)
(5) shroud conductivity (day and night)
(6) sensor specific heat
(7) lunar soil specific heat
(8) soil density
(9) soil conductivity
(10) lunar soil adiabatic depth

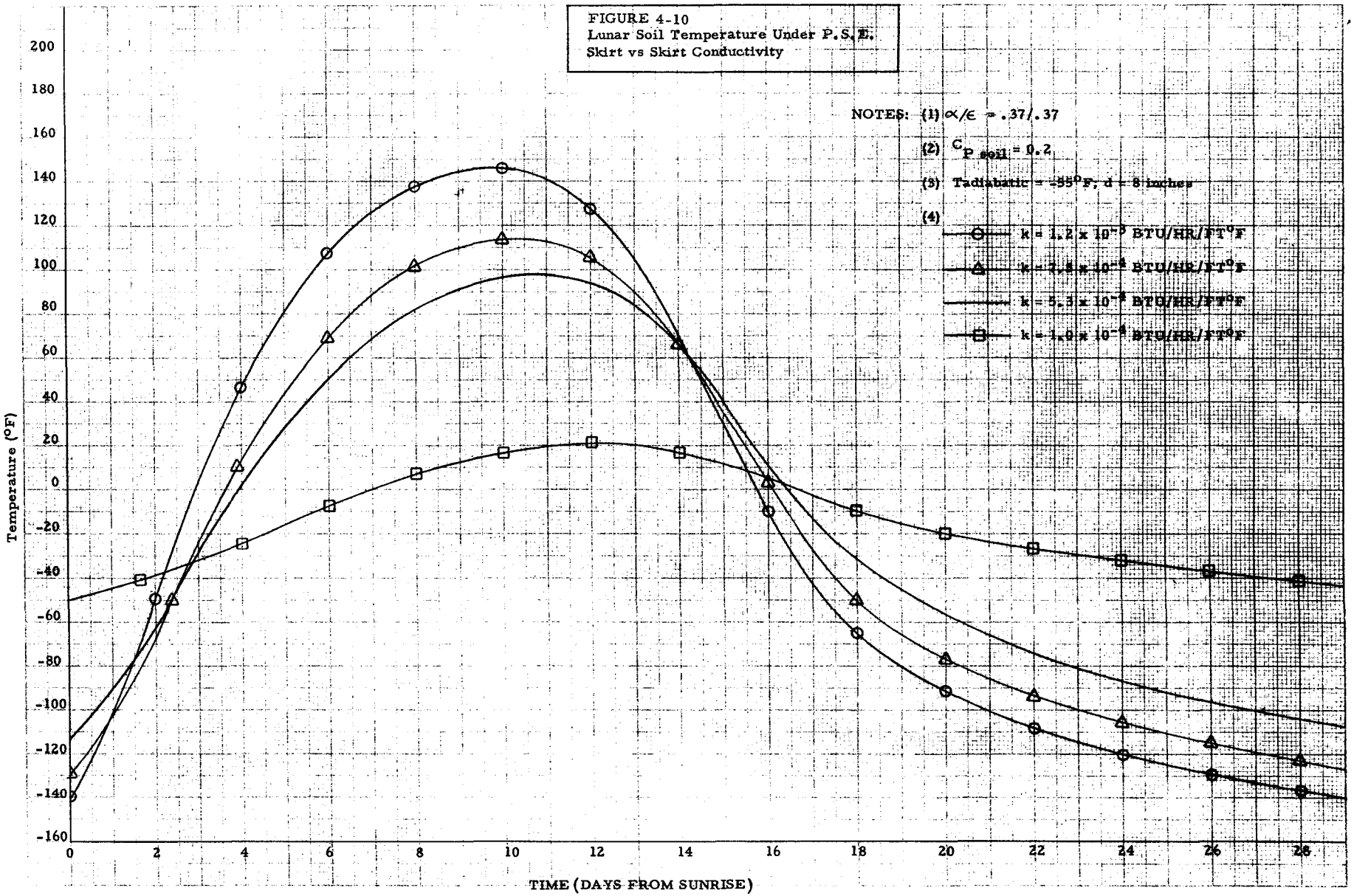
FIGURE 4-10
Lunar Soil Temperature Under P.S.E.
Skirt vs Skirt Conductivity
NOTES: (1) ∝/ϵ = .37/.37
(2) $C_{P\ soil}$ = 0.2
(3) Tadiabatic = -55°F, d = 8 inches
(4)
k = 1.2 x 10⁻³ BTU/HR/FT°F
k = 7.8 x 10⁻⁴ BTU/HR/FT°F
k = 5.3 x 10⁻⁴ BTU/HR/FT°F
k = 1.0 x 10⁻⁴ BTU/HR/FT°F
Temperature (°F)
200
180
160
140
120
100
80
60
40
20
0
-20
-40
-60
-80
-100
-120
-140
-160
0
2
4
6
8
10
12
14
16
18
20
22
24
26
28
TIME (DAYS FROM SUNRISE)

(11) lunar soil adiabatic temperature

(12) internal power dissipation (day and night)

(13) cable and stool thermal resistance

(14) multilayer insulation blanket

Several items in the simulation were difficult to take into consideration and hence some basic assumptions were made.

(1) The tunneling of solar and reflected energy to the sensor base is difficult to determine analytically, and hence assumed not to occur.

(2) The weight of the Flight 1 sensor is 19.26 pounds. Since the sensor is constructed primarily of beryllium a specific heat of 0.28 Btu/lb°F is assumed. Therefore, the value of the sensor capacitance is 5.5 Btu/°F.

(3) Nominal α_s/ϵ_{ir} measurements of aluminized mylar yield values of 0.2/0.37. However, the insulation skirt is visibly degraded by ruffles, creases and wrinkles as well as dust. To account for this non-ideal surface, the values of α_s/ϵ_{ir} are taken to be 0.37/0.37.

(4) The power dissipation within the sensor is assumed to be 1.0 watts for sensor temperatures above 126°F. This includes 0.75 watts of electronics dissipation and 0.25 watts of heater power while in the automatic mode. For sensor temperatures below the set point of 126°F an internal power dissipation of 3.25 watts is assumed.

With the above underlying set of assumptions and assumed parameter values, several transient computer runs were made. The matching of the sensor temperature decay after lunar sunset was first attempted. Using a skirt conductivity of 5.3×10^{-4} Btu/hr/ft°F and a shroud conductivity of 7.5×10^{-4} Btu/hr/ft°F for both day and night, correlation was achieved within 3°F.

At the beginning of the study it was assumed that the adiabatic temperature and depth beneath the skirt remained at -55 °F and 8 inches, respectively, and not influenced by the presence of the blanket. However, if a second iteration attempt is made to determine a new adiabatic temperature and depth under the skirt assuming new surface boundary conditions, a temperature of -32 °F and a depth of 8 inches is obtained.

To correlate lunar day results is a much more difficult task than lunar night. A number of other variables must be considered other than insulation conductivity. If a nominal deployment of the PSE and nominal surface properties are assumed it is not possible to get a good correlation with Flight 1 data. Uncertainties such as dust degradation of optical properties, skirt location and condition, in addition to effective skirt and shroud conductivity, make the correlation a formidable task. As a result, combinations of parameters must be evaluated separately.

Analysis of the Surveyor III equipment retrieved during the Apollo 12 mission showed the sandblasting effects of the LM during lunar landing (reference 20). This is an effect which would be difficult to assess analytically.

To date the correlation within 3 °F of Flight 1 data has been obtained by assuming that the east side and top of the cylindrical shroud having a nominal $\alpha_s/\epsilon_{ir} = 0.73/0.73$. The west side remains in the undegraded state. The present correlation also requires the following:

(1) $k_{skirt} = 5.3 \times 10^{-4}$ Btu/hr/ft °F (day and night)

(2) $k_{shroud} = 7.5 \times 10^{-4}$ Btu/hr/ft °F (day and night)

(3) $k_{soil} = 1.1 \times 10^{-3}$ Btu/hr/ft °F

(4) $\rho_{soil} = 6.14 \times 10^{-2}$ lb/in^3

(5) $C_{p\ soil} = 0.2$ Btu/lb °F

(6) $C_{p\ sensor} = 0.28$ Btu/lb °F

(7) $\alpha/\epsilon_{skirt} = 0.37/0.37$

(8) $$Q = \begin{cases} 1.0 \text{ watts for } T_{sensor} > 126°F \\ \\ 3.25 \text{ watts for } T_{sensor} < 126°F \end{cases}$$

The first, second and third days of lunar operation of Flight 1 are shown in Figure 4-11. Some typical parametric effects are shown in Figures 4-12 and 4-13. The best correlation to date is presented in Figure 4-14. Note the 24-hour phase shift of peak sensor temperature and the dip in temperature with respect to Flight 1 data.

A summary of the maximum and minimum sensor temperature extremes as a function of the parameters is presented in Table 4-1.

Using the subsurface and PSE nodal model shown, in Figure 4-14 correlation with the second day, Flight 1 PSE thermal data has been attained within 3°F. A 24-hour phase lag of the thermal model peak temperature with respect to flight data is present, suggesting minor modeling errors or improper selection of parametric values. However, the usefulness of the simulation to analytically evaluate possible design modifications is not diminished.

Thermal model results indicate that the Flight 1 PSE reaches a low temperature of 73°F just before lunar sunrise. This temperature was unknown since the off-scale lower limit is 107°F, but was previously estimated by curve fitting methods to be approximately 75°F. The model predicts a maximum temperature of 142.5°F whereas a Flight 1 maximum of 142.0°F is reported for the second day.

During the time intervals in which the sensor is below the set point (i.e., either heating up at lunar sunrise or cooling off at sunset), the temperature rise or decay rates compare very favorably. Thermal model and Flight 1 temperature rise rates are 0.85°F/hr.

FIGURE 4-11

BENDIX AEROSPACE SYSTEMS DIVISION - THERMOPHYSICS GROUP

APOLLO LUNAR SURFACE EXPERIMENTS PACKAGE (FLIGHT 1 - APOLLO 12) - 4 TH ALSEP LUNATION

SUNRISE DAY 046 (FEBRUARY 15, 1970) AT 1600 GMT

SUNRISE DAY 076 (MARCH 17, 1970) AT 0600 GMT

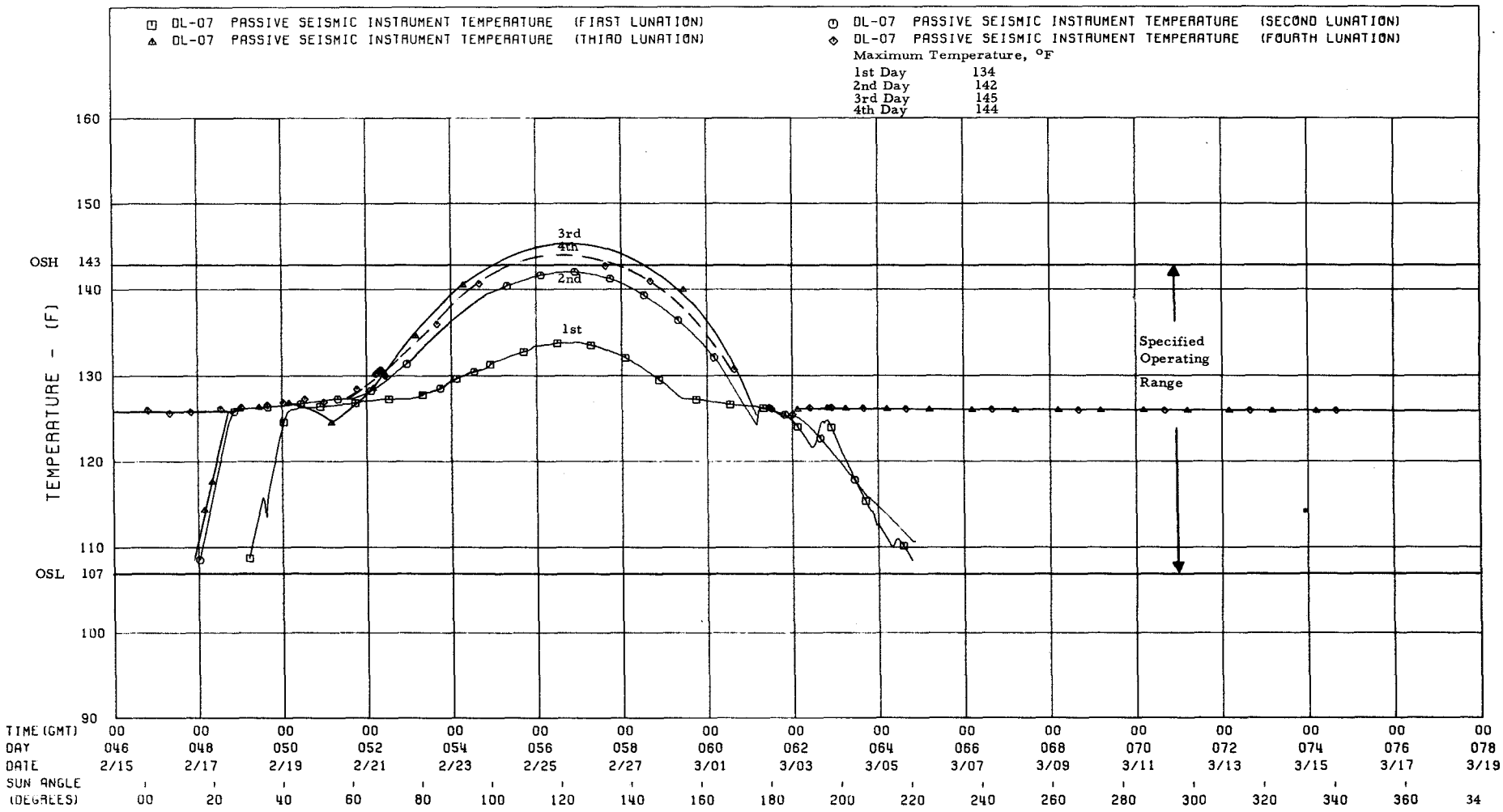

FIGURE 4-12 PARAMETRIC EFFECTS ON PSE TRANSIENT TEMPERATURES

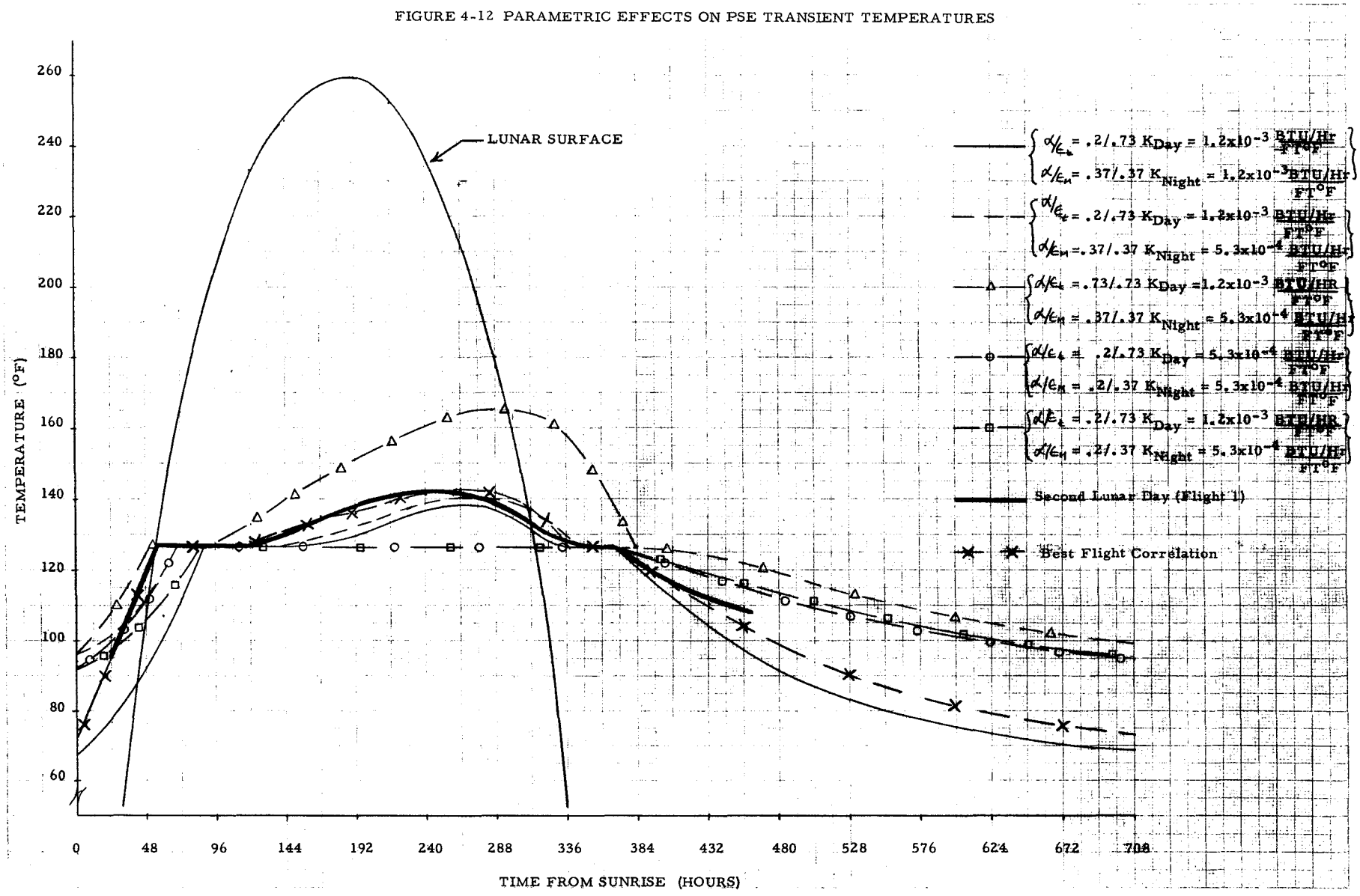

FIGURE 4-13 PARAMETRIC EFFECTS ON PSE TRANSIENT TEMPERATURES

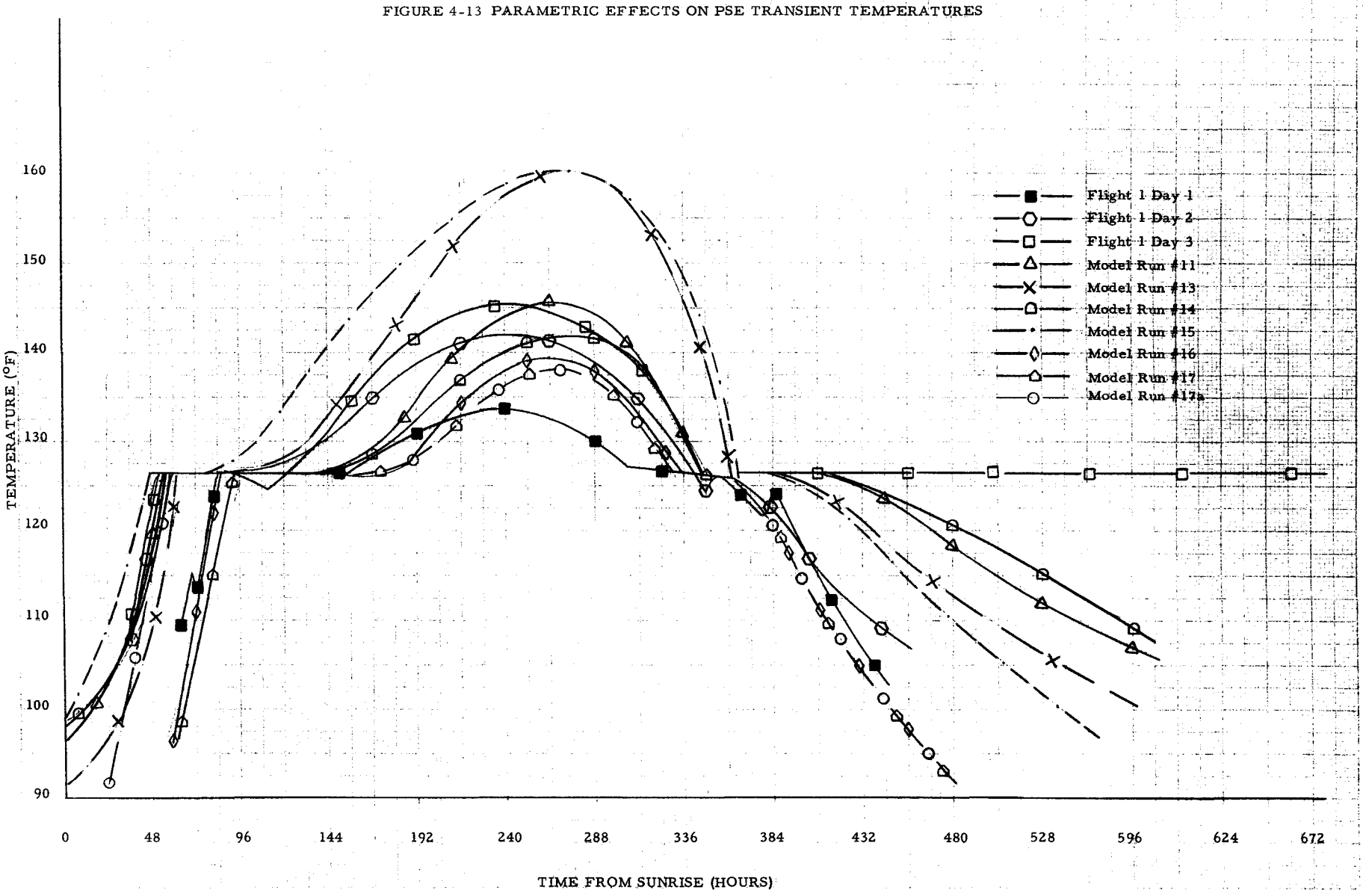

FIGURE 4-14

BENDIX AEROSPACE SYSTEMS DIVISION
PASSIVE SEISMIC EXPERIMENT THERMAL MODEL
A/E=.20,.73/.73;.37/.37; K-SKIRT=5.3E-04; K-SHROUD=7.5E-04 BTU/HR/FTF Q-DAY=1.W

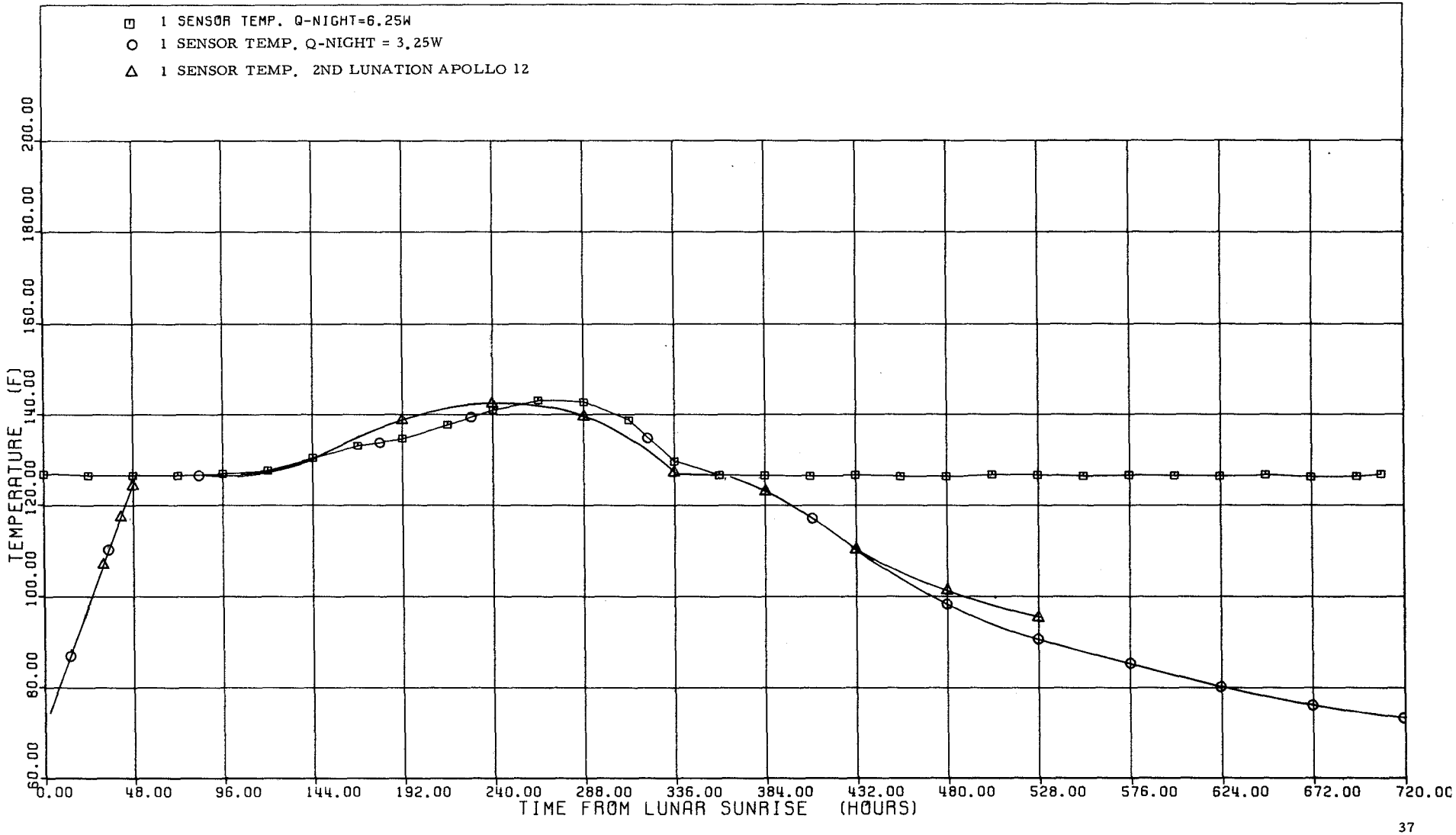

TABLE 4-1 SUMMARY OF PASSIVE SEISMIC EXPERIMENT THERMAL MODEL RESULTS

Run #	α/ϵ Shroud	α/ϵ Skirt	Skirt Conductivity (BTU/hr./ft.^{o}F) Day	Skirt Conductivity (BTU/hr./ft.^{o}F) Night	Shroud Conductivity (BTU/hr./ft.^{o}F) Day	Shroud Conductivity (BTU/hr./ft.^{o}F) Night	C_p (BTU/^{o}F) Sensor	C_p (BTU/^{o}F) Soil	Soil Density (lbm/in^3)	Soil Conductivity (BTU/hr./ft.^{o}F)	Source of Lunar Surface Properties	Sensor Power Dissipation (Watts) Ti < 126^{o}F	Sensor Power Dissipation (Watts) Ti > 126^{o}F	Sensor Temp. (^{o}F) Max.	Sensor Temp. (^{o}F) Min.
1	.2/.73	.2/.37	5.3×10^{-4}	5.3×10^{-4}	5.3×10^{-4}	5.3×10^{-4}	0.38	0.2	3.24×10^{-2}	2.42×10^{-3}	LED-520	3.25	1.0	126.5	93
2	.2/.73	.37/.37	1.2×10^{-3}	5.3×10^{-4}	1.2×10^{-3}	5.3×10^{-4}	"	"	"	"	"	"	"	141	96
3	.2/.73	.37/.37	"	1.2×10^{-3}	1.2×10^{-3}	1.2×10^{-3}	"	"	"	"	"	"	"	138	68
4	.2/.73	.2/.73	"	5.3×10^{-4}	1.2×10^{-3}	5.3×10^{-4}	"	"	"	"	"	"	"	126.5	93
5	.2/.73	.37/.73	"	"	1.2×10^{-3}	5.3×10^{-4}	"	"	"	"	"	"	"	126.5	90
6	.73/.73	.37/.37	"	"	1.2×10^{-3}	5.3×10^{-4}	"	"	"	"	"	"	"	166	99
* 7	.2/.73	.37/.37	"	"	1.2×10^{-3}	5.3×10^{-4}	"	"	"	"	"	"	"	139.6	104
8	.2/.73	.2/.73	1.0×10^{-4}	1.0×10^{-4}	1.0×10^{-4}	1.0×10^{-4}	"	"	"	"	"	"	"	126.5	126.5
9	.73/.73	.73/.73	1.0×10^{-4}	1.0×10^{-4}	1.0×10^{-4}	1.0×10^{-4}	"	"	6.14×10^{-2}	1.1×10^{-3}	APOLLO 11	"	"	126.5	126.5
10	.2/.73	.37/.37	1.2×10^{-3}	5.3×10^{-4}	1.2×10^{-3}	5.3×10^{-4}	"	"	"	"	"	"	"	142.5	99.5
11	.2/.73	.37/.37	"	"	1.2×10^{-3}	5.3×10^{-4}	0.28	"	"	"	"	"	"	145.7	98
12	.2/.73	.37/.37	"	"	1.2×10^{-3}	5.3×10^{-4}	"	"	"	"	"	"	"	126.5	89
13	.2/.73	.37/.37	"	"	1.2×10^{-3}	5.3×10^{-4}	0.38	0.05	"	"	"	"	"	160	91.6
** 14	.2/.73	"	"	"	1.2×10^{-3}	5.3×10^{-4}	"	0.2	"	"	"	"	"	142	80
15	E .73/.73 T .73/.73 W .2/.73	"	"	"	1.2×10^{-3}	5.3×10^{-4}	"	"	"	"	"	"	"	160.5	100
16	E .37/.73 T .2/.73 W .2/.73	.37/.37	1.2×10^{-3}	1.2×10^{-3}	1.2×10^{-3}	1.2×10^{-3}	0.38	0.2	6.14×10^{-2}	1.1×10^{-3}	APOLLO 11	3.25	1.0	139.5	69
17	.2/.73	"	"	"	1.2×10^{-2}	1.2×10^{-3}	"	"	"	"	"	"	"	138	69
18	E .73/.73 T .73/.73 W .2/.73	"	7.5×10^{-4}	7.5×10^{-4}	"	"	"	"	"	"	"	"	"	148	71
19	E .37/.73 T .37/.73 W .2/.73	"	"	"	"	"	"	"	"	"	"	"	0.75	128	61

* with multilayer blanket
** 1/2 leg and cable resistance

TABLE 4-1 SUMMARY OF PASSIVE SEISMIC EXPERIMENT THERMAL MODEL RESULTS (CONT)

Run #	α/ϵ Shroud	α/ϵ Skirt	Skirt Conductivity (BTU/hr./ft.°F) Day	Skirt Conductivity (BTU/hr./ft.°F) Night	Shroud Conductivity (BTU/hr./ft.°F) Day	Shroud Conductivity (BTU/hr./ft.°F) Night	C_p (BTU/°F) Sensor	C_p (BTU/°F) Soil	Soil Density (lbm/in^3)	Soil Conductivity (BTU/hr./ft.°F)	Source of Lunar Surface Properties	Sensor Power Dissipation (Watts) $T_i < 126°F$	Sensor Power Dissipation (Watts) $T_i > 126°F$	Sensor Temp. (°F) Max.	Sensor Temp. (°F) Min.
20	E.73/.73 T.37/.73 W.2/.73	.37/.37	5.3×10^{-4}	5.3×10^{-4}	1.2×10^{-2}	1.2×10^{-3}	0.33	0.2	6.14×10^{-2}	1.1×10^{-3}	APOLLO 11	3.25	1.0	126.5	62
21	E.73/.73 T.37/.73 W.15/.73	"	"	"	"	"	"	"	"	"	"	"	"	126.5	62
22	E.73/.73 T.37/.73 W.2/.73	"	"	"	1.2×10^{-3}	5.3×10^{-4}	"	"	"	"	"	"	"	129.5	85
23	E.73/.73 T.73/.73 W.2/.73	"	"	"	5.3×10^{-4}	"	"	"	"	"	"	"	"	140	85
24	E.73/.73 T.73/.73 W.2/.73	"	"	"	1.2×10^{-3}	7.5×10^{-4}	"	0.1	"	"	"	"	"	152	70
25	E.73/.73 T.9/.73 W.2/.73	"	"	"	"	"	"	"	"	"	"	"	"	154	70
26	E.73/.73 T.9/.73 W.2/.73	"	"	"	"	"	"	0.2	"	"	"	"	"	142.5	73
27	E.73/.73 T.73/.73 W.2/.73	"	"	"	7.5×10^{-4}	"	"	"	"	"	"	"	"	143.5	73
** 28	E.73/.73 T.73/.73 W..2/.73	"	"	"	"	"	"	"	"	"	"	"	"	151	75
29	E.2/.73 T.2/.73 W.2/.73	"	1.2×10^{-3}	5.3×10^{-4}	"	"	"	"	"	"	"	"	"	152	75

** No cable or legs

4.5 SOLAR ILLUMINATION TRANSIENTS AT LUNAR SUNRISE AND SUNSET

This study was conducted to determine the transient solar illumination effect. Specifically to determine the thermal response during sunrise, of the external surfaces of the PSE deployed on the lunar equator.

At lunar sunrise two effects must be considered:

4.5.1 Shadowing Effect

The top of the package is illuminated first; the demarcation line between light and shadow travels down the vertical side of the package at a variable rate until the base is also illuminated.

4.5.1.1 Level Terrain

The height (h) of the package determines the angle (θ) through which the moon must rotate in order to bring the entire package out of the shadow. The geometry of this problem is illustrated in Figure 4-15. For small angles ($\theta \leq 3°$) the sine of the angle is equal to the angle itself expressed in radians. Therefore we have

$$\theta \cong \sqrt{1 - \cos^2\theta}$$

where

$$\cos^2\theta = \frac{R_m^2}{(R_m + h)^2} = \frac{1}{(1 + \frac{h}{R_m})^2}$$

and

h = height of the package in feet

R_m = radius of the moon (5.7024×10^6 ft)

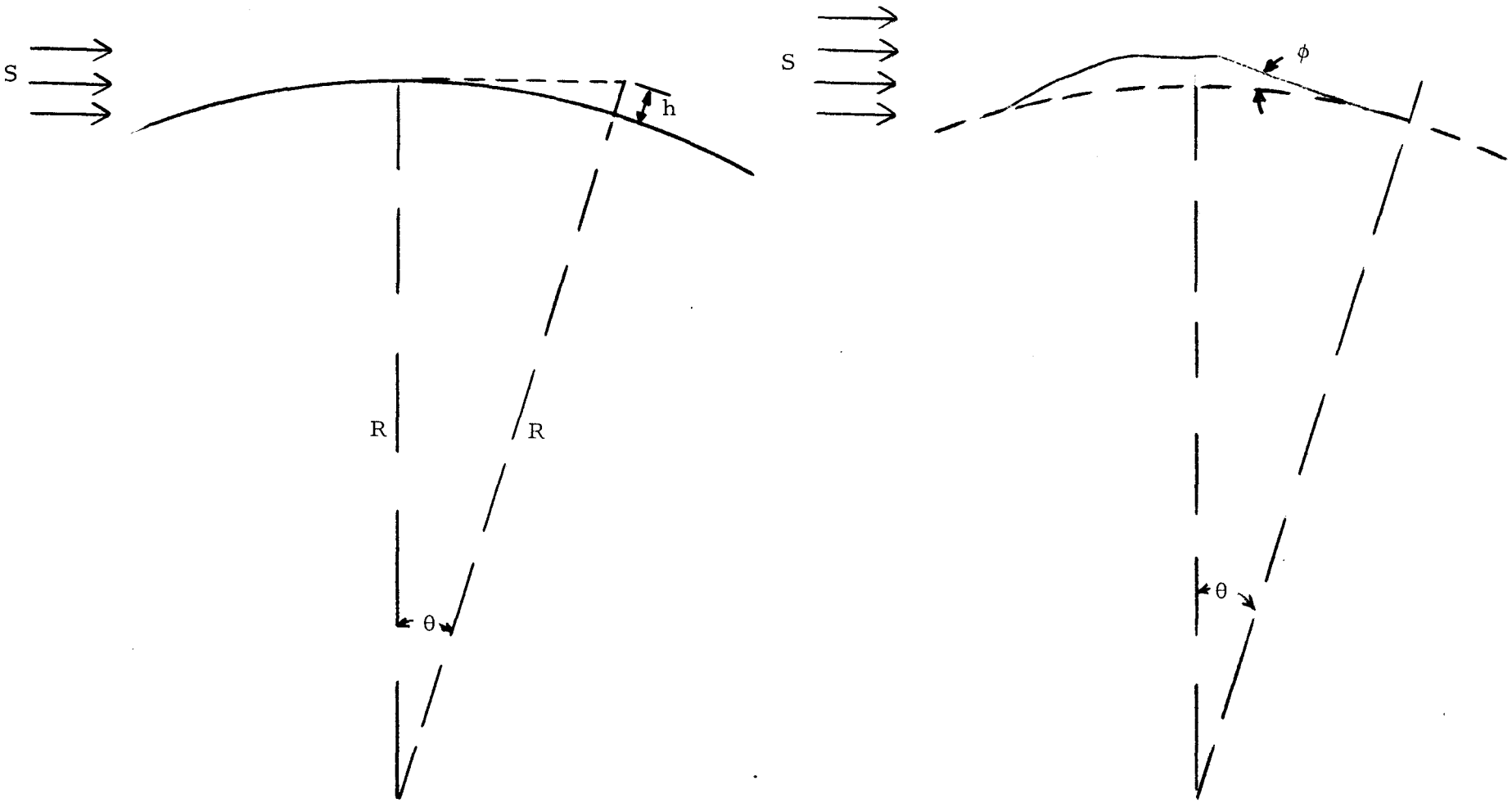

a. Level Terrain

b. Sloped Terrain

FIGURE 4-15 LUNAR SUNRISE GEOMETRY

from which

$$\theta = \sqrt{1 - \frac{1}{(1 + \frac{h}{R_m})^2}}$$

The time (t) required for the moon to rotate through the angle θ is given by:

$$t = \frac{\theta}{\dot{\theta}}$$

where

$\dot{\theta}$ = rotation rate of the moon (8.8655×10^{-3} radians/hr)

The results, which are presented in Figure 4-16, show that the demarcation line between shadow and light travels down a vertical surface at a rate that depends upon the height. At heights between 4 and 5 feet the rate exceeds 1 ft/min. At heights between 1 and 2 feet the rate has slowed to approximately 0.6 ft/min. The top of the PSE, for example, will be illuminated for approximately 4 minutes prior to the illumination of the skirt.

4.5.1.2 Sloped Terrain

A local slope, ascending from the object, causes the local sunrise to be delayed from that predicted for a particular location. The angle (ϕ) of the local slope is the additional angle through which the moon must rotate before the actual sunrise occurs. The geometry is illustrated in Figure 4-15b.

Note that when sunrise does occur, the demarcation line travels down the vertical surface in the time interval:

$$\Delta t = \frac{\phi}{\dot{\phi}}$$

FIGURE 4-16 TIME REQUIRED FOR SOLAR ILLUMINATION TO TRAVEL FROM TOP TO BASE OF VERTICAL OBJECT ON THE LUNAR SURFACE

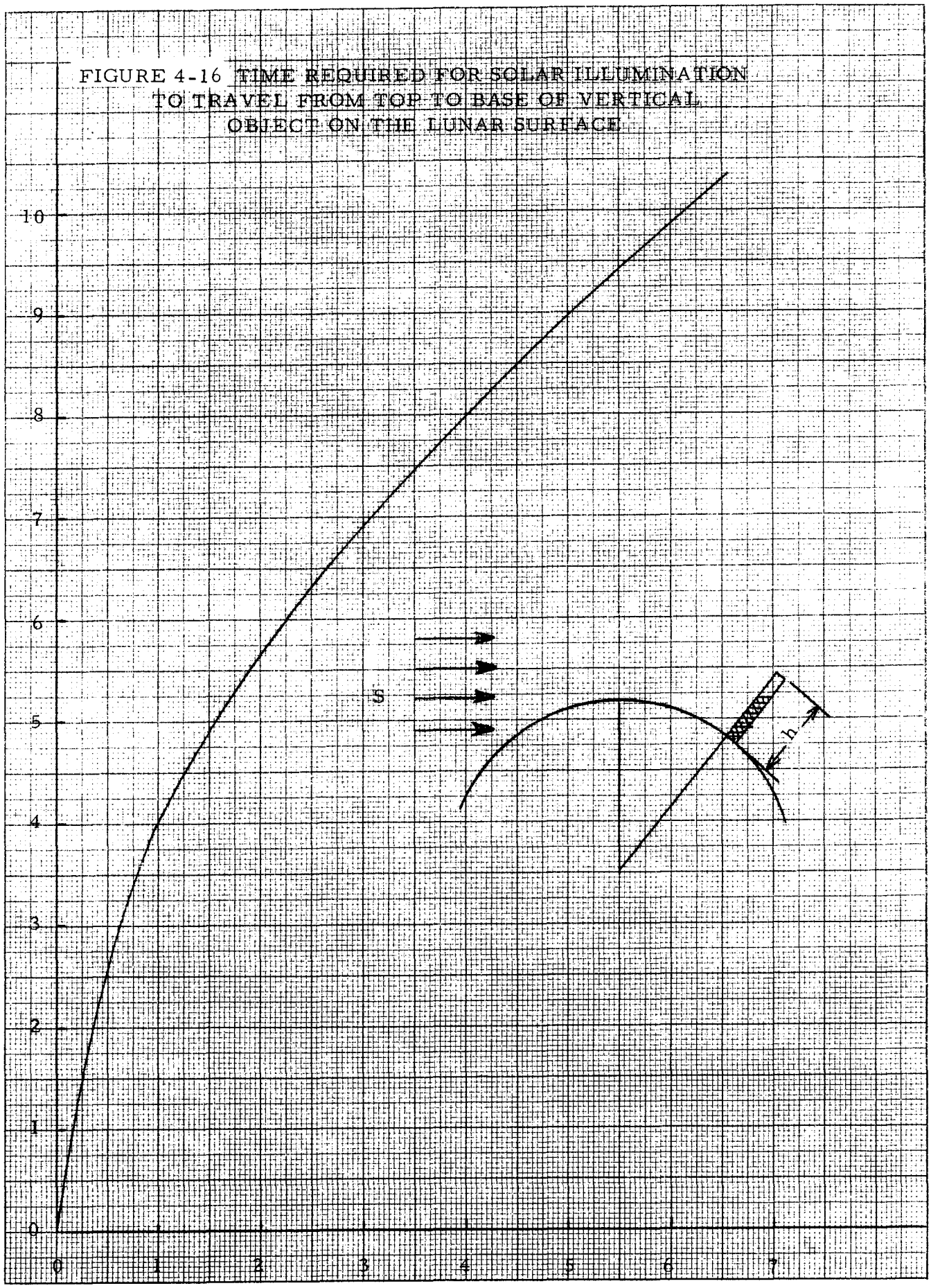

which yields the results shown in Table 4-2, below:

TABLE 4-2

SUNRISE DELAY DUE TO LOCAL SLOPE CONDITIONS

Local Slope Angle (ϕ)		Sunrise Delay
(°)	(Radians)	(Hrs)
1	0.017	1.97
2	0.035	3.94
3	0.052	5.91
4	0.070	7.87
5	0.087	9.84

4.5.2 Eclipse Effect

At the beginning of lunar sunrise (first contact) only a very small portion of the solar disk emerges above the horizon and it is only after some time that the entire disk clears the horizon (last contact). However, the solar constant is based upon the entire solar disk being visible and therefore an effective solar constant must be determined.

$$S_e = \frac{A's}{As} S$$

where

S = Solar Constant (130 w/ft^2)

A'_s = Projected area of the solar disk above the lunar horizon

A_s = Total projected area of the entire solar disk

We have that

$$A_s = \pi R_s^2 \quad \text{(where } R_s = \text{radius of the solar disk)}$$

and

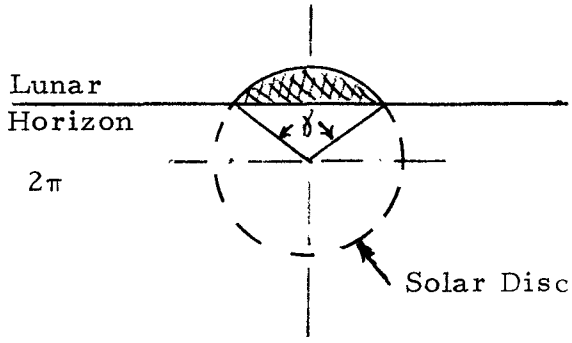

$$A'_s = \frac{\pi R_s^2 \gamma}{360} - \frac{R_s^2}{2} \sin\gamma \ , \quad 0 \leq \gamma \leq 2\pi$$

from which

$$S_e = (0.361 \text{ w/ft}^2)\ \gamma - (20.690 \text{ w/ft}^2) \sin\gamma \ (\gamma \text{ in degrees})$$

where

$$\frac{\gamma}{2} = \arcsin\left(\frac{t}{S_\gamma/2\theta}\right) = \arcsin\left(\frac{t}{29.5 \text{ min}}\right) \ , \quad 0 \leq t \leq 29.5 \text{ min.}$$

and

$$\frac{\gamma}{2} = \pi - \arcsin\left(\frac{59 \text{ min} - t}{29.5 \text{ min}}\right) \ , \quad 29.5 \text{ min} \leq t \leq 58 \text{ min.}$$

and

t = Time interval between the first and last contacts of the solar disk with the lunar horizon ($0 \leq t \leq 59$ min)

S_γ = Angular diameter of the solar disk (8.724×10^{-3} radians)

The results are listed in Table 4-3 and plotted in Figure 4-16. The data show that the effective solar constant builds up very slowly for the first 20 minutes, then achieves more than 90% of the full value during the next 20 minutes (20 to 40 min). By the end of 48 minutes, the effective solar constant has reached 99% of the full value.

TABLE 4-3

EFFECTIVE SOLAR CONSTANT DURING LUNAR SUNRISE

Time (min)	S_e (w/ft^2)	Time (min)	S_e (w/ft^2)	Time (min)	S_e (w/ft^2)
0	0.00	20	10.20	40	121.43
1	0.00	21	12.09	41	122.85
2	0.01	22	14.26	42	124.08
3	0.03	23	16.80	43	125.34
4	0.07	24	19.75	44	126.04
5	0.14	25	23.22	45	126.82
6	0.24	26	27.40	46	127.48
7	0.38	27	32.59	47	128.04
8	0.56	28	39.38	48	128.50
9	0.81	29	49.91	49	128.89
10	1.11	30	80.09	50	129.19
11	1.50	31	90.62	51	129.44
12	1.96	32	97.41	52	129.62
13	2.52	33	102.60	53	129.77
14	3.18	34	106.78	54	129.87
15	3.96	35	110.25	55	129.93
16	4.66	36	113.20	56	129.97
17	5.92	37	115.74	57	129.99
18	7.15	38	117.91	58	130.00
19	8.57	39	119.80	59	130.00

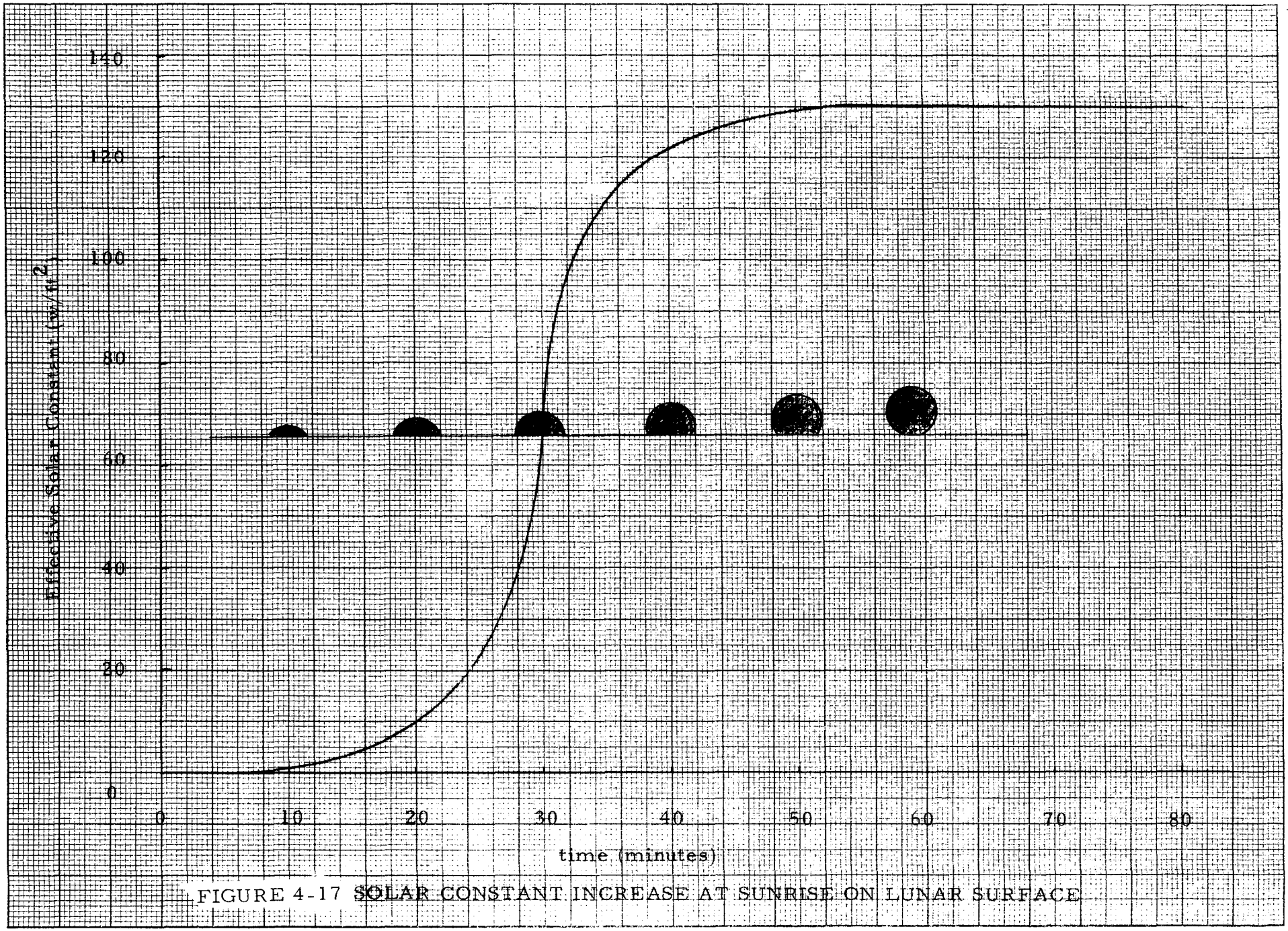

FIGURE 4-17 SOLAR CONSTANT INCREASE AT SUNRISE ON LUNAR SURFACE

4.5.3 Lunar Sunrise Transient Study

In order to study the thermal response of components during lunar sunrise, a simplified thermal math model was developed. The math model consists of 14 nodes representing four 12" x 12" plates, the lunar surface and space as shown in Figure 4-18. The plates are perpendicular to the lunar surface and perfectly insulated on their backsides and edges. The frontside of each plate is assumed dust degraded with an α/ϵ of 0.3/0.9 and is illuminated by the sun.

The first plate is 0.015" thick and is subdivided into 5 equal nodes (nodes 1, 2, 3, 4, 5) with their long dimension parallel to the lunar surface. Time zero is defined as the instant at which the demarcation line between light and shadow crosses the center of node 1. From this time on, the solar energy incident on node 1 is programmed as shown in Table 4-3. At t + 0.57 min the process is repeated for node 2. Similarly, the process is repeated for nodes 3, 4 and 5 at times t + 0.66 min, t + 0.79 min and t + 1.40 min respectively.

The second plate, consists of a single node (node 6). At time zero, the entire plate is illuminated with one solar constant (130 w/ft^2).

The temperature responses of these plates during lunar sunrise are shown in Figures 4-19 and 4-20 As can be seen, the second plate (node 6) reaches its equilibrium temperature in about 12 minutes whereas the first plate requires approximately 55 minutes to achieve this condition. Evident too, is the fact that the top-to-bottom temperature gradient in plate No. 1 reaches its maximum value (~ 48F) at approximately t + 30 minutes.

The analysis, as discussed above, is repeated for the third and fourth plates which are thicker by a factor of 20. The results for these thicker plates are presented in Figure 21. The plates mass has the effect of damping the thermal shock beyond the time period in which the solar constant is arriving to its full value.

It is concluded that the thermal shock which occurs on the vertical surfaces of the PSE thermal shroud during lunar sunrise is partially compensated for by the transient nature of the solar constant buildup. On the thicker sections, however, thermal inertia overrides the effect of the solar constant build-up.

This transient thermal effect occurs in reverse during sunset; however, the thermal shock is not as severe since the lunar surface at this point in the lunation is still warm, and gradually cooling.

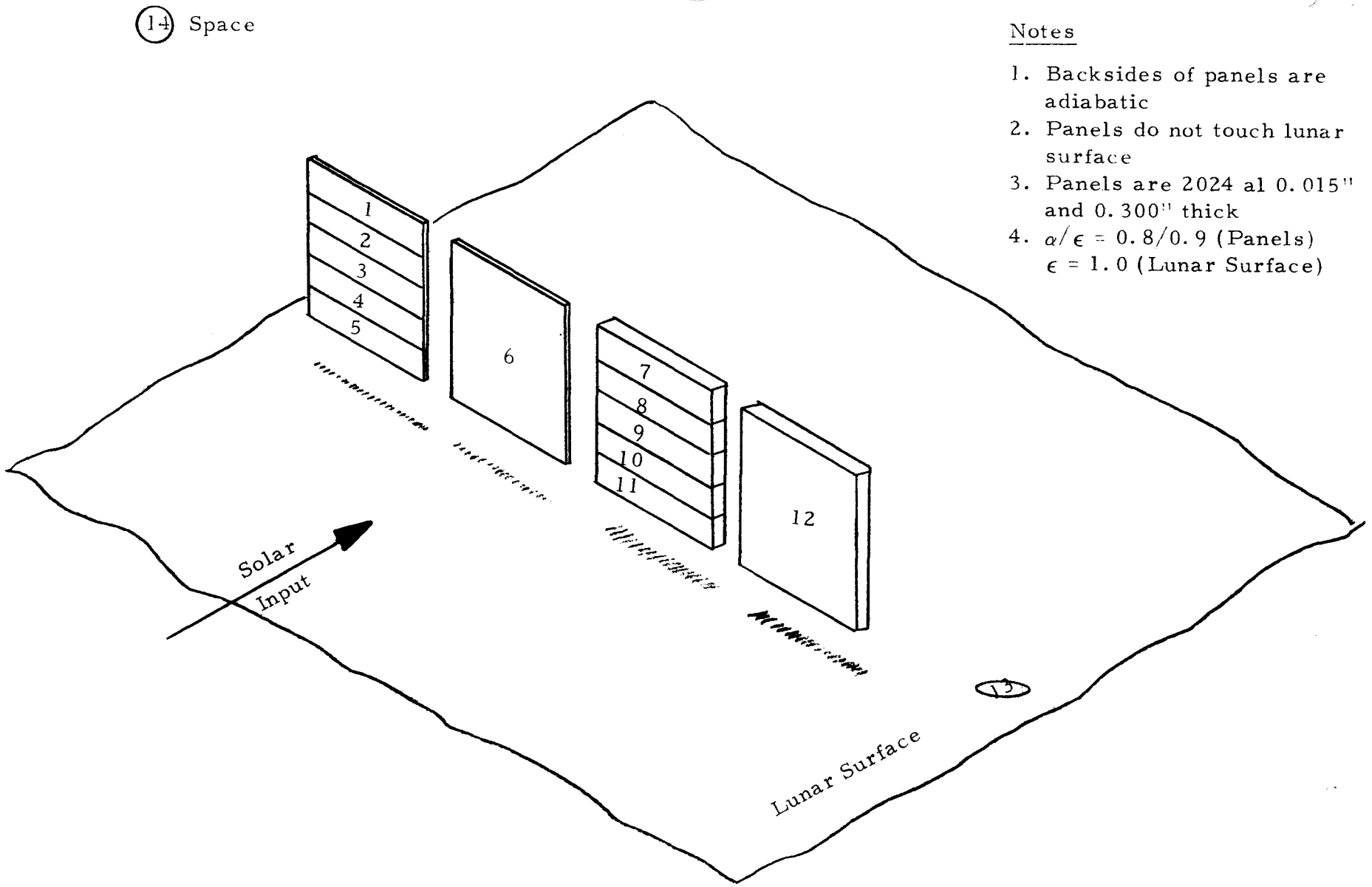

FIGURE 4-18 THERMAL MATH MODEL - LUNAR SUNRISE TRANSIENT STUDY

LUNAR SUNRISE TRANSIENT STUDY

ALSEP 01

Figure 4-19

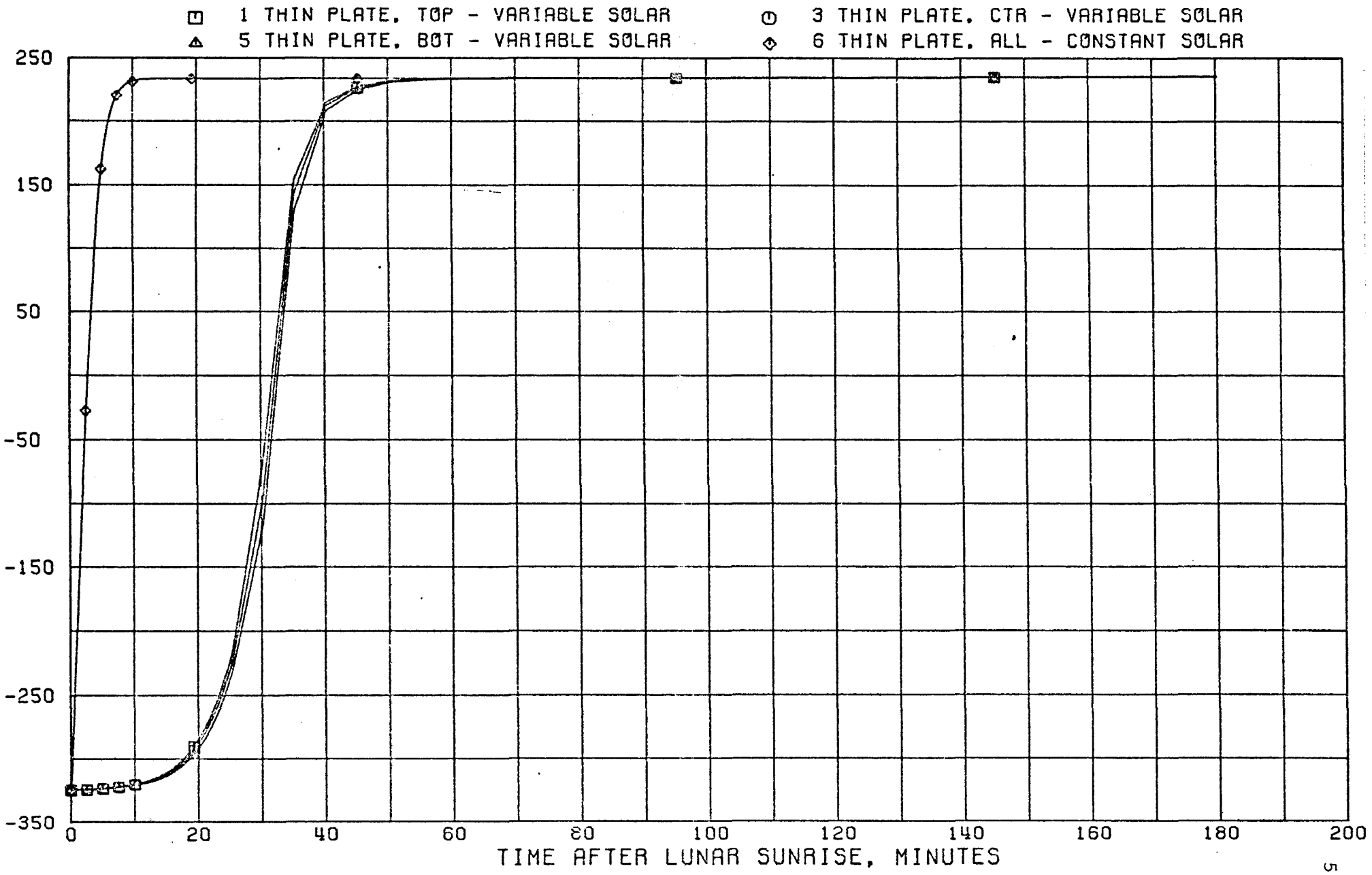

LUNAR SUNRISE TRANSIENT STUDY

ALSEP 01

Figure 4-20

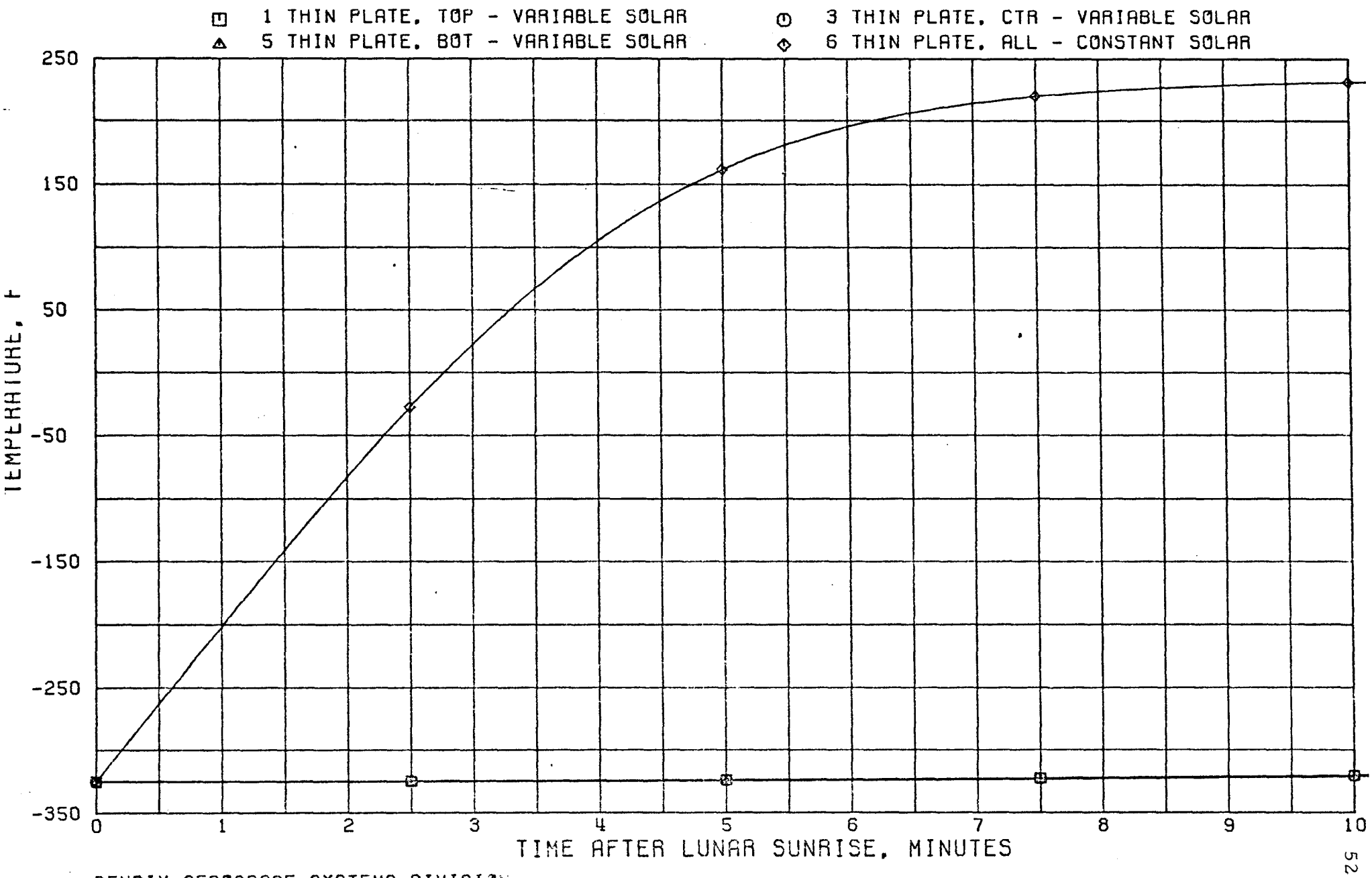

LUNAR SUNRISE TRANSIENT STUDY

ALSEP 01

Figure 4-21

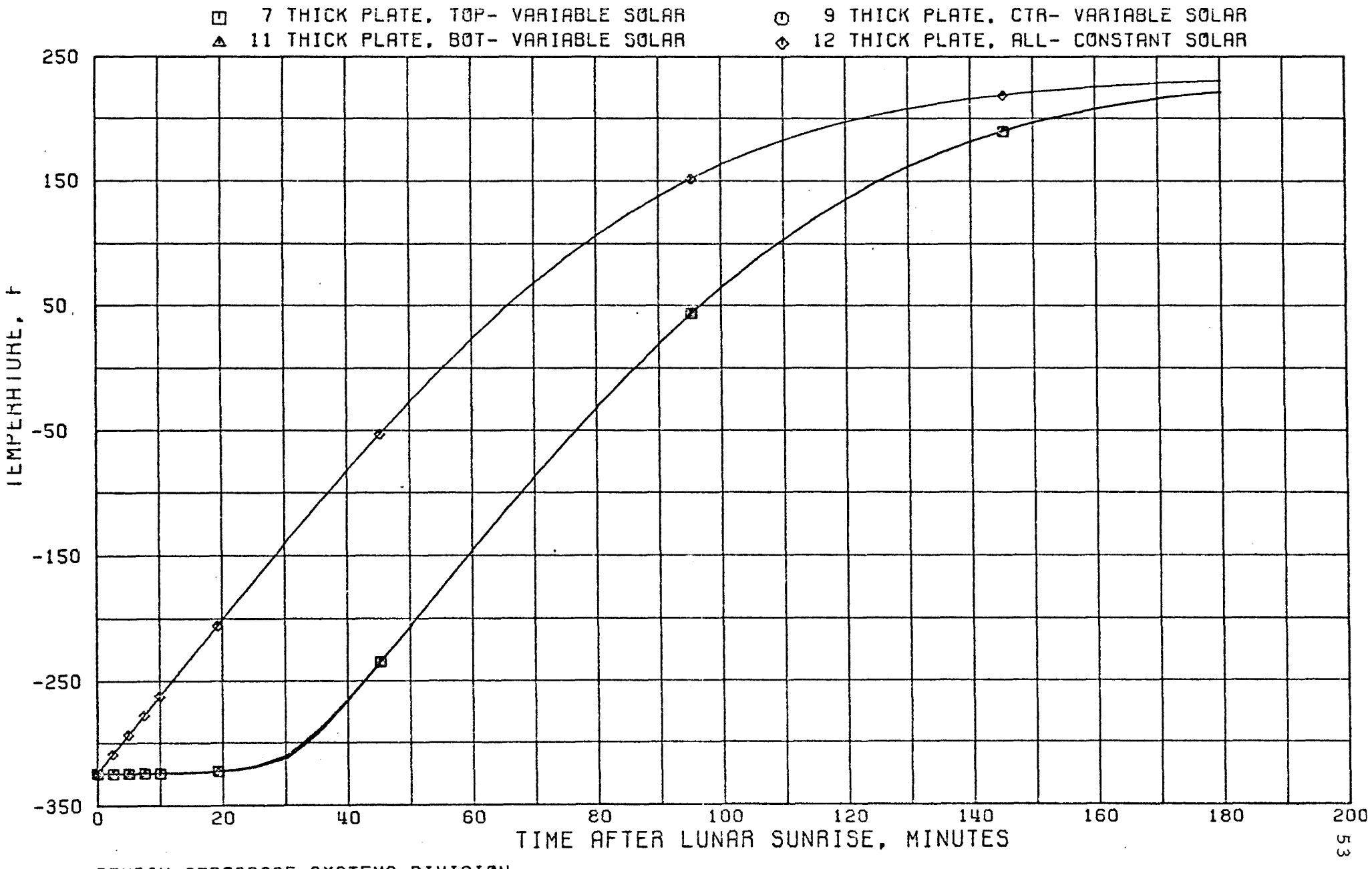

BENDIX AEROSPACE SYSTEMS DIVISION

5.0 THERMAL CONTROL OF HEATER TRANSISTORS

The additional heater power needed to maintain sensor temperature at 126°F during lunar night required a design modification of the heater electrical circuit. Transistors (2N2102) with more power dissipation resulted in a thermal control problem of the semiconductor devices themselves. Cooling by free convection cannot be considered due to the absence of a medium. Cooling by conduction and radiation from the case are the only possible means of removing the internally generated heat.

The maximum power dissipation within a transistor that is not temperature compensated is limited primarily by a regenerative condition known as "thermal runaway" which results in a melting of the silicon wafer. Additional factors which require a limit on the power dissipation and hence the temperature are the yield point of the solder and the efficiency of heat removal among other things.

5.0.1 Thermal Analysis

A thermal analysis (reference 31) was performed on the two 2N2102 transistors located on the "W" board of the PSE electronics assembly to determine their steady state collector-base junction temperatures. A maximum temperature of 200°C is specified for this semiconductor. However, a derated maximum temperature of 100°C is desirable for reliability considerations. The present application of the 2N2102 transistor requires it to be mounted on a thermally low conducting fiberglass board.

A six node thermal model of the transistor as shown in Figure 5-1 was used to determine the junction temperature, T_1. The model accounts for all paths of heat transfer by conduction and radiation from the transistor to the board and its surroundings which are assumed to be a 126°F heat sink.

The power dissipated in a physical transistor is not distributed uniformly across the wafer, but is concentrated in the collector-base junction area. However, in this model a uniform distribution throughout node 1 is assumed. A nominal power of 0.8 watts was used.

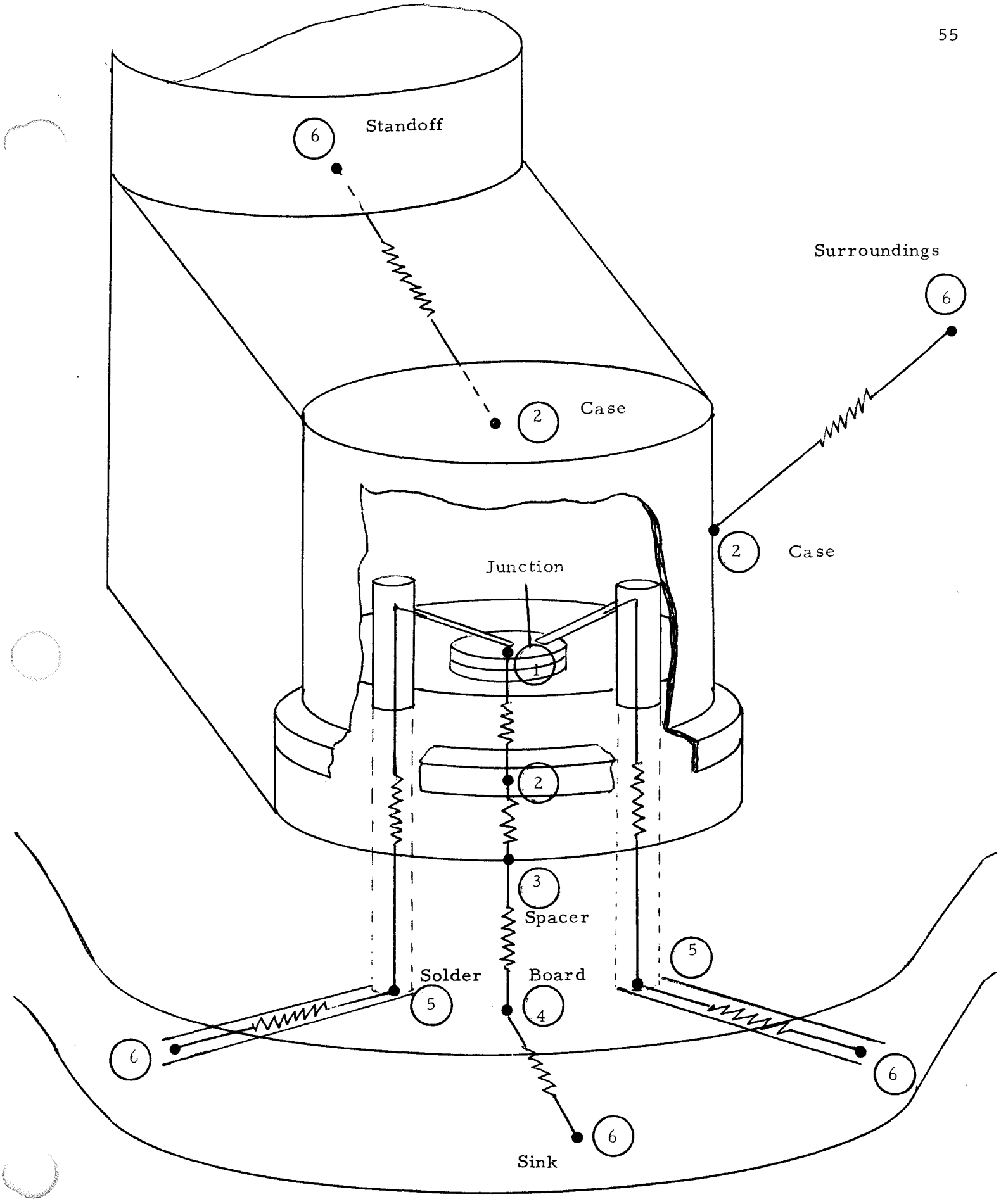

Figure 5-1 Thermal Model of Q24 and Q25 with Standoff

It was assumed that the three gold leads from the junction area were 0.1" in length and 0.019" diameter as specified in Figure 5-2. Three conduction paths leading from the solder connection on the copper etched board to the heat sink were assumed to be of 3" in length, 0.005" thick and 0.06" wide.

The transistor case is coated with a conformal coating having an infrared emittance of approximately 0.8. The infrared emittance of the surroundings is assumed to be 0.9. A geometric view factor from the case to the surroundings of 1.0 is assumed.

A junction to case thermal resistance of 35°C/watt (18.4 hr°F/Btu) was obtained from the data sheet on the 2N2102 transistor.

The heat flow through the board from the transistor to the surroundings was assumed to take two paths. One path leads to the 1/4" diameter aluminum standoff located approximately 3/4" from the transistor seating plane. A second path leads to a cylindrical heat sink 3" from the seating plane. Due to the physical location on the "W"-board as shown in Figure 5-3, edge effects were accounted for by doubling the calculated value of thermal resistance along the second path.

To reduce collector-base junction temperatures, potting the transistors with Stycast 2850 FT epoxy to the aluminum standoffs was investigated analytically using the thermal model. Since the PSE is to be maintained at 126°F it could be used as a heat sink if the transistor case is thermally coupled to it. The thermal resistance between the transistor case and the standoff was computed assuming a path between the two was filled with the epoxy resin. Dimensions of the resin slab were taken as the height of the transistor case (0.38") and diameter of the transistor case (0.32"). A mean length of 0.75" between the case and the standoff was assumed.

A summary of the parameter values used in the analysis are as follows:

(1) R_{J-C} = 35°C/watt (18.4 hr°F/Btu)

(2) K_{board} = 0.2 Btu/hr/Ft°F

JEDEC TO-5

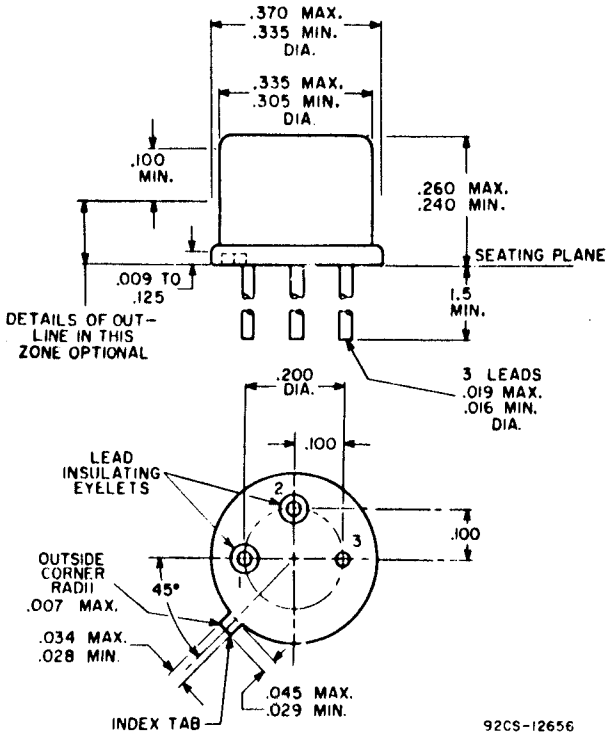

Figure 5-2 Dimensions of the 2N2102

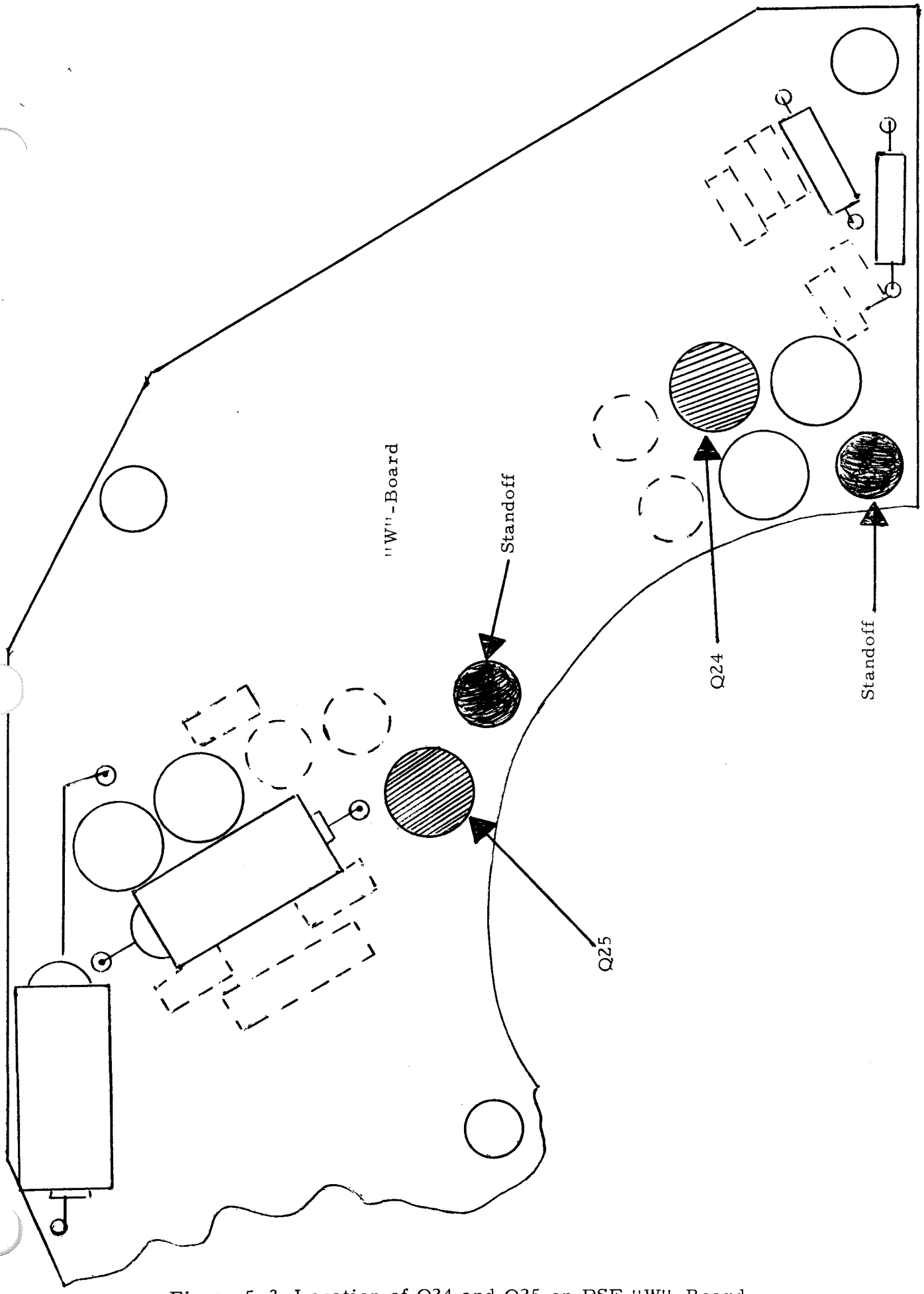

Figure 5-3 Location of Q24 and Q25 on PSE "W"-Board

(3) K_{AU} = 170 Btu/hr/Ft°F

(4) K_{CU} = 218 Btu/hr/Ft°F

(5) K_{nylon} = 1.2 Btu/hr/ft°F/in.

(6) $K_{beryllia}$ = 9.52 Btu/hr/Ft°F

(7) $K_{Stycast}$ = 0.592 Btu/hr/Ft°F

(8) ϵ_T = 0.8

(9) ϵ_S = 0.9

(10) t_{board} = 0.060"

(11) t_{nylon} = 0.020"

(12) $t_{beryllium}$ = 0.060"

(13) t_{cu} = 0.005"

(14) lead diameter = 0.019"

A summary of the steady state junction and case temperatures is presented in Table 5-1 for several transistor configurations. It is immediately evident that the nylon spacers raise the junction temperature significantly and should be replaced by the beryllium oxide spacers. The relatively low thermal conductivity of nylon effectively insulates the seating plane from the board.

Configuration	Junction Temp (°F)	Junction Temp (°C)	Case Temp (°F)	Case Temp (°C)
Nylon spacer	363.7	183°	336	168.5
Nylon spacer with Stycast potting	269	131.5	254	123
Beryllium spacer	277	136	241	116
Beryllium spacer with Stycast potting	244	117.5	222	105

TABLE 5-1

Transistor Temperatures for Nominal Dissipation of 0.8 Watts

The analysis showed that the concept described above would not maintain junction temperatures below the desired 100°C at a nominal power dissipation of 800 milliwatts. Maximum allowable transistor power dissipations were determined for these two configurations. In Figures 5-4 and 5-5 case and junction temperatures are shown as a function of dissipated power.

A modification was proposed in reference 32 to reduce the transistor temperatures. A study was made assuming that a copper strap was used to provide a highly conductive thermal path from the case to the sensor base. To maintain electrical isolation from the transistor case, a beryllium oxide spacer is epoxied to the transistor top separating the copper strap and transistor case.

In the analysis it was assumed that the copper strap was attached as shown in Figure 5-6. The transistor cap diameter of 0.25 inches was assumed to be the width of the copper strap. Location of the W-board in relation to the sensor base attachment point requires a length of copper of approximately two inches. To determine the strap thickness, several steady state computer runs were made using the nodal model shown in Figure 5-1. The results are presented in Figure 5-7. It is apparent that the heat sink thermal control technique effectively reduces case and junction temperatures. To maintain junction temperatures below 100°C limit a strap thickness of approximately 1/16" is required. A transistor power dissipation of 800 milliwatts was assumed in the analysis and a heat sink temperature of 52°C (126°F).

Using the analytical thermal model it was shown feasible to maintain the desired temperatures. The concept remained to be verified in the laboratory by tests.

5.0.2 Thermal-Vacuum Testing of Heater Circuit Transistors

A thermal-vacuum test of the Q24 and Q25 2N2102 transistors was performed to verify the analytical predictions of the thermal control techniques proposed (reference 33). The test of the transistors was performed in an environment simulating very closely the surroundings of the transistors when mounted in the PSE electronics stack.

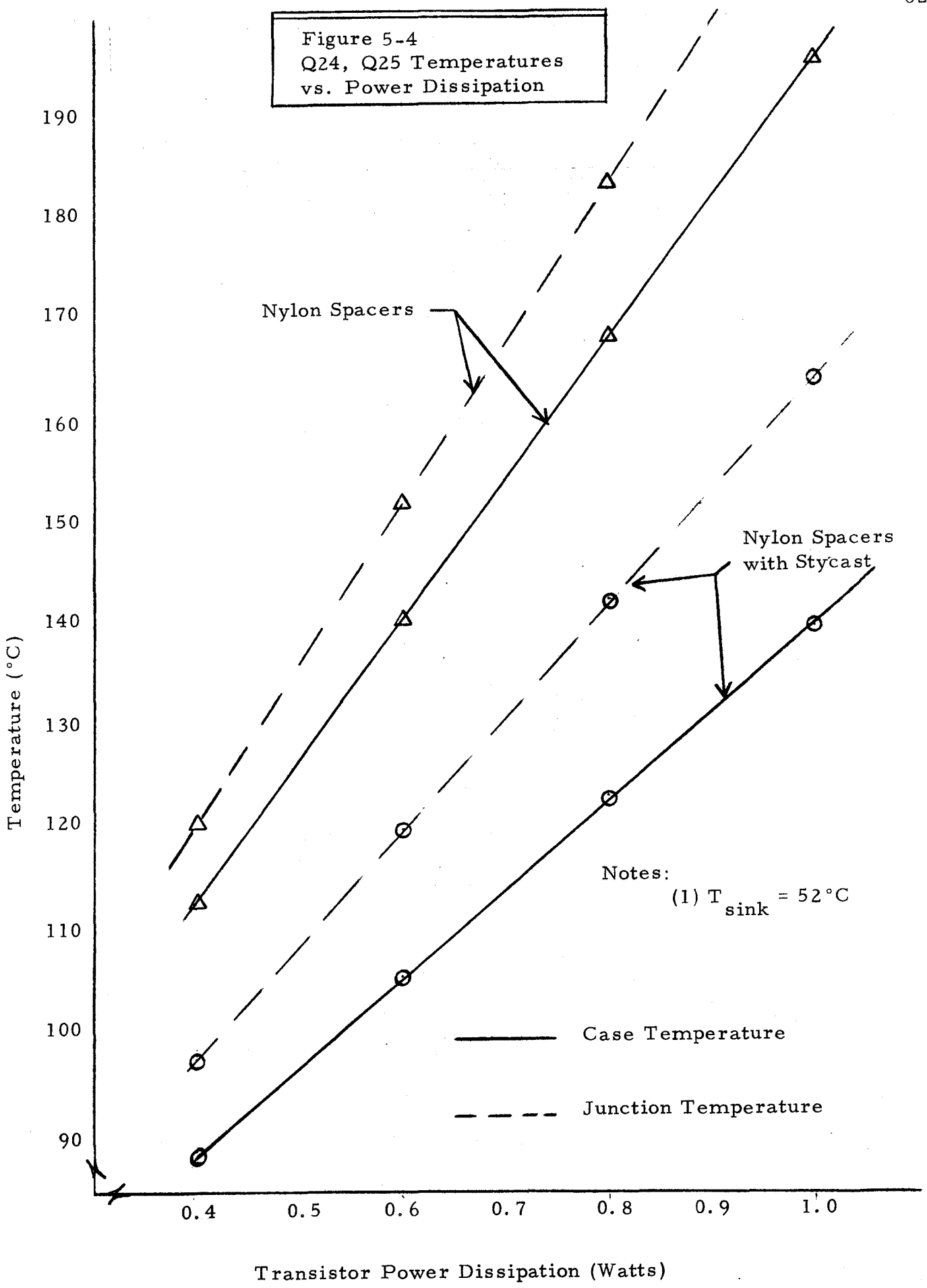
Figure 5-4
Q24, Q25 Temperatures
vs. Power Dissipation
190
180
170
160
150
140
130
120
110
100
90
Temperature (°C)
Nylon Spacers
Nylon Spacers
with Stycast
Notes:
(1) T_{sink} = 52°C
Case Temperature
Junction Temperature
0.4
0.5
0.6
0.7
0.8
0.9
1.0
Transistor Power Dissipation (Watts)

Figure 5-5
Q24, Q25 Temperatures
vs. Power Dissipation

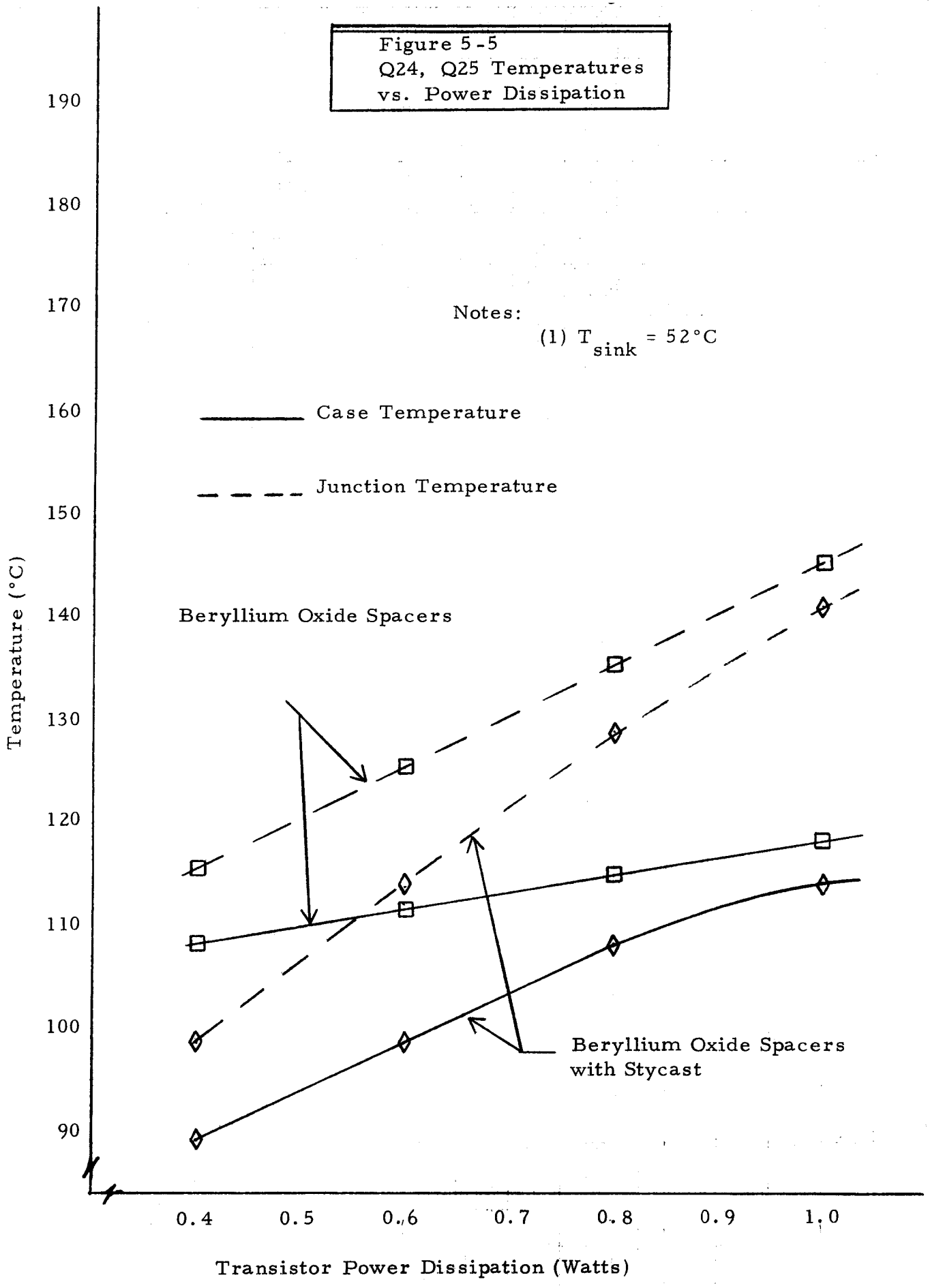

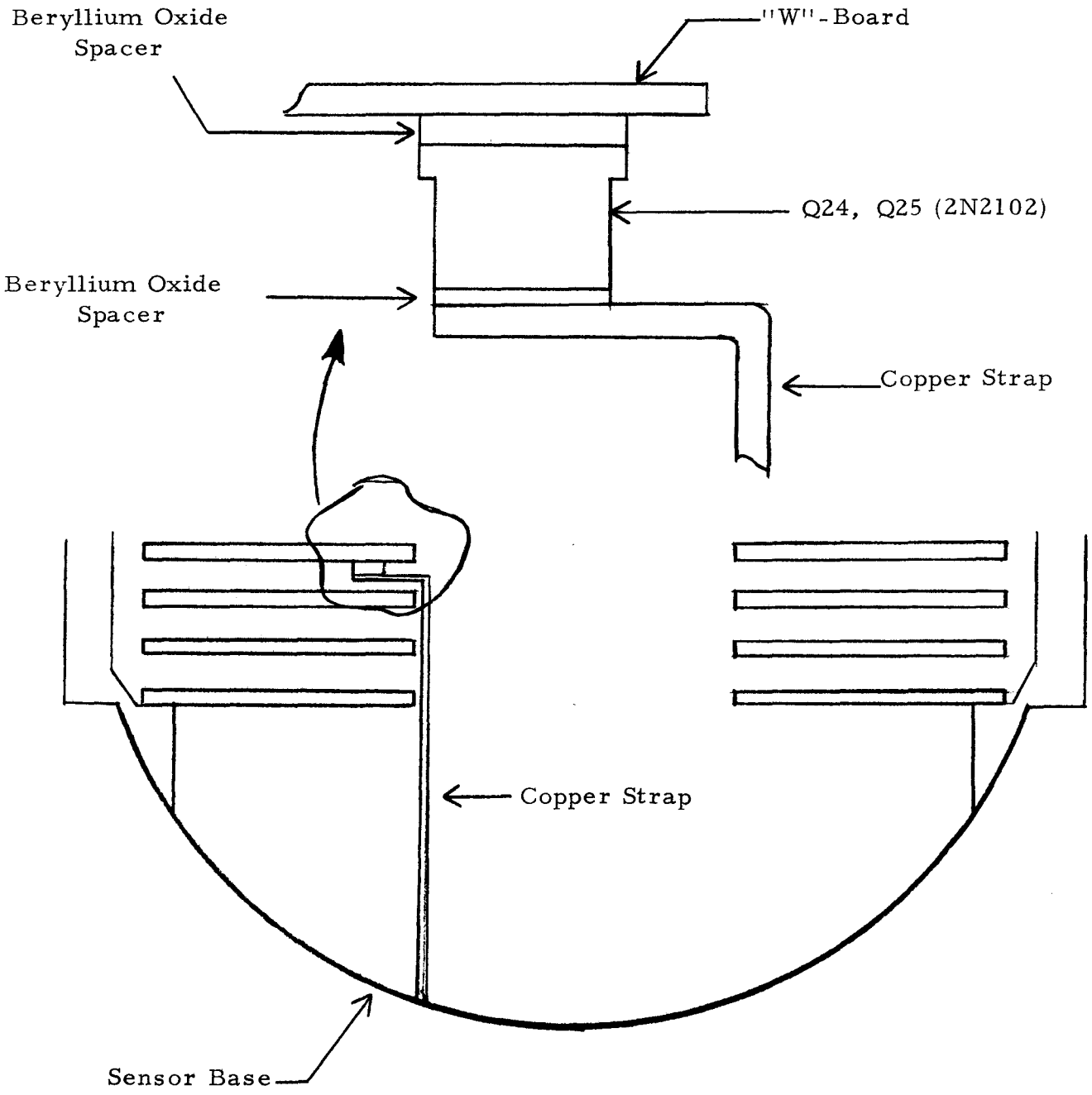

Figure 5-6 Q24, Q25 Heat Sink Technique

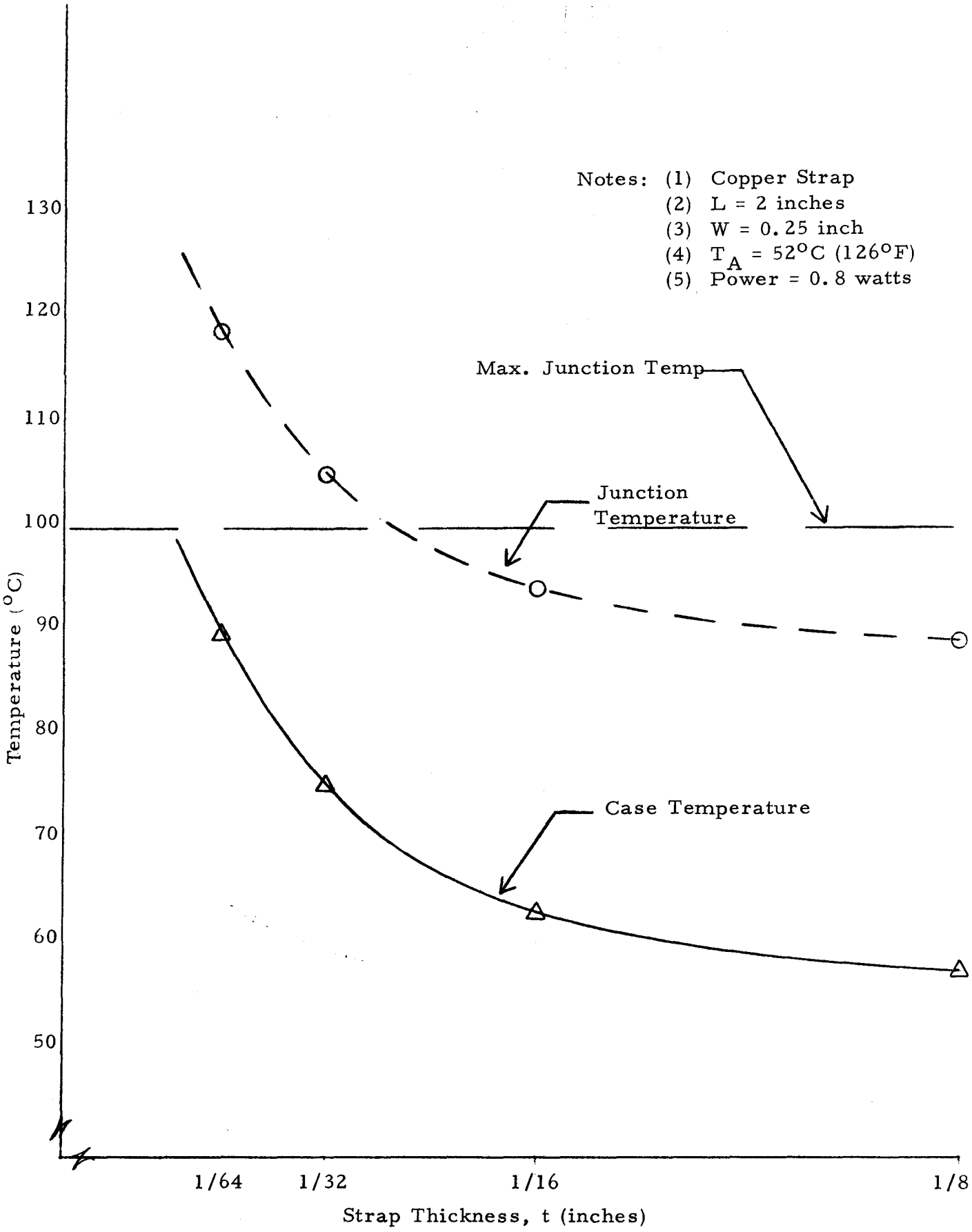

Figure 5-7 Q24, Q25 Temperatures vs. Copper Strap Thickness

A diagram of the test setup is shown in Figure 5-8. The "W" board was mounted to the cover of a minibox using four 3/8" O. D. aluminum standoffs each 1/2 inch in length. The component side was face down as shown in the figure.

A thermally conducting silicone grease was used to insure good thermal contact between the minibox cover and the 15" diameter copper thermal plate. A 9" x 7" x 2" minibox was used to form an enclosure around the "W" board assembly. To simulate the surroundings of the "W"-board, a high emittance (ϵ = 0.9) black paint was used to coat the insides and cover of the aluminum minibox. Finally several layers of multilayer insulation were secured over the outside of the minibox to help maintain uniform temperatures throughout the enclosure.

It was recommended that a two-inch length copper strap 1/4" wide and 1/16" thick be used to provide an adequate thermal path from the transistor case to base. However, the actual lengths of the copper strips used were 6 inches.

Due to the unavailability of 0.060" beryllium oxide spacers at the time of the test, the copper strip was attached to the top of the transistor case using Stycast 2850 FT epoxy.

Temperature measurements were made using #40 gauge copper-constantan thermocouples located on the test items. The thermocouples were epoxied on the side of Q24 and Q25, the "W"-board, the thermally controlled heat sink and the minibox cover as shown in Figure 5-8. A Wheatstone Bridge was used to read out voltages used to determine temperatures by resistance thermometer methods.

The results of the test were in excellent agreement with those predicted using the analytical model. Under vacuum conditions, case temperatures differed by only 2 °C at most. The summary of test and analytical results is presented in Table 5-2 along with the analytical prediction of corresponding junction temperatures.

A brief description of the test conditions follows:

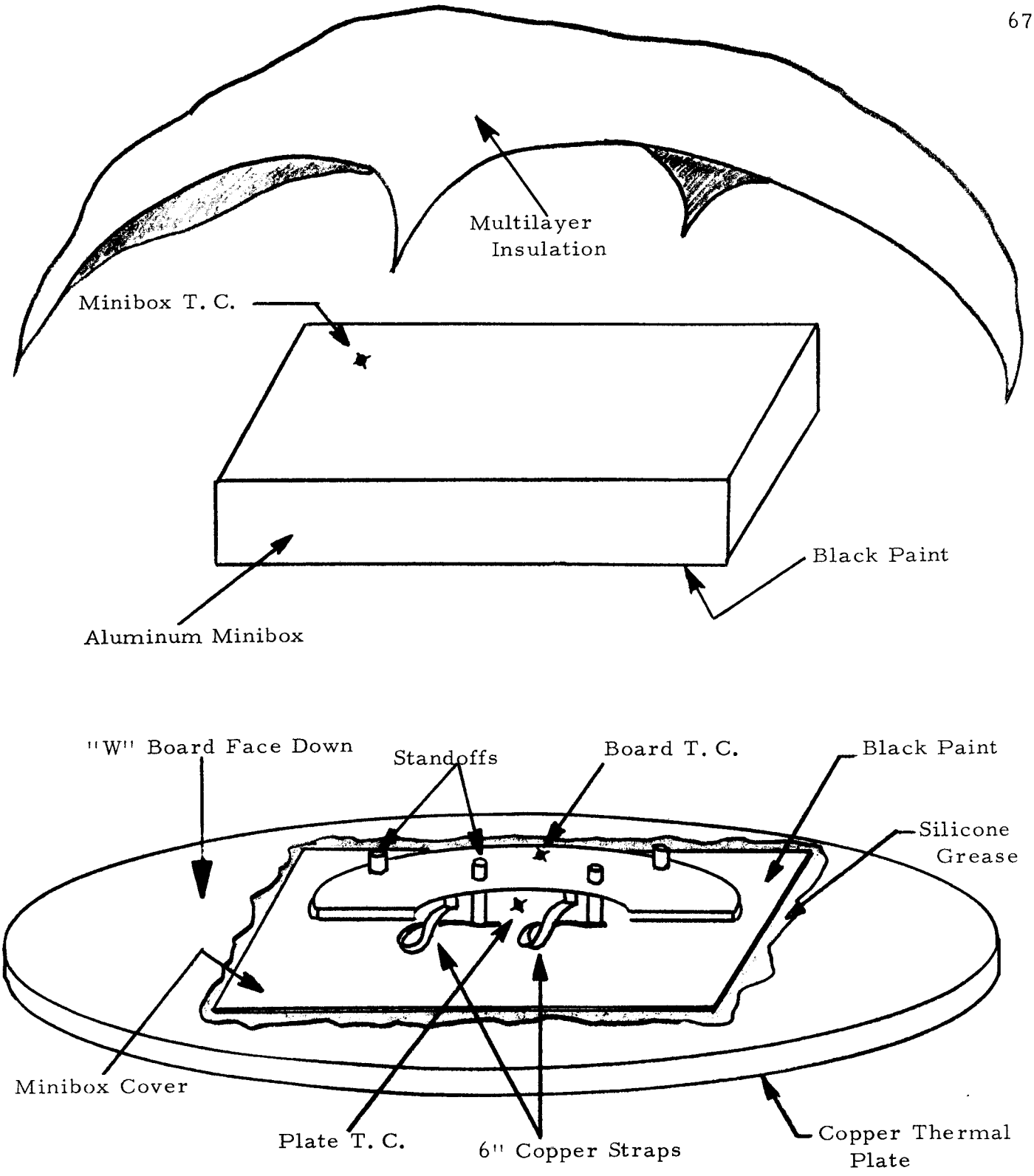

Figure 5-8 Test Simulation of Q24 and Q25 Thermal Environment

Test #	Q24 Temperatures (°C)			Q25 Temperatures (°C)		
	CASE		JUNCTION	CASE		JUNCTION
	Test	Analytical	Analytical	Test	Analytical	Analytical
1	61.0	66.6	93.1	63.0	67.3	92.7
2	29.5	31.2	47.2	27.0	25.5	25.5
3	96.4	98.4	152.1	30.0	27.9	27.9
4	86.5	88.1	115.1	88.0	87.7	113.8
5	117.0	118.1	173.2	54.5	53.0	53.0

Table 5-2 Comparison of Test and Analytical Case Temperatures and Corresponding Predicted Junction Temperatures

Test #1: Operation in Ambient Air.

Free air curves can not be used in the specification of maximum power dissipation since the transistors were mounted to the "W" board which in turn is mounted on the thermal plate. A run was made to determine case temperatures in this configuration. The thermal plate and "W" board temperatures were 25.5 and 30.0°C, respectively.

Test #2: Q25 Failed Due to Short-In Vacuum at Ambient Temperatures

In this test the thermal plate and "W" board were 25.5 and 29.5°C respectively as Q25 was electrically shorted out. The bell jar had been evacuated to 0.5×10^{-4} microns.

Test #3: Q25 Failed Due to Open Circuit-In Vacuum at Ambient Temperatures

This test was conducted in a vacuum with plate and board temperatures of 27.9 and 27.9°C respectively. The Q25 transistor was opened resulting in Q24 carrying the entire load. The bell jar was evacuated to 0.5×10^{-4} microns.

Test #4: Normal Operation Temperature Environment-In Vacuum

The temperatures of the thermal plate and board were recorded to be 51.5 and 54°C respectively. Both transistors were dissipating nominal power. The bell jar was evacuated to 0.5×10^{-4} microns.

Test #5: Q25 Failed Due to Open Circuit. Normal Temperature Environment in Vacuum.

The test was made in the actual environment to be encountered. The thermal plate and board temperatures were 52 and 56°C, respectively. Twice the nominal power dissipation occured in Q24. The bell jar was evacuated to 0.5×10^{-4} microns.

Test Results

An abbreviated summary of the test results is presented in Table 5-3. Thermal plate, board and transistor temperatures are presented as well as the required voltages needed to calculate transistor power dissipations.

TEST #	VAC OR AIR	PLATE TEMP.	BOARD TEMP.	$T_{CASE\ Q_{24}}$	$T_{CASE\ Q_{25}}$	V_C	I_H	$V_{R_{38}}$	$V_{R_{39}}$
		(°C)	(°C)	(°C)	(°C)	(VOLTS)	(MA)	(MV)	(MV)
1	AIR	25.5	30.0	61.0	63.0	10.5	175	560	540
2	VAC	25.5α	29.5	29.5	27.0	1.45	258	175	1450
3	VAC	27.9	33.8	96.4	30.0	17.0	115	680	0
4	VAC	51.5	54.0	86.5	88.0	10.9	172	540	520
5	VAC	52.0	56.0	117.0	54.5	17.5	112	670	0

Table 5-3 Abbreviated Summary of Test Results

Presented in Figure 5-9 is the schematic used to determine the dissipations. A nominal electrical resistance of 5.9 ohms for R_{38} and R_{39} was assumed in the determination of the currents through the components. The resulting power dissipations of Q24 and Q25 are presented in Table 5-4.

Using the calculated power dissipations of Q_{24} and Q_{25} from electrical measurements made in the test as inputs to the thermal model, the junction and case temperatures were determined using the Thermal Analyzer Computer Program. These temperatures are presented in Table 5-2.

5.0.3 Correlation of Thermal Model and Test Results

The correlation of thermal model temperatures with test data is excellent indicating a good modeling of the transistors and test conditions. Case temperatures differed at most by 6 °C in the first test run under ambient conditions in air.

Since heat transfer by free convection was not considered in the analytical model, it is to be expected that case temperatures in the first test should run lower than predicted by the model. All other correlations agree well with case temperatures differing by 2 °C at most. A comparison of analytical and test results is presented in Table 5-2.

Comments

The overall thermal simulation of the "W" board and its environment was ideal. All conditions were matched very closely. The minibox and cover were very near uniform temperatures at all times simulating the massive PSE heat sink and surroundings. The black coating of the box simulated well the high emittance fiberglass boards ($\epsilon = 0.8$) and surroundings. The aluminum standoffs were flight type hardware.

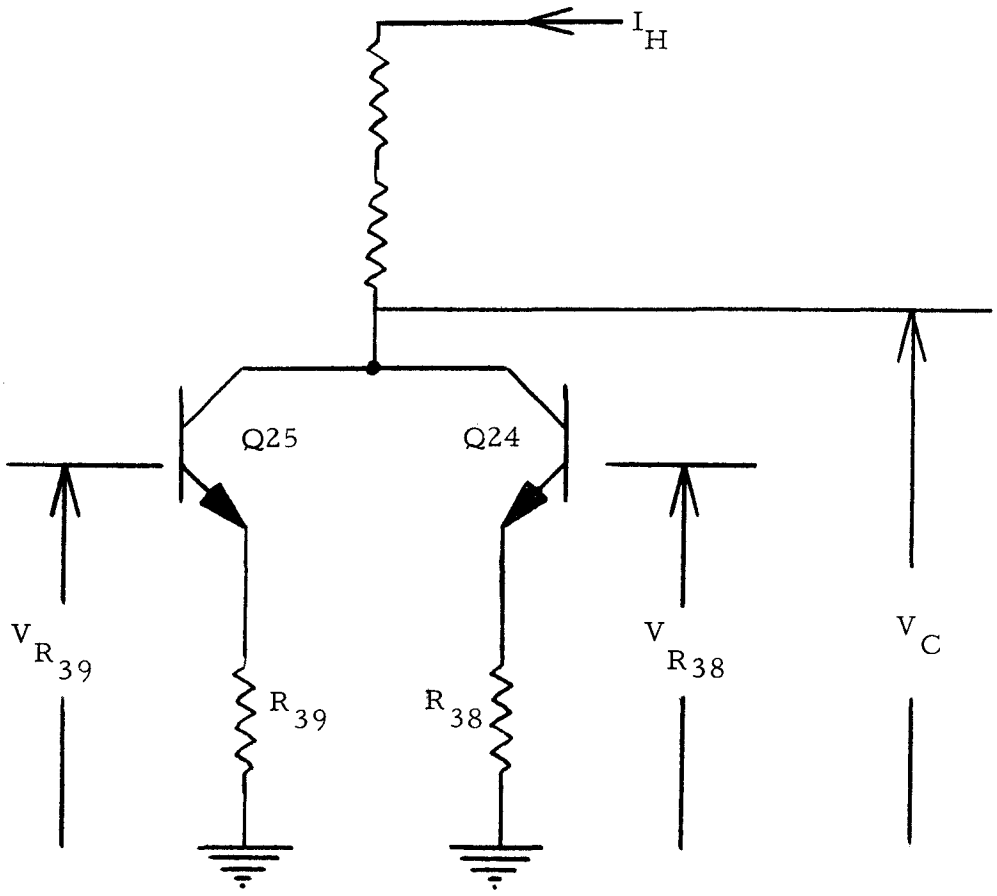

$$R_{38} = R_{39} = 5.9$$

$$I_{Q24} = \frac{V_{R_{38}}}{5.9} \qquad I_{Q25} = \frac{V_{R_{38}}}{5.9}$$

$$P_{24} = (V_C - V_{R_{38}})\ I_{Q24} \qquad P_{25} = (V_C - V_{R_{39}})\ I_{Q25}$$

Figure 5-9 Schematic Used to Determine Transistor Power Dissipation

TEST #	Q_{24} POWER DISSIPATION (WATTS)	Q_{25} POWER DISSIPATION (WATTS)
1	0.943	0.9116
2	0.037	0
3	1.881	0
4	0.948	0.9149
5	1.911	0

TABLE 5-4

Summary of Calculated Power Dissipations

5.0.4 Final Thermal Control Design of Heater Transistors

The thermal control concept of heat sinking the transistors to the PSE base was demonstrated by tests as well as analytically. However, the final design required that the transistor cases be provided with heat sinking to the aluminum standoffs which separate the electronic boards. A final thermal analysis of the design was reported in reference 34. In Figure 5-10 a sketch of the final design is shown.

Clearance and assembly tolerances required that the nylon spacer be used instead of the more thermally desirable beryllium oxide material. Figure 5-11 presents steady state case and junction temperatures as a function of the transistor power dissipation using the analytical thermal model verified by test. The analytical results show that it is possible to maintain junction temperatures below 100°C while dissipating the nominal 800 milliwatts of power.

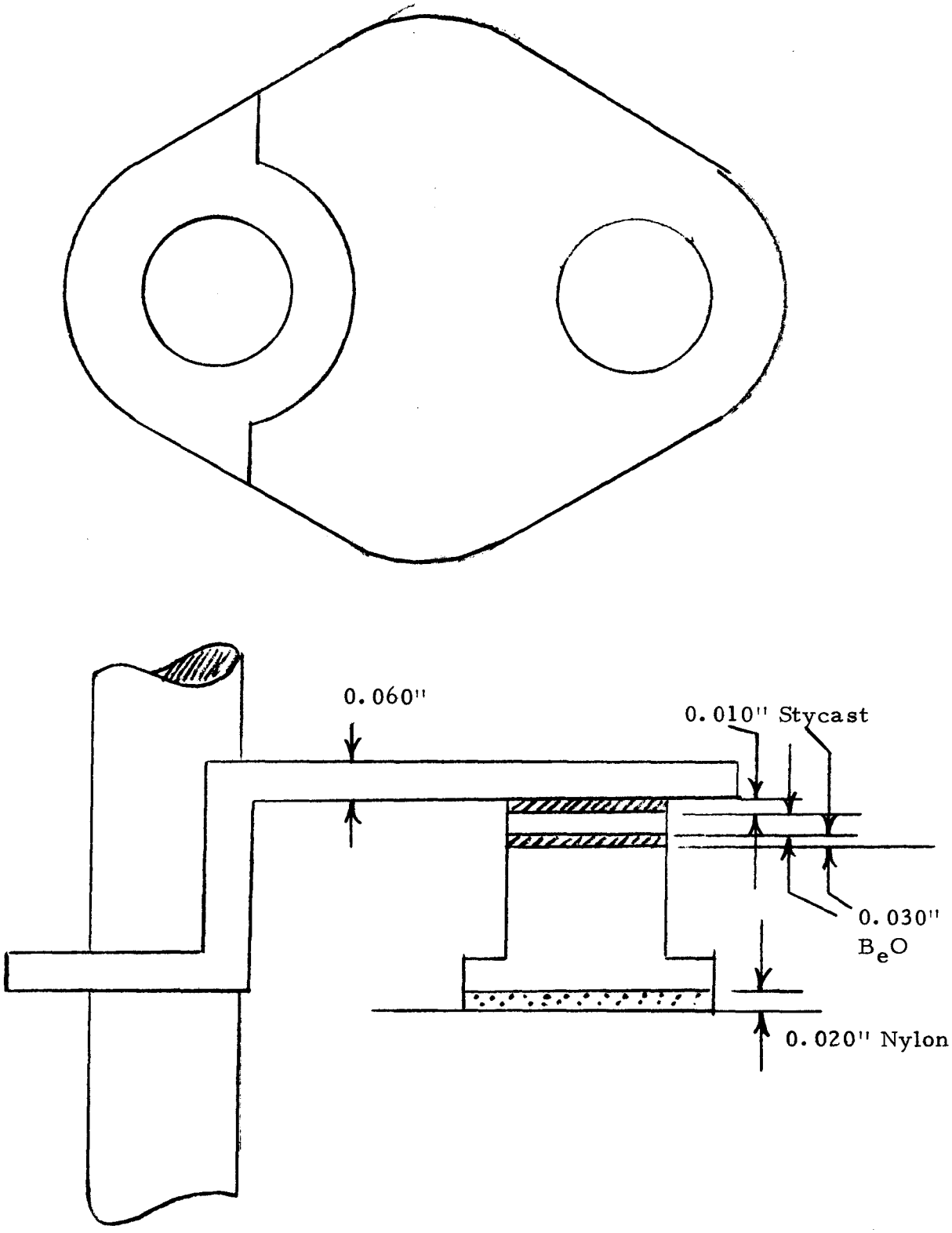

Figure 5-10 Q_{24} Heat Sink Attachment to Stand off

Figure 5-11

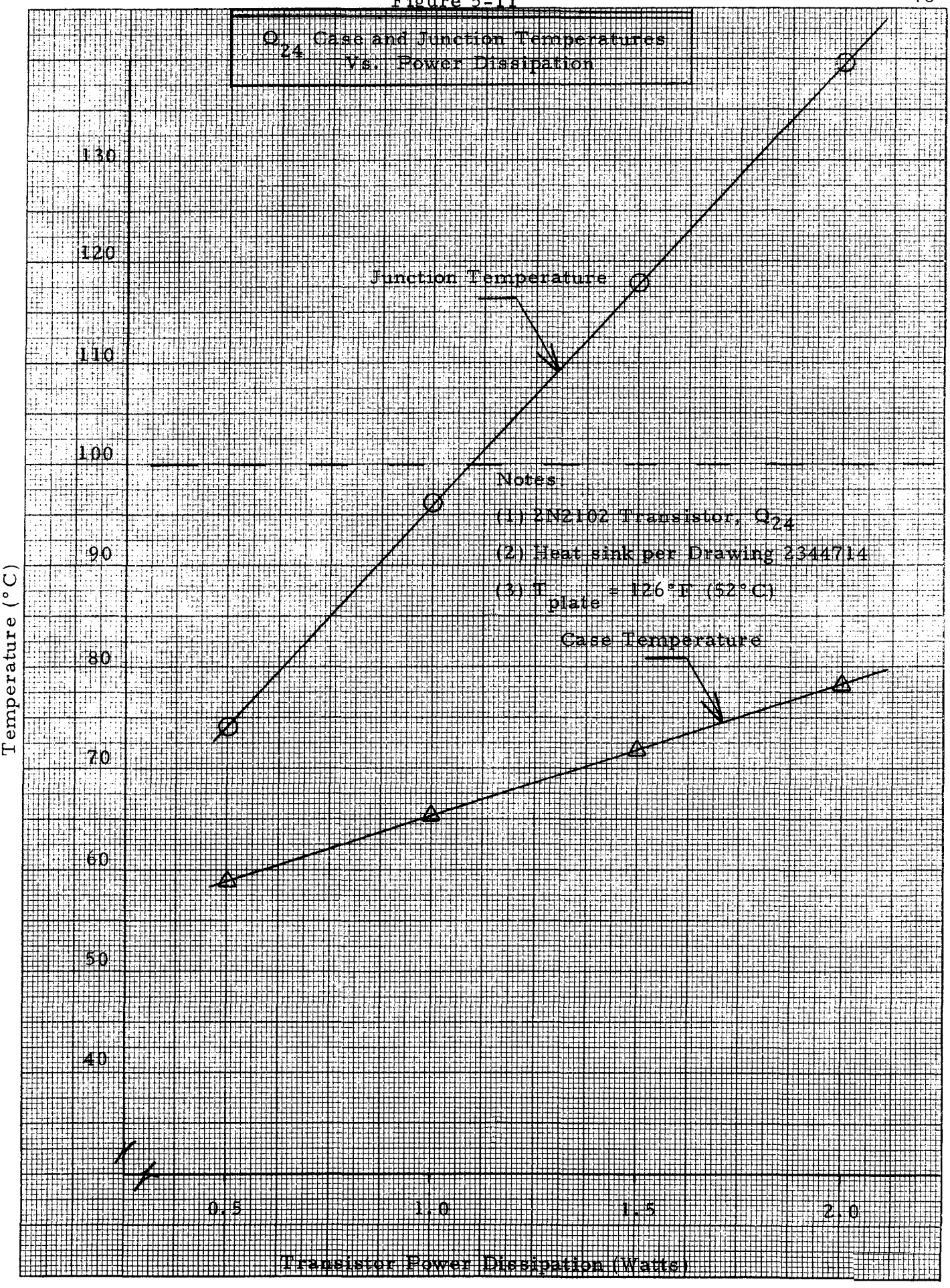

5.1 FLIGHT-4 (APOLLO 14) HEATER POWER DISSIPATION

The design modification to increase heater power during lunar night is presented and the dissipations documented for future use.

Heater power was set in the bypass mode. The nominal heater circuit current and voltage are 200 ± 10 Ma and 29 VDC, respectively. Recorded current and voltage levels taken from an engineering model in free air with case temperature of 85°C were 190 Ma at 29 VDC. This results in a heater power of 5.52 watts. It is assumed that the power in the auto mode is identical to that set in the bypass mode.

Manual power was determined from heater circuit current and voltage measurements. A current of 192 ma at 29 VDC results in a manual heater power of 5.57 watts.

Finally, survival power with the present heater modification is 0.628 watts. Flight 1 survival power was 0.725 watts.

A summary of the heater power dissipations of the Flight-4 PSE is presented in Table 5-5. The powers were obtained from reference 17.

Mode of Operation	New Heater Design Power (watts)	Original Heater Design Power (watts)
Auto	5.52	2.35
Manual	5.57	2.9
Survival	0.628	0.725

Table 5-5 Summary of Flight-4 Heater Power Modifications

5.2 MATERIAL EVALUATION

In reference 1 the optical properties used were those determined from absorptance and emittance measurements of samples taken at BxA and other reliable sources. Results of measurements taken on exposed external surfaces such as aluminized mylar and aluminized teflon were reported in references 8, 26, 27, and 28. The results of optical measurements taken on PSE beryllium and other internal components were presented in references 27 and 29.

The importance of the external surface properties on the performance of the PSE thermal shroud was elaborated in reference 1. Specifically, it was recommended that a layer of 2 mil aluminized teflon be added to the external surface of the skirt to reduce the external surface temperature of the skirt and consequently maintain the sensor temperature at its set point of 126°F during lunar day. The thermal stress to the external surface of the skirt would decrease accordingly during terminator crossing. To further reduce external temperatures of the shroud, the attachment of 2 mil silverized teflon to the outer layer was suggested due to the improved optical properties of silver. Since then a material evaluation has been conducted and reported in reference 2. The purpose of the evaluation was to (1) summarize all available data on the surface properties of aluminized and silverized teflon films, (2) perform measurements on available material samples such as that used on the Apollo 13 PSE shroud modification and compare these measurements with the survey and (3) summarize or determine the status of long term degradation of teflon films by charged particles and fields in the lunar environment.

To this end, informal contacts with personnel from the Goddard Space Flight Center (refs. 35, 38, and 40), Dupont Co. (ref. 37), Ultrainsulation Co. (ref. 36), Schjeldehl Co., Norton Co. and Coburn Coating Corp. have been made. Material samples from each of these sources were obtained and optical measurements made. These measured values were compared with data presented by each respective source and any other available data. The nominal (i.e., undegraded) solar absorptance and infrared emittance of aluminized and silverized teflon films have been established. Table 5-6 presents the range of values established for the 2 mil teflon films and clearly shows the advantage of silverized teflon.

TABLE 5-6

SURFACE PROPERTIES OF 2 MIL METALLIZED TEFLON FILMS

Metal Coating	Solar Absorptance (α_s)	Infrared Emittance (ϵ_{ir})	$\frac{\alpha_s}{\epsilon_{ir}}$
Aluminum	.124-.213	.65-.73	.19-.3
Silver	.04-.07	.64-.67	.07-.11

Teflon is inert to ultraviolet radiation for short durations or long durations when partially filtered by the earth's atmosphere. For long durations in a lunar environment it is generally accepted as inert; however, conclusive data is not available to verify this. 40 KEV proton bombardment has a negligible effect for fluence levels up to 2×10^{14} particles/cm^2. Degradation increases progressively from this level. At fluence levels greater than 1×10^{16} particles/cm^2 degradation is considerable. For example, the solar absorptance of 2 mil aluminized teflon degrades 50% at fluence levels of 1.8×10^{16} particles/cm^2. At fluence levels of 1.7×10^{16} 2 mil silverized teflon degrades 67%. It has been shown that the percent degradation gradually decreases with increasing thickness. (reference 39).

5.3 REQUIRED MODIFICATIONS - APOLLO 14

All of the proposed modifications to the Apollo 14 PSE thermal shroud will not require requalification; however, a few will require simple engineering evaluation tests.

The modifications implemented on the Apollo 13 thermal shroud modification shown in Figures 5-12 and 5-13 are again required. These modifications require no evaluation testing and are itemized as follows:

1. Perforation of the mylar insulation layers in the thermal skirt including the 1/2 mil non-aluminized mylar sheet. Vent holes of 1/8 inch diameter are required with alternate patterns in adjacent sheets.

2. A layer of 2 mil FEP Type-A teflon aluminized or silverized on one side over the entire external surface including the leveling support structure. The teflon film will be the exposed surface. Film will be stitched where possible and bonded only where necessary.

3. Incorporation of Mallory 1000 weights to each deployment tab. The weights will be sewn firmly to the tabs by Tufbraid 50 DOR 16.

4. (a) Loose buttoning through thermal skirt of 8, 16 and 32 buttons in three concentric circles of 8, 16 and 28 inch radii. Buttons will be 5 mil Kapton 3/8 inches in diameter.

   (b) Loose stitching the periphery of skirt 1/2 inch from edge with 1/2 inch stitches.

The implementation of each of these modifications are required for the following purposes:

1. This modification assures positive venting of any air entrapped during stowage. As a result, both stowage and deployment are improved. Possible rupture of the shroud during the launch and transit phases is eliminated.

FIGURE 5-12 APOLLO 13 PASSIVE SEISMIC EXPERIMENT INSULATION SKIRT MODIFICATION

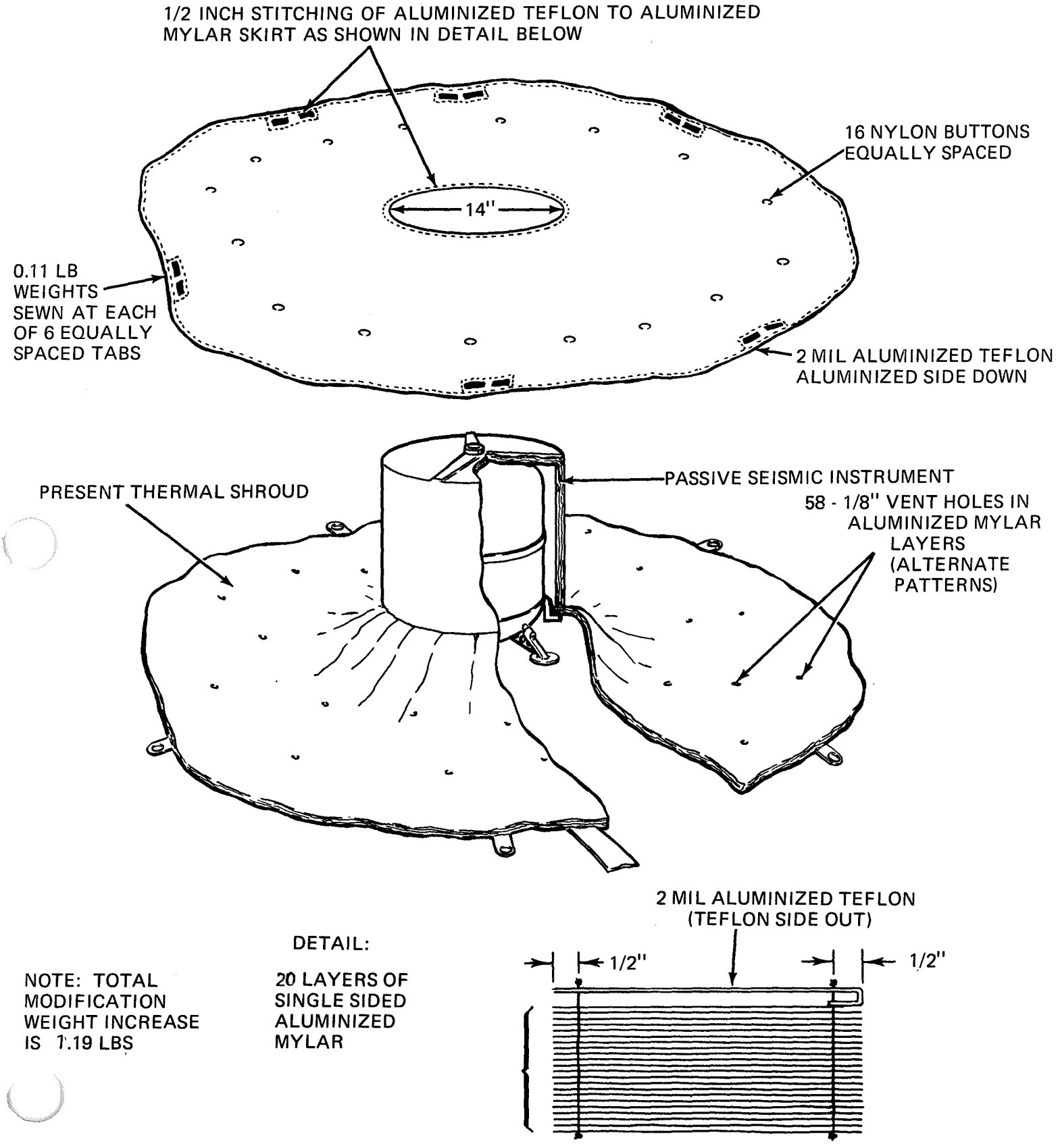

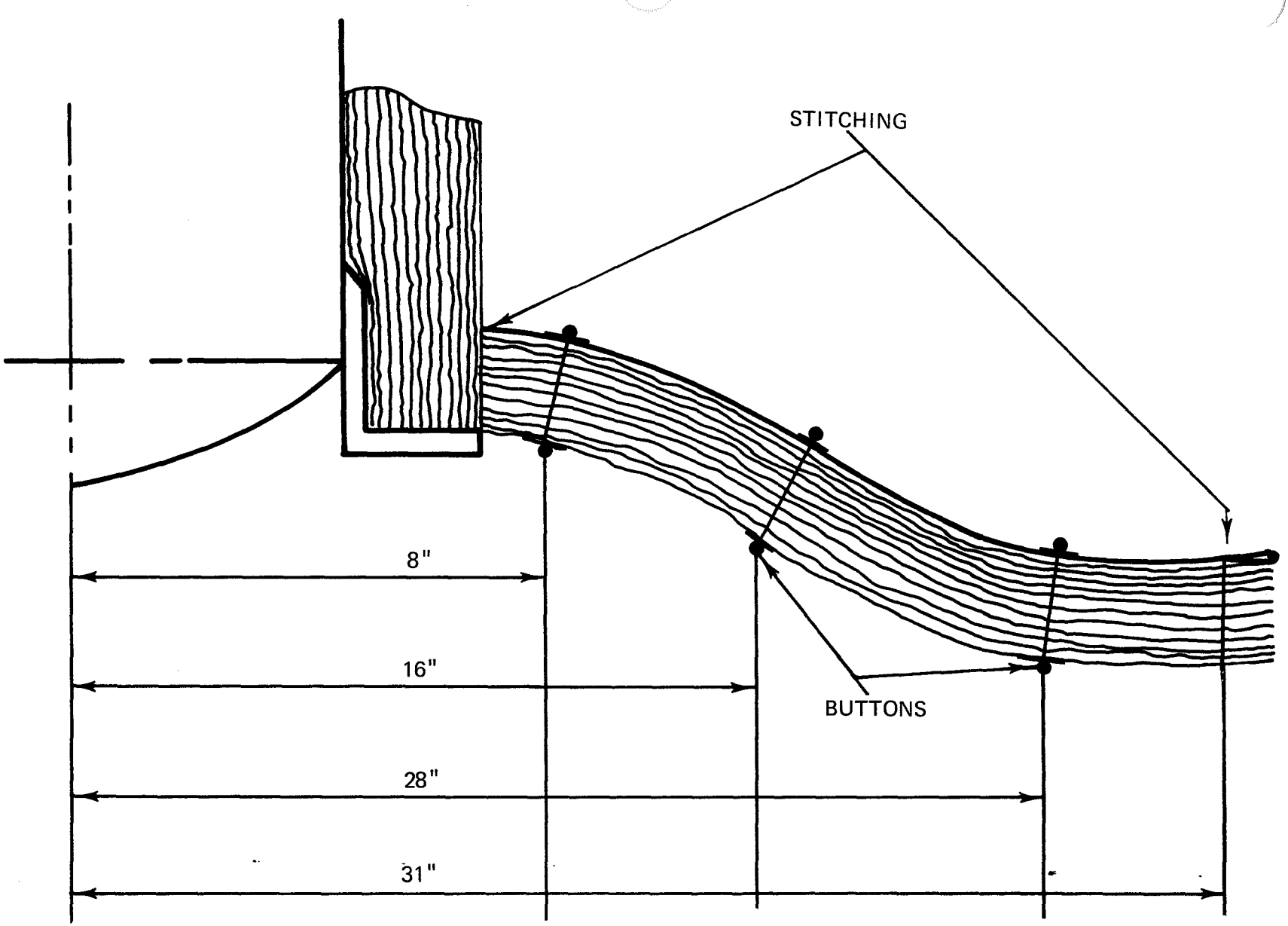

FIGURE 5-13 STITCHING AND BUTTON LOCATIONS

2. The present thermal skirt consists of an outer layer of 1/4 mil aluminized mylar with the mylar film exposed. The annular surface from the cylindrical cannister out to a radius of 14.5 inches is covered with an additional layer of 2 mil aluminized teflon film which is spot bonded to the mylar film. Mylar degrades (i.e., the solar absorptance increases) considerably with exposure to the ultraviolet radiation present in the lunar environment. Also, the annular teflon layer tends to delaminate at the bonding sites, which further increases the effective solar absorptance (Refs. 10, 11 and 12). With an undegraded undelaminated surface the peak temperature of the skirts external surface will be reduced. Accordingly, the temperature excursion of the lunar soil beneath the sensor will be reduced providing a more effective heat sink for the sensor.

   The outer surface of the cylindrical cannister is 2 mil aluminized teflon bonded to the outermost layer of mylar with the exception of the compass rose which is 5 mil aluminized mylar. The same tendency to delaminate at the bonding sites is observed. Thus, the additional layer of aluminized teflon attached without bonding will assure reduced peak temperatures on the cannister and result in reduced heat loads to the sensor.

3. Incorporating weights to the deployment tabs will improve deployment since the skirt will tend to settle into its required configuration more readily. The adverse thermal effects of tunnelling are minimized and thermal isolation is improved.

4. The buttons and stitching will eliminate the repelling and pealing back of individual layers due to electrostatic charges and will keep the skirt in tact when impinged by LM exhaust gases and debris during ascent.

In addition to these modifications, the following modifications are recommended:

1. An increase in heater power dissipation in the auto mode from 2.5 to 5.5 watts by replacing present resistance heaters. Per reference 17 the manual mode power dissipation will increase from 2.9 to 5.57 watts.

2. Ten additional insulation layers to thermal skirt of 1/4 mil mylar aluminized one side. Each layer inserted between two existing layers with the mylar side up.

3. Mechanically decouple thermal skirt from sensor in an interim manner such as shown in Figure 5-14.

4. A 2 mil teflon compass rose bonded over the present 5 mil mylar compass rose.

5. A temperature sensor added to either the underside of the skirt or to the cable approximately one foot from the sensor.

All of these latter five modifications require a simple engineering evaluation test with the exception of item 5 which will require an electrical continuity check.

The purposes for implementation of these modifications are:

1. During the Apollo 12 mission, it was found that by actuating the 3 watt leveling motor during lunar night, the sensor could be maintained at its temperature set point of 126°F. By increasing heater power dissipation in the auto mode by 3 watts, the sensor will be self-regulated.

2. Increasing the number of insulation layers in the skirt effectively decreases the skirt thermal conductivity. The decrease in thermal conductivity reduces (1) the temperature excursion of the lunar surface beneath the skirt and (2) the effect of degradation on the outer surface properties of the skirt due to dust accumulation, vacuum-radiation effects or charged particles.

3. Mechanically decoupling the skirt from the sensor will tend to minimize the possible tension force buildup or release on the sensor due to thermal contraction or expansion on the outer surface layer of the skirt. This contraction expansion is readily evident during terminator crossings (ref's 2, 3, 5 and 9).

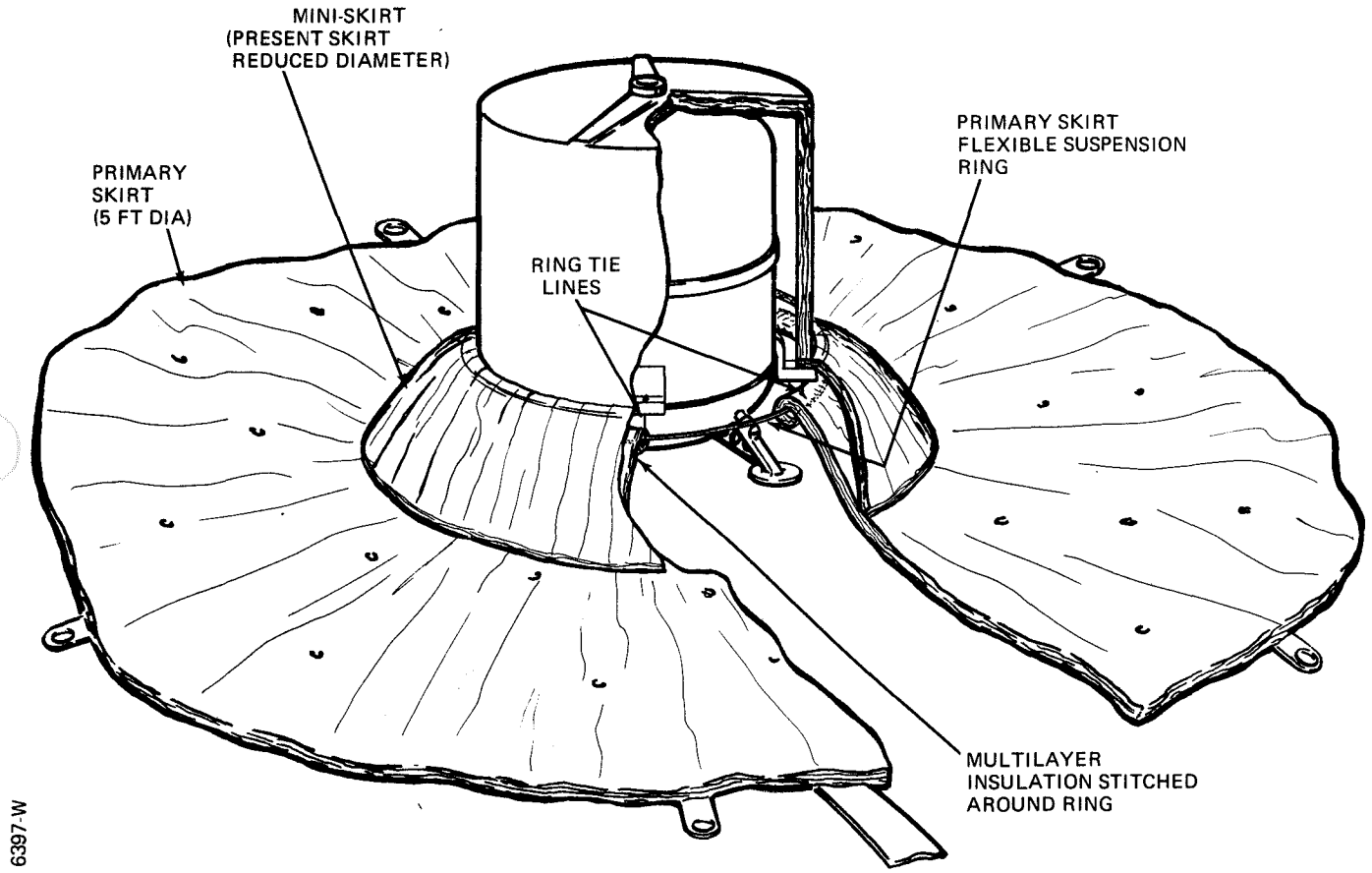

Figure 5-14 Interim Decoupled Shroud Concept

4. The present mylar compass rose will degrade due to ultraviolet radiation and charged particles present in the lunar environment. The teflon compass rose is inert to the lunar environment and will result in lower cannister temperatures.

5. The addition of a temperature measurement external to the sensor but below the thermal shroud will simplify the task of deducing the thermal sink temperature of the soil beneath the sensor. The heat losses from the sensor could then be evaluated more effectively.

6.0 PREDICTIONS FOR POSSIBLE APOLLO 14 DEPLOYMENT SITES

Operational sensor temperatures have been predicted for the Littrow Rille landing site located at 22°N latitude. The lunar surface temperature and set of one dimensional time varying boundary conditions determined in Section 4.2.2 were input to the analytical model. A total power dissipation of 1.0 watts during lunar day and 6.25 watts during lunar night is assumed. Computer analyses show that the sensor will be maintained at 126.0°F during both lunar day and night. In Figure is the plot of the predicted sensor temperature through an entire lunation. The results are presented for a partially degraded skirt (α_s/ϵ_{ir} = 0.37/0.73) and totally degraded shroud (α_s/ϵ_{ir} = 0.73/0.73) as well as for the undegraded case (α_s/ϵ_{ir} = 0.2/0.73). Effective thermal conductivities of the skirt and shroud are assumed to be 5.3×10^{-4} and 7.5×10^{-4} Btu/hr/ft°F, respectively.

For the possible deployment of the PSE at the Frau Mauro site a constant sensor temperature of 126.0°F is predicted.

7.0 FUTURE EFFORT RECOMMENDATIONS

The Apollo 11 and 12 missions have revealed that the lunar soil is similar to the dust design properties of reference 13. The thermal analyses to date have considered only the most likely soil properties as obtained from references 14 and 15. It is likely that at the higher lattitudes a harder substrate with radically different thermal-physical properties will exist. The most probable is a surface of high thermal conductivity and density such as the rock design properties of reference 13. To account for this posibility, a thermal analysis is recommended to evaluate the PSE thermal control system at deployment sites of high thermal conductances and densities. Thermal performance at the equator and at various lattitudes up to 45 degrees will be considered.

The Apollo 12 mission has indicated that seismic activity appears to occur at the sunrise and sunset terminator crossings. This activity could be due to a number of phenomena. Among these are: (1) thermal expansion or contraction of the thermal shroud and cable, (2) a gradual settling of the sensor into the lunar soil, (3) thermal expansion or contraction of the local lunar soil and substrate.

The latter phenomena is beyond the realm of the study and is not considered. The present sensor is mechanically attached to the thermal shroud by nylon screws at the four mounting tabs. The skirt on the Apollo 12 mission was weighted by Boyd Bolt guide cups and lunar rocks emplaced by the astronauts to keep the individual skirt layers from separating. This provided an additional constraint on the shroud. Thermal contraction or expansion in the outer layers of the thermal shroud could cause tension loads or the relief of previous loads on the sensor. These forces tend to rotate the sensor beyond the threshold limit of 5×10^{-7} radians per references 2 and 3. In reference 9 it was shown that thermal contraction or expansion of the electronics cable could cause changes in suspended cable length or curvature which would also tend to rotate the sensor beyond the threshold limit of 5×10^{-7} radians.

On Apollo 14, modifications are proposed to the present thermal shroud to minimize the mechanical coupling of the shroud and sensor. To determine the effectiveness of the decoupling, the Apollo 12 long-period and tital data will be reviewed in detail. Subsequent to Apollo 14 deployment, the long-period and tidal data will again be studied to determine the precise effect of the interim decoupling.

To positively eliminate any torque on the sensor by the thermal shroud during terminator crossing, a totally decoupled shroud is required. To this end, a thermal design study is recommended to evaluate totally decoupled shroud concepts. The study will include the effect of various geometries such as the hemispherical and conical shrouds shown in Figure 7-1. The effect of lunar surface area protected by the thermal shroud for the ALSEP design range of soil thermal-physical properties will be studied. Mechanical stowage and crew requirements will be considered in any recommendations from this study.

A new foot pad design has been proposed in reference 17 to minimize settling and to assure positive clearance of the bottom of the sensor. The modified design reduces the pad pressure by increasing the contact area of the pads and extends the isolator buttons on the ring of the leveling stool to increase clearance. The present isolater buttons are fiberglass. The proposed extensions are beryllium to minimize thermal stresses. Due to the new materials and possible change in contact area with the sensor base, a thermal analysis is required to determine the effect of this modification on the thermal control of the sensor.

Additional areas requiring future effort are:

1. Evaluation of the thermal-physical properties of the Apollo 12 and 14 lunar soil samples to incorporate in subsequent correlation studies.

2. Correlation of Apollo 14 flight data.

3. Further evaluation of silverized teflon films for long-term stability in charged particle environments. Intensity and integrated flux flight data from the ALSEP charged particle experiments will be necessary for proper evaluation.

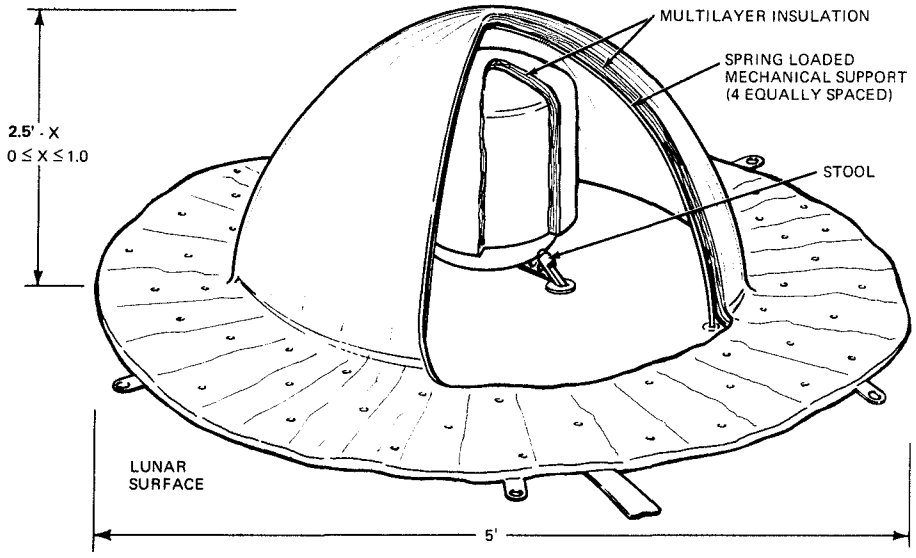

HEMISPHERICAL – DECOUPLED DESIGN

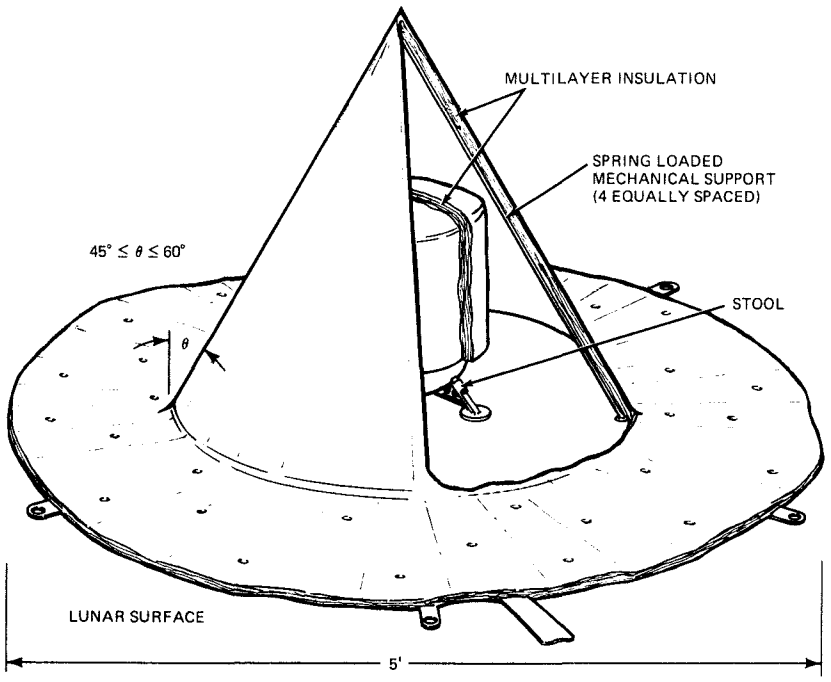

CONICAL – DECOUPLED DESIGN

Figure 5-15 Totally Decoupled Shroud Concepts

8.0 REFERENCES

1. ATM-862, "ALSEP Flight 1 PSE Thermal Anomaly Study", 4/2/70

2. BxA Memo 70-210-121,"PSE Anomaly at Terminator Crossing", 4/20/70

3. BxA SSED-57(d), (e) and (f), "Interim Report - Investigation of PSE Anomalies - Apollo 12 Mission", 4/21/70

4. BxA Memo 70-210-135, "Concept to Reduce the Influence of PSE Skirt Thermal-Mechanical Stressing on Sensor Data", 5/5/70

5. BxA SSED-436, "Technical Review Meeting with LDGO", 4/30/70 and 5/1/70

6. BxA Memo 70-210-143, "PSE, One-Dimensional Thermal Analysis of Various Lunar Soils at Off-Equator Latitudes", 5/8/70

7. BxA SSED-443, "Heater Modification Meeting", 5/3/70

8. BxA Memo 70-210-165, "Surface Properties of Metallized Teflon Films", 5/22/70

9. BxA Memo 70-210-175, "Influence of Electronic Cable and Skirt Design on PSE Terminator Anomaly", 6/1/70

10. BxA Memo 9713-10-3344, "Delamination of Aluminum Coating from Teflon on PSE Thermal Shrouds", 10/17/69

11. BxA Memo 9713-10-3352, "PSE Thermal Shrouds - Aluminum-Teflon Delamination", 10/30/69

12. BxA Memo 9713-10-3359, "PSE Thermal Shroud Covering Delamination - Effect of Material Thickness", 11/19/69

13. GAC Document No. LED-520-IF, "LM Design Criteria and Environments", 5/15/66

14. Science Vol. 167, No. 3918, 30 January 1970

15. R. Birkebak, C. Cremers, J. Dawson, "Thermal Radiation Properties and Thermal Conductivity of Lunar Material." Science Vol. 167, No. 3918, 30 January 1970, pp. 724-726.

16. R. Fryxell, D. Anderson, D. Carrier, W. Greenwood, G. Heiken, "Apollo 11 Drive-Tube Core Samples: An Initial Physical Analysis of Lunar Surface Sediment." Science Vol. 167, No. 3918, 30 January 1970, pp. 734-737

17. BxA SSED-57, "Investigations of PSE Anomalies - Apollo 12 Missions", 5/28/70

18. BxA Contact Report SSED-448, "PSE Seismometer-Terminator Anomaly Investigation", 5/14/70

19. Simms, R. J., "Solar Illumination Transients at Lunar Sunrise," 6/1/70, BxA Memo 70-210-191

20. NASA News Release No. 70-23, "LM Shower on Surveyor III", 2/17/70

21. AIAA Paper No. 67-289, "Diurnal Lunar Temperatures", April 1967

22. "Thermal Radiation Exchange of PSE Sensor with the Lunar Surface", BxA Memo 9713-10-3292, 8/15/69.

23, "Internal Configuration Factors for PSE." BxA Memo 9713-10-917, 16 July 1968; "A Computer Program to Supplement CONFAC II." BxA Memo 9713-10-916, 17 July 1968

24. "Summary of PSE Thermal Control System - BxA ALSEP Systems Thermal/Vacuum Tests" BxA Memo 9713-10-3060, 20 February 1969

25. "PSE Thermal Performance During Lunar Night" BxA Memo 9713-10-3069, 26 February 1969

26. "Change Order No. 11 Spectral Reflectivity Curves" Letter from J. Clerk to M. Osmun (BxA), 17 July 1967

27. "Results of Reflectance Tests" BxA Memo 974-1012, 26 September 1968

28. "Surface Properties of PSE Thermal Shroud Simulator" BxA Memo 9713-10-3378, 9 December 1969

29. "Surface Properties of PSE Beryllium Components" BxA Memo 9713-10-3357, 13 November 1969

30. "Analysis of Apollo 12 PSE Data Anomaly" MSC TWX-BG93/ L115-70/T94, 13 February 1970.

31. "Thermal Analysis of Q24 and Q25 Transistors on the PSE "W"-Board", BxA memo 70-210-170, 26 May 1970

32. "Q24, Q25 Transistor Thermal Control - Proposed Modification", BxA memo 70-210-174, 28 May 1970

33. "Correlation of Q24 and Q25 Thermal-Vacuum Tests with Thermal Model Predictions", BxA memo 70-210-180, 3 June 1970

34. "Thermal Performance of Q24 Transistor with Copper Cup and Nylon Spacers", BxA memo 70-210-186, June 5, 1970

35. BxA contact report 70-210-07CR, "Metallized Teflon Films", 2/6/70

36. Ultrainsulation letter F. Bjorklund to M. Skerritt, 2/19/70

37. BxA contact report 70-210-08CR, "FEP Type A Teflon - Optical Properties", 2/23/70

38. BxA letter No. 70-210-30, G. Psaros to K. Jacobs (GSFC), 4/27/70

39. Boeing Progress Report to GSFC, "Degradation Tests on Thermal Control Materials", January 1970

40. GSFC letters from W. T. Chen to G. Psaros, 5/21/70 and 6/3/70.